DYNAMICS OF ION EXCHANGE COLUMNS IN SEPARATION OF LITHIUM-ION BATTERY METALS

Lappeenranta–Lahti University of Technology LUT

Master's Program in Chemical Engineering, Master's Thesis

2022

Alexander Tuhkunen

Examiners: Prof. Tuomo Sainio

D.Sc. Sami Virolainen

Abstract

Lappeenranta–Lahti University of Technology LUT

LUT School of Engineering Science

Chemical Engineering

Alexander Tuhkunen

Dynamics of ion exchange columns in separation of lithium-ion battery metals

Master's thesis

2022

73 + (15) pages, 28 + (36) figures, 9 tables and 2 appendices

Keywords: battery metals, lithium-ion battery, ion exchange, simulation, modelling, recycling, hydrometallurgy, cobalt, lithium, nickel, kinetics, TP260 resin

Examiners: Prof. Tuomo Sainio

D.Sc. Sami Virolainen

The number of lithium-ion batteries (LIB) is increasing drastically in everyday-life. Its usage in portable devices like mobile phones and laptops has increased every year. Also increasing number of electric vehicles has increased the LIBs demand. This demand also means there is a large number of batteries that need to be recycled. LIBs contain several valuable metals that can be recycled. The most valuable of them are Co, Li, and Ni.

In this thesis, the target was to gather data and simulate a loading of the ion exchange of LIB metals. Lewatit TP260 resin was used to study the breakthrough of the Al, Co, Cu, Fe, Li, Mn, Na, and Ni in a ~1 M H_2SO_4 solution. Each LIB metal was studied separately with the presence of Na, SO_4, and H ions. Experiments were conducted at pH 0, 1, and 1.8 at 60 °C. Elution and regeneration were performed with 2 M H_2SO_4 solution. For elution of Al and Fe, 0.4 M $(COOH)_2$ (oxalic acid) was used.

Laboratory experiments were used to fit the simulated breakthrough curves of each metal by utilizing NICA-IX equilibrium model. Affinity constant and pore diffusion coefficient had the focus of this study. The NICA-IX model gave promising results and the fit of the simulated loading cycle was able to be made accurately in most cases. Fe had the largest affinity constant, and Li, Co, and Ni had the lowest. Al, Cu, and Mn affinity values were between the Fe and Li, Co, and Ni. Fitted values and gathered data can be used for the development of multi-metal ion exchange systems.

Tiivistelmä

Lappeenrannan–Lahden teknillinen yliopisto LUT

LUT Teknis-luonnontieteellinen

Kemiantekniikka

Alexander Tuhkunen

Ioninvaihtokolonnin dynamiikka akkumetallien erotuksessa

Kemiantekniikan diplomityö

2022

73 + (15) sivua, 28 + (36) kuvaa, 9 taulukkoa ja 2 liitettä

Avainsanat: akkumetallit, litiumioniakku, ioninvaihto, simulointi, mallinnus, kierrätys, hydrometallurgia, koboltti, litium, nikkeli, kinetiikka, TP260 hartsi

Tarkastajat: Prof. Tuomo Sainio

D.Sc. Sami Virolainen

Litiumioniakkujen määrä on noussut merkittävästi jokapäiväisessä elämässä. Niiden käyttö kannettavissa laitteissa kuten puhelimissa ja kannettavissa tietokoneissa on kasvanut joka vuosi. Lisäksi sähköautojen määrän kasvu on lisännyt litiumioniakkujen kysyntää maailmalla. Tämän kysyntä myös tarkoittaa, että kierrätettävien akkujen määrä on kasvanut. Litiumioniakuissa on monia arvokkaita metalleja, jotka voidaan kierrättää. Arvokkaimmat metallit ovat Li, Co ja Ni.

Tässä työssä tavoitteena oli kerätä dataa ja simuloida litiumioniakkumetallien ionivaihtoa. Läpäisykäyräkokeissa tutkittiin Al, Co, Cu, Fe, Li, Mn, Na ja Ni metalleja ~1 M H_2SO_4 liuoksessa ja hartsina käytettiin Lewatit TP260. Jokaista akkumetallia tutkittiin erikseen samalla kun liuoksessa oli Na, SO_4 ja H ioneita. Testit tehtiin pH arvoilla 0, 1 ja 1.8 kun lämpötila oli 60°C. Eluointi ja hartsin regenerointi tehtiin 2 M H_2SO_4 liuoksella. Al ja Fe eluointiin käytettiin 0.4 M $(COOH)_2$ (oksaalihappo) liuosta.

Laboratoriotestien tuloksia käytettiin simuloitujen läpäisykäyrä kuvaajien sovittamisessa NICA-IX tasapainomallilla. Tutkimuksessa keskityttiin selvittämään affinititeettikertoimia ja huokosten diffuusiokertoimia metalleille. NICA-IX antoi lupaavia tuloksia ja simulointien sovittaminen tarkasti onnistui hyvin useimmissa tapauksissa. Fe:llä oli suurin affiniteettikerroin arvo kun taas Li, Co ja Ni:oli pienimmät arvot. Al, Cu ja Mn affinitteikertoimet olivat Fe:n ja Li, Co ja Ni arvojen välissä. Saatuja arvoja voidaan käyttää monimetalli systeemien ionivaihdon kehittämiseen.

Foreword

This Master's Thesis was a part of the BATix project funded by Metallinjalostajien rahasto (Metallinjalostajat ry.) where the goal is to achieve a continuous ion exchange process where high purity Ni/Co/Li raffinate can be produced in a single unit operation step. This process could be then used in lithium-ion battery recycling processes. This thesis was done in the Department of Chemical Engineering at Lappeenranta-Lahti University of Technology LUT between October 2021 and December 2022.

I would like to thank Tuomo Sainio and Sami Virolainen for this opportunity and support in this work. I also want to thank Tobias Wesselborg for offering and giving help whenever I needed it. Also, thanks to Liisa Puro for her help with ICP analysis and Santeri Kurkinen for additional help in the laboratory. Finally, I also thank my family and friends who supported me during this long process.

Lappeenranta, 6th of December 2022.

Alexander Tuhkunen

Table of contents

Symbols

A	Anion
a_{H+}	Activity of proton, -
a_r	Equilibrium constant, $(L/mg)^{\beta}$
b_i	Constant for Extend Freundlich model, -
c	Concentration, mol/L
$c_{i,l}$	Concentration of component i in the liquid, mol/L
$c_{i,r}$	Concentration of component i in the resin, mol/L
c_n	Concentration at point n, mol/L
c_{n+1}	Concentration at point n+1, mol/L
c_p	Molar concentration in pore, mol/L
c_0	Feed concentration, mol/L
Cl	Reactive part of the resin (anionic cases)
D_{ax}	Axial dispersion coefficient, m^2 /s
D_p	Pore diffusion coefficient, m^2 /s
d_s	Diameter, m
F	Faraday constant, J/(mol·K)
H	Reactive part of the resin (cationic cases)
h	Ion-specific non-ideality constant ($0 < h \leq 1$), -
J	Diffusion flux, mol/(m^2s)
K	Affinity constant, -
K^A_B	Equilibrium coefficient between A and B, -
k_l	Equilibrium constant, L/g
k_f	Equilibrium constant, $(mg/g)(mg/L)^{1/n}$
$k_{f,i}$	Equilibrium constant for component i, $(mg/g)(mg/L)^{1/n}$
k_m	Mass transfer coefficient, m/s
M	Cation
m_{vap}	Mass of evaporated water per g of wet resin, g
N	The end of data set
N_{tot}	Solution normality, mol/kg

$N_{0.5n-1}$	The last point before the accumulated surface area of absorbance is ≤ 0.5 of the total surface area
$N_{0.5n+1}$	The first point after the accumulated surface area of absorbance is ≥ 0.5 of the total surface area
n_a	Adsorption intensity, -
$n_{f,i}$	Constant for Extend Freundlich model, -
p	Site-specific non-ideality constant describing the adsorption site heterogeneity ($0 < p \leq 1$), -
q	Amount of component bound onto resin sites, mol/kg
q_e	Amount of metal in resin per mass of the dry resin, meq/g
q_{max}	Maximum amount of adsorption for resin, mol/kg
R	Gas constant, J/(molK)
R_e	Resin which is insoluble to the solution
r	Radial coordinate, m
T	Temperature, K
t	Time, s
t_{inj}	Injection time of the solution, s
t_{pmc}	Time value of the peak mass center, s
$t_{tube\ void}$	Time delay caused the volume of tubes and measuring devices, s
$t_{0.5n-1}$	Time of the measured y-value at the last point before the accumulated surface area of absorbance is ≤ 0.5 of the total surface area, s
$t_{0.5n+1}$	Time of the measured y-value value at the first point after the accumulated surface area of absorbance is ≥ 0.5 of the total surface area, s
Δt	Time interval, s
V_{Bed}	Volume of the resin bed, dm^3
$V_{Bed,\ void}$	Volume of the void of the resin bed, dm^3
v	Flow rate, L/s
x_i	Constant for Extend Freundlich model, -
x_M	Equivalent factor of component A and B, -
x_x	Axial coordinate (length), m
y_i	Constant for Extend Freundlich model, -
y_M	Equivalent factor of component A and B, -

y_n	Absorbance of point n, -
y_{n-1}	Absorbance of point n-1, -
y_{n+1}	Absorbance of point n+1, -
z	Charge of component, -
z_c	Charge of cation, -
z_n	Number of charges or/and stoichiometry, -
z_R	Charge of resin functional group, -

Greek letters

β	Isotherm exponent, -
γ	Activity coefficient of component at bulk phase, -
$\overline{\gamma}$	Activity coefficient of component at resin phase, -
$\Theta_{i,t}$	Degree of coverage for component i on site t, -
$\rho_{b,vet}$	Density of wet resin, g/L
ε_{Bed}	Bed porosity, -
ε_{resin}	Resin porosity, -
$\varepsilon_{tot,}$	Total porosity, -
φ	Electric potential, V

Subscripts

A	Component in MAIX model
B	Component in MAIX model
elu	Elution
H	Proton
i	Component
j	Component
loa	Loading
n	Data point

Abbreviations

BV	Bed volume
B-to-T	Bottom to top (When describing flow direction)
LIB	Lithium-ion battery
LFP	Lithium iron phosphate
LMO	Lithium manganese oxide
LTO	Lithium titanate
LCO	Lithium cobalt oxide
MAIX	Mass action ion exchange
NCA	Lithium nickel cobalt aluminum
NICA	Non-ideal competitive adsorption
NMC	Lithium nickel manganese cobalt
T-to-B	Top to bottom (When describing flow direction)

1. Introduction

The electrification of the world has created an ever-increasing need for energy and portable energy storages. Laptops, mobile phones, mobile accessories, cars, ships, and airplanes use different kinds of batteries and when the use of fossil fuels will be reduced and eventually given up entirely, demand for batteries will increase even more. At the same time, the number of spent batteries is increasing without an effective recycling process that is needed to handle all the produced battery waste. Another aspect that needs to be solved is to meet the future demand with the limited presence of raw materials on Earth. In the case of batteries, this is quite crucial because batteries use metals, like Co, Li, and Ni, that are quite rare and couple of them are listed in the European union's critical raw-material list. (European Commission, 2020)

The rapid change toward electrification of transportation is mostly caused by political decisions addressing the climate change. Utilization of fossil fuels in transportation is reduced and replaced by other energy sources such as lithium-ion batteries (LIB). New battery chemical factories, battery metal mines, and refineries are being opened all around the world. At the same time the number of studies about recycling is increasing to find a solution to meet the huge demand of battery metals. The demand of batteries was 180 GWh in 2018 and it has been predicted to increase to 2623 GWh by 2030 (*A Vision for a Sustainable Battery Value Chain in 2030: Unlocking the Full Potential to Power Sustainable Development and Climate Change Mitigation.* 2019). This is a huge number of batteries that are needed to recycle at some point, and they contain a large amount of valuable metals that can be reused after recycling. Batteries are also hazardous waste so recycling them is a good idea for the environment.

One of the most common battery types, are LIBs which are used in portable and moving electric machines. They have a high energy density, reasonably long lifespan, and can be recharged many times before they lose significant amount of their capacity. (Scrosati, 2011) Batteries vary in size and composition quite a lot with each other which makes it hard to develop one unified recycling process. The

amounts of different metals and compositions can vary immensely. (Warner, 2015) Because of this, the recycling process needs to be versatile so it can handle different kind of battery wastes. In the case of LIB, the situation is the same, in one kind of battery type can have many variations in compositions. The goal is to separate and recover valuable pure metals out of the process as effectively as possible at the same time at a low cost.

Performing the recycling of LIB waste by hydrometallurgy is one possibility. Hydrometallurgical processes consist of several different processes. One of these processes is ion exchange. Ion exchange is a method that can be used to separate different components from each other. Ion exchange is utilized in hydrometallurgical processes and one common application is water purification. Ion exchange reaction is reversible, and resins can be regenerated providing thousands of cycles of usage. (Free, 2022)

This master's thesis is part of BATix project whose goal is to develop a recycling process for LIB waste metals by ion exchange. This work's purpose is to get more information of ion exchange system where Al, Cu, Fe and Mn are separated from Co, Li and Ni. Current challenges are lack of information for simulations and two-step elution. Used methods are a short literature review of the current situation, single metal column laboratory experiments, and simulation of the ion exchange with non-ideal competitive adsorption ion exchange (NICA-IX) model. The metals were simulated one LIB metal at a time making it easier to determine kinetic values. Affinity constants and pore diffusion were studied in this study. The purpose of simulating LIB metals alone is to be able to simulate multi-metal systems by using the same values as in single-metal simulations.

2. Lithium-ion batteries and their recycling

Lithium-ion batteries have been on the market and utilized in several commercial applications since the 1970s. One advantage of lithium-ion batteries is higher energy density which means lighter, and smaller batteries. This advantage made it

possible to improve and develop new small portable, and handheld devices such as pacemakers, mobile phones, laptops, and other devices. Another improvement that came along with the lithium-ion batteries was a higher voltage which made it possible to use fewer batteries in series to achieve the needed voltages. (Scrosati, 2011)

Nowadays lithium-ion batteries are also used in transportation like hybrid vehicles, plug-in hybrid vehicles, and electric vehicles. Grid applications of LIBs have been developed to smooth out consumption spikes and to support wind and solar energy (Choi *et al.,* 2021). Spent electric vehicle batteries can be used as energy storage in electric grids (Abdel-Monem *et al.,* 2017; Choi *et al.,* 2021). This end-use increases the lifetime of batteries, but it does not remove the need for recycling at the end of batteries lifetime. Currently, the interest in recycling LIBs has been increasing. There are studies that handle LIB waste recycling in different ways. Some existing recycling processes already use pyrometallurgy, hydrometallurgy, and combinations of these two. However, there are a lot of shortcomings and lots of metals and other materials are lost during these processes. (Velázquez-Martínez *et al.,* 2019; Sommerville *et al.,* 2021)

2.1. Lithium-ion batteries

The lithium-ion batteries consist of cathodes, anodes, material in between the cathode and anode working as a separator, case, and Al and Cu foils (Vanderbruggen *et al.,* 2021). One kind of lithium-ion battery structure is presented in Figure (1). Table (I) shows metal concentrations of LIB waste leachate. Li can be used to produce several different kinds of cathodes for batteries. Every cathode compound has its own properties that are needed in different applications. This makes the LIB waste so diverse.

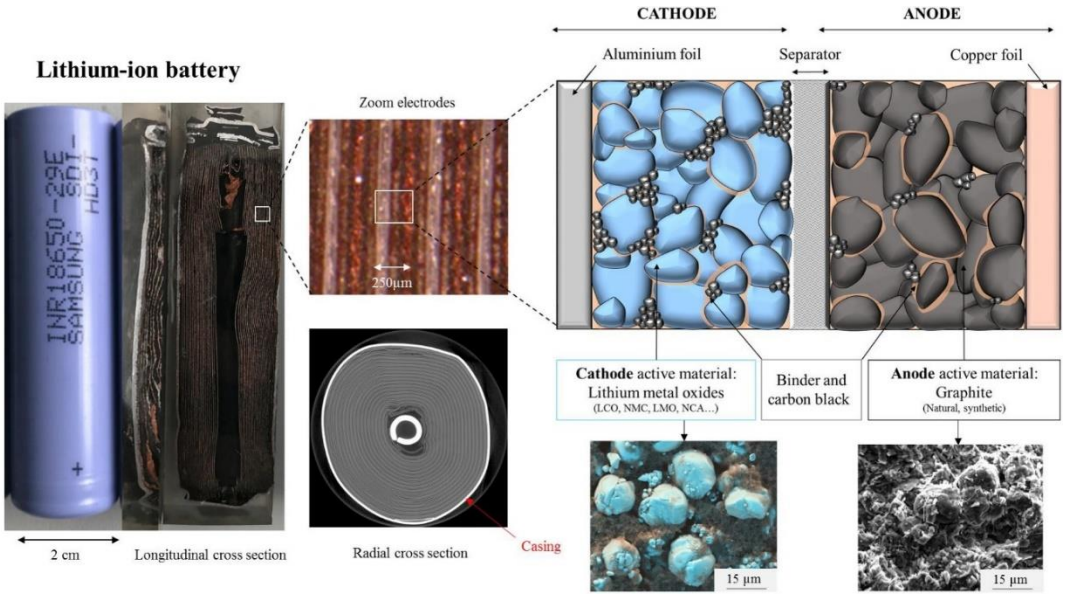

Figure 1 Structure of an 18650 lithium-ion battery (left), structure of LIB cells (top right) and SEM image on LCO (bottom right) (Vanderbruggen *et al.*, 2021).

Table I Metal content in LIB waste leachate (Porvali *et al.*, 2019).

Metal	**Concentration, mg/L**
Li	2548
Co	16817
Ni	1996
Mn	2146
Cu	2145
Al	1519
Fe	741

Lithium-ion battery's cathodes can be made from many different compounds such as lithium iron phosphate (LFP), lithium manganese oxide (LMO), lithium titanite (LTO), lithium cobalt oxide (LCO), lithium nickel cobalt aluminum (NCA), and lithium nickel manganese cobalt (NMC). The energy capacities, life cycles, costs, and temperature range of operating the battery vary a lot between different cathode materials. (Warner, 2015) Because there are several different cathodes that have different metals and metal ratios in them the metal concentrations in Table (I) are

not universal. In hydrometallurgical LIB recycling, waste has been leached usually with H_2SO_4 and HCl (Georgi-Maschler *et al.*, 2012; Porvali *et al.*, 2019). However, different kinds of chemicals are tested, for example, organic acids such as glycine (Chen et al. 2021).

2.2. Main metals of LIBs

The most valuable metals in lithium-ion batteries are Co, Li, and Ni. Co content is high in some lithium-ion batteries cathode and in its leachate. The Co concentration is high in the LIB waste leachate presented in Table (I). Other metals were around 2 g/L which is much less than the Co amount but some of them have significant values in them. The values of battery metals are presented in Figure (2).

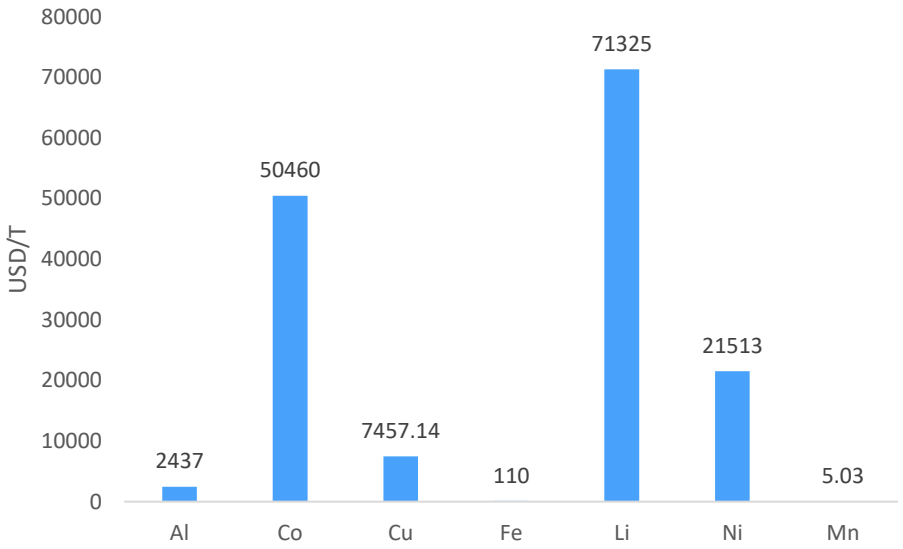

Figure 2 Market prices of battery metals on 26.7.2022 (*Trading Economics.* 2022).

Li is currently the most valuable metal in this group and its value has increased 1229 % between 2020 and 2022 (*Trading Economics.* 2022). Other valuable metals are Co and Ni. The recycling of these metals is profitable in several cases depending on the recycling method used. The value of metals can change quite quickly like in

the case of Li. However, because the usage of battery metals is going to increase, the value of battery metals most probably continues to increase or remains around the same level with some dips and spikes from time to time. New inventions can change the demand for metals in the future which also affects the price of these metals.

Co is mainly mined as a byproduct of other metals such as Ni and Cu (Fisher, 2011). The largest Co producers in 2021 were DR Congo, Russia, and Australia (U.S. Geological Survey, 2022). There is a supply risk for Co which is mainly caused by the DR Congo's political instability (Helbig *et al.*, 2018). Co consumption has been estimated to grow from 2007 50 kt/year to 2050 190 kt/year (Tisserant and Pauliuk, 2016).

Li is mostly produced from brines. Li is also produced from spodumene, lepidolite, amblygonite, and eucryptite minerals. (Peiró *et al.*, 2013). The biggest Li producers are Australia, Chile, and China (U.S. Geological Survey, 2022). Li mine production in 2010 was 25300 metric tons and the amount increased to about 100000 metric tons in 2020 (U.S. Geological Survey, 2011; U.S. Geological Survey, 2022).

The third most valuable metal in LIB waste is Ni. Ni is produced from laterites and magnetic sulfide deposits (U.S. Geological Survey, 2021). Ni usage has increased from 1.465 Mt in 2010 to 2.385 Mt in 2020. (International Nickel Study Group, 2021). Worlds main producers of Ni are Indonesia, the Philippines, and Russia (U.S. Geological Survey, 2022).

2.3. Current recycle processes

The market for recycling lithium-ion batteries was 1.7 billion USD in 2020 and this amount is expected to increase in the future (*Lithium-Ion Battery Recycling Market.* 2021). There are several companies that recycle lithium-ion batteries already. Many of these companies like Accurec, Umicore, and ERAMET utilize pyrometallurgical processes. Hydrometallurgical processes are greatly used by TOXCO, Green Eco-Manufacture Hi-Tech Co, and Bangpu Ni/Co High-Tech Co. However, many of

these companies use both pyrometallurgy and hydrometallurgy in their processes. (Liu *et al.,* 2019; Sommerville *et al.,* 2021) The world's largest battery recycling company Brunp Recycling Technologies is located in China. Its capacity is 100 000 tons/year, and it utilizes pyro- and hydrometallurgical processes when handling the recycling. (Baum *et al.,* 2022)

The recycling processes are complex and consist of several steps. For example, comminution is a common step in recycling. Here the battery waste is crushed and grinded to finer particles. AkkuSer in Finland also makes size separation during the comminution step. AkkuSer uses magnetic separation, and the end product is black mass and foils (Pudas *et al.,* 2015; Sommerville *et al.,* 2021).

In pyrometallurgical processes, the downsides are the material losses during the process and high energy consumption. There are also losses of metals to side streams/slag and for example, Li is lost in the side streams in some cases (Velázquez-Martínez *et al.,* 2019). However, currently Li is a valuable metal so losing it is not a desirable outcome. Advantages in pyrometallurgical processes are a high capacity and simplicity (Zheng *et al.,* 2018). When recycling battery waste with pyrometallurgy Cu, Co, Ni, and Fe can be recovered. (Gaines, 2018).

Common process steps in hydrometallurgy are leaching, extraction, and precipitation. Hydrometallurgical processes are less energy intensive than pyrometallurgical processes. Hydrometallurgical processes do not often need high temperatures compared to pyrometallurgy where temperatures can be over 1000 °C (Li *et al.,* 2016). Hydrometallurgical processes have often lower capital cost. Another advantage is the possibility to achieve high purities in products. However, the chemical consumption is high in these processes and amount of produced wastewater is high. (Zheng *et al.,* 2018; Jung *et al.,* 2021)

3. Ion exchange

Ion exchange is a versatile and effective hydrometallurgical method to separate different metal ions and other ionic substances from each other. By understanding the methods and its functions, most metals and compounds can be separated via ion exchange. For example, ion exchange has been used for purification of water. Ion exchange is used to purify solutions from impurities before further processing like electrowinning. (Sole *et al.*, 2016; Free, 2022) For example, Glencore Nikkelverk AS refinery uses ion exchange to separate Co and Ni from each other. Ni is sorped into activated carbon and Co continues to a recovery step. (Brückner *et al.*, 2020)

There are chelating, cationic and anionic ion exchange resins that can interact with the ions of the solution. There are weak basic and acid ion exchange resins and in addition, there are also strong basic and acid ion exchange resins. (Shamsuddin, 2021) Ion exchange resins can be chosen or prepared for different separation needs. For example, the resin can be chosen in a way it interacts mostly with the target ion and let other ions pass through without too much interaction. (Luca *et al.*, 2009; Lebron *et al.*, 2021) Separation's core idea is to let different ions out of the columns at different times and in different cycles. Target ions can be sorped and then collected during an elution cycle, or impurities are sorped and target ions collected in the raffinate.

On the surface and inside of the resins are functional groups that can perform the ion exchange. The original counter ion of the functional group is replaced with an ion from a treated solution. Depending on the functional groups of the resin, the selectivity can be affected greatly. Metal ions can be selectively removed from the liquids onto the resin. The functional groups can form chemical bounds with metal ions and complexes. The metal ion interactions can be represented as a reaction to cationic exchange case in Equation (1) and anionic case in Equation (2). The ion reacts with the functional group of the resin in an equilibrium reaction and the capacity of the resin is limited. (Shamsuddin 2021)

$$z_n HR_e(s) + M^{z_n+}(aq) \rightleftarrows MR_e(s) + z_n H^+(aq) \quad (1)$$

$$z_n R_e Cl(s) + A^{z_n-}(aq) \rightleftarrows R_e A(s) + z_n Cl^-(aq) \quad (2)$$

Where	*A*	Anion
	Cl	Counter ion of the resin (anionic cases)
	H	Counter ion of the resin (cationic cases)
	M	Cation
	z_n	Number of charges or/and stoichiometry
	R_e	Resin which is insoluble to the solution

Other phenomena in the ion exchange column are film diffusion and particle diffusion. The whole reaction process can be presented in five steps: 1. diffusion of metal ion from bulk phase to the boundary layer of the resin, 2. diffusion of the metal ion into the resin's pores, 3. metal ions ion exchange with the resins functional group, 4. counter ions diffusion out of the resin and 5. protons diffusion from the boundary layer to bulk phase. In case of the elution and adsorption the reaction process is quite the same but another way around. In adsorption metal ions come from the bulk and in elution the replacing ion, for example, protons come from the bulk phase. (Shamsuddin, 2021) Figures (3) and (4) present adsorption and ion exchange resin-packed column and their working principle.

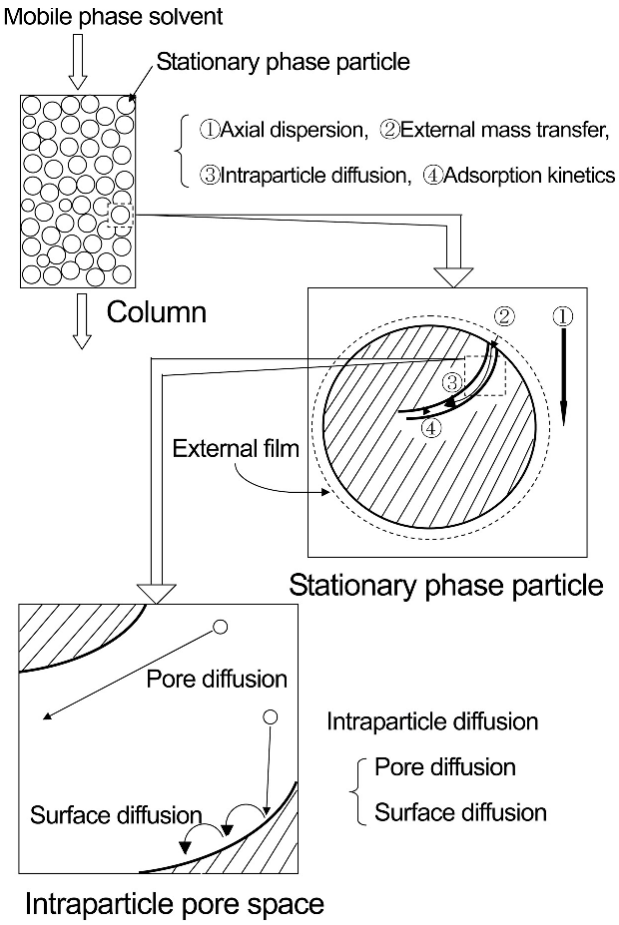

Figure 3 Kinetics and dynamics of adsorption/ion exchange column (Miyabe and Guiochon, 2003).

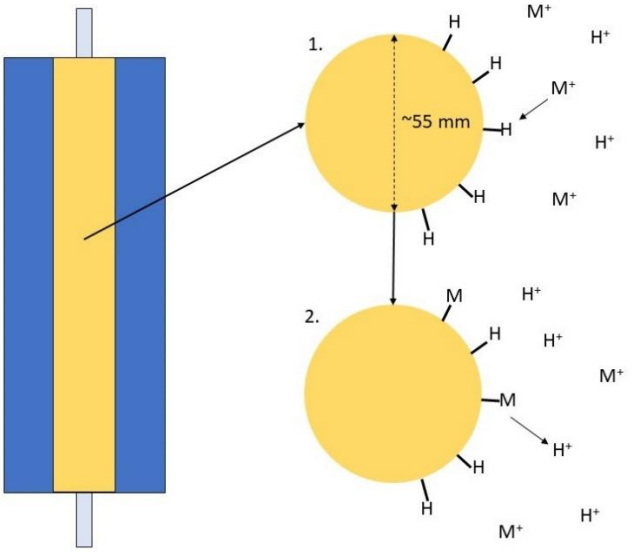

Figure 4 Simplified working principle of ion exchange. At point 1 the resin functional group has its original counter ion, and the cation is in the liquid phase. At point 2 the cation has bound to the site and the counter ion is in the liquid phase.

Pores of the resin also affect the ion exchange of the system. Figure (3) presents the pore of one particle and how particles or ions move near and inside the resin particle. The pore diffusion is the phenomenon that describes particle movement inside the resin pores. This will affect how pores fill up during the loading and get replaced during the elution. When the resin is very porous this will make a difference when the system is being simulated. Depending on the pore diffusion, the time needed to fill the whole resin bed will vary between different ions.

Ion exchange columns are operated in different cycles. During loading, a solution that contains ions is injected into the column and the target ions are absorbed onto the resin. Other ions go through the column without strong interactions with the resin and separation is achieved. Columns are often operated as long as the impurities of the raffinate are at acceptable level. (Kaukinen, 2019; Virolainen *et al.,* 2021) Depending on the product being made, the required purity varies, for example, for battery metals the target purity is around 99.5 % (European Lithium, 2020). After loading, the column is washed. Column is rinsed with purified water because there is still feeding solution inside the column, and it is not wanted to mix with other solutions. Column is rinsed also after elution. In case of the eluates there can be risk for precipitation for example with $(COOH)_2$ and Cu. After washing, the process is continued with elution, another washing phase, regeneration phase, and last washing phase. In elution, sorped ions are replaced with resins functional groups counterion (for example with H^+) and previously adsorbed ion move into eluate. The resin can be regenerated in this step, or it is regenerated separately in the regeneration step and after wash, the resin can be used again for ion exchange. Resins are often operated for hundreds or thousands of cycles before replacing it. (Kaukinen, 2019; Virolainen *et al.,* 2021) Depending on the used resin and solution the lifetime of the ion exchange resin can be long but in harsh conditions, the resin wears out quickly. (*DuPont Ion Exchange Resins Resin wear-out guidelines.* 2019)

3.1. Mathematical models for adsorption and ion exchange equilibrium

There are several mathematical models for describing adsorption processes. Some of these can be used also for the ion exchange processes but they usually need to be modified first before use. Depending on solutions, resins, and conditions of the system, different mathematical models are chosen or developed. The more there is species competing the adsorption sites, the more complex the model is. One basic mono-component adsorption is Langmuir isotherm model which is in Equation (3) (Langmuir, 1918).

$$q_i = \frac{q_{max} k_{l,i} c_i}{1 + k_{l,i} c_i} \tag{3}$$

Where

c_i	Concentration of component i, mol/L
$k_{l,i}$	Equilibrium constant for component i, L/mg
q_i	Amount of component i bound onto sites, mol/kg
q_{max}	Maximum amount of sites, mol/kg

Here is assumed only one molecule can be adsorbed onto one site. Sites on the resin are on a solid surface and each of the sites are energetically equivalent. Also, adsorbed molecules/ions do not interact with other adsorbed molecules. (Ruthven, 1984) Langmuir equations are usually used for adsorption. In the case of a multi-component system, it has its own models. For Langmuir, there is non-modified competitive Langmuir in Equation (4) (Gupta and Balomajumder, 2015; Lebron *et al.*, 2021).

$$q_i = \frac{q_{max,i} k_{l,i} c_i}{1 + \sum_{j=1}^{N} (k_{l,j} c_j)} \tag{4}$$

Where c_j Concentration of component *j*, mol/L

$k_{l,j}$ Equilibrium constant for component *j*, L/mg

In these models the different compounds are taken into account and as the name implies, they compete with each other for adsorption sites of the resin. In modified competitive Langmuir is also additional *n*-parameter that works as correction factor. The *n*-parameter can be calculated using experimental data. (Girish, 2017)

Other common mathematical model is Freundlich isotherm model which is in Equation (5) (Naushad and Al-Othman, 2013; Gupta and Balomajumder, 2015).

$$q_i = k_f c_i^{1/n_a} \tag{5}$$

Where k_f Equilibrium constant, $(mg/g)(mg/L)^{1/n}$

n_a Adsorption intensity, -

Where is assumed a heterogenic surface where multilayer adsorption is possible (Naushad and Al-Othman, 2013). The Freundlich equation is suitable for fitting most of adsorption and desorption data and especially when the sorbent is heterogeneous. However, at high concentrations, it cannot be used to predict adsorption equilibrium and at very low concentrations, it cannot present the system linearly (Naushad and Al-Othman, 2013). For the Freundlich model, there is also Extended Freundlich in Equation (6) (Gupta and Balomajumder, 2015).

$$q_i = \frac{k_{f,i} c_i^{\frac{1}{n_{f,i}+x_i}}}{c_i^{x_i} + y_i c_j^{b_i}} \tag{6}$$

Where $k_{f,i}$ Equilibrium constant for component i, $(mg/g)(mg/L)^{1/n}$

b_i, $n_{f,i}$, x_i, and y_i Constants of component *i*, -

Third common isotherm model is Redlich-Peterson and a modified competitive Redlich-Peterson is in Equation (7) (Gupta and Balomajumder, 2015; Girish, 2017).

$$q_i = \frac{k_{r,i}(\frac{c_i}{n_i})}{1 + \sum_{j=1}^{N} a_{r,j}(\frac{c_j}{n_j})^{\beta_j}} \quad (7)$$

Where a_r Equilibrium constant, $(L/mg)^{\beta}$

k_l Equilibrium constant, L/g

β Isotherm exponent, -

β_j Isotherm exponent of component *j*, -

Redlich-Peterson model is combination of the Langmuir and Freundlich models. This model is suitable for a wide range of concentrations in the system. At high the model is closer at Freundlich model and in the high concentration its closer to Langmuir. At the modified competitive Redlich-Peterson is added interaction parameter *n* that is calculated from experimental data. This model is suitable for multicomponent systems. (Girish, 2017)

When modeling ion exchange, assumptions are made for simplification. Thus, assumptions are being made to describe the ion exchange process. In ion exchange model's electro neutrality is assumed (Inglezakis and Zorpas,2012). More advanced model for ion exchange is mass action ion exchange (MAIX) model. MAIX is a stoichiometric exchange model. MAIX equilibrium is presented in Equation (8). (Laatikainen, 2014)

$$K_B^A = (\frac{y_{M,A}^{|z_B|} x_{M,B}^{|z_A|}}{x_{M,A}^{|z_B|} y_{M,B}^{|z_A|}})(\frac{\bar{\gamma}_A^{|z_B|} \gamma_B^{|z_A|}}{\gamma_A^{|z_B|} \bar{\gamma}_B^{|z_A|}})(\frac{q_i}{N_{tot}})^{|z_B|-|z_A|} \quad (8)$$

Where K^A_B Equilibrium coefficient between A and B, -

N_{tot}	Solution normality, mol/kg
$x_{M,A}$ and $x_{M,B}$	Equivalent factor of component A and B, -
$y_{M,A}$ and $y_{M,B}$	Equivalent factor of component A and B, -
z_A and z_B	Charge of component A and B, -
γ_A and γ_B	Activity coefficient of component A and B at bulk phase, -
$\overline{\gamma}_A$ and $\overline{\gamma}_B$	Activity coefficient of component A and B at resin phase, -

MAIX is a phase equilibrium model, and it is used to model the equilibrium of the ions between liquid and solid phases (Laatikainen, 2014). Another more advanced ion exchange equilibrium model is the NICA-IX model, derived from the NICA model whose equations are presented in Equation (9) and Equation (10). Derived NICA-IX is in Equation (11). (Kinniburgh *et al.*, 1999; Laatikainen, 2014).

$$\theta_{i,t} = \frac{(K_i c_i)^{h_i}}{\sum_i (K_i c_i)^{h_i}} * \frac{[\sum_n (K_i c_i)^{h_i}]^p}{1 + [\sum_n (K_i c_i)^{h_i}]^p} \quad (9)$$

Where	$\Theta_{i,t}$	Degree of coverage for component i on site t
	h_H	Ion-specific non-ideality constant for the proton, ($0 < h_H \leq 1$)
	h_i	Ion-specific non-ideality constant for the component i, ($0 < h_i \leq 1$)
	K_i	Affinity constant for component i, -
	p	Site-specific non-ideality constant describing the adsorption site heterogeneity ($0 < p \leq 1$)

$$q_i = \theta_{i,t} * \frac{h_i}{h_H} q_{max,H} \quad (10)$$

Where q_i Adsorption of component i, mol/kg

$q_{max,\,H}$ Maximum adsorption of the proton, mol/kg

$$q_i = q_{max}\frac{|z_R||z_i|}{|z_i|}\frac{h_i(K_i|z_i|c_i)^{h_i}}{\sum_j|z_j|h_j\,(K_j|z_j|c_j)^{h_j}} \quad (11)$$

Where z_i Ion charge of component i

z_R Ion charge of the resin functional group

The q-values are used for the calculation of specific ions or components' sorped amount into the resin. When the amount of the resin is known the amount of a specific component in the resin can be calculated. For the NICA-IX model with several components bound to the resin, the component of interest's adsorption value can be calculated while at the same time taking into account each active component in the solution. In the NICA-IX model stoichiometry of the resin and components, competition, and affinity constants are taken into consideration (Kinniburgh *et al.*, 1999; Laatikainen, 2014).

3.2. ResMod simulation tool

Simulations are helpful when planning chemical processes such as ion exchange. Laborious tests can be avoided when a working simulation can be done. Results can be used for sizing the equipment, evaluating quantities of needed chemicals, and the capacity of the process. Simulations need mathematical models that can describe well reactions of the process. In this study ResMod toolbox and NICA-IX equilibrium model were used. ResMod is an Excel toolbox that can be used for simulating ion exchange processes. The mass balance of the fixed bed in ResMod is presented in Equation (12). (Laatikainen, 2014)

$$\frac{\partial c_{i,l}}{\partial t} + v\frac{\partial c_{i,l}}{\partial x_x} + \frac{(1-\varepsilon_{bed})}{\varepsilon_{bed}}\frac{6k_{m,i}}{d_s}(c_{i,l} - c_{i,r}) - D_{ax}\frac{\partial^2 c_{i,l}}{\partial {x_x}^2} = 0 \quad (12)$$

Where	$c_{i,r}$	Concentration of component i in the resin, mol/L
	$c_{i,l}$	Concentration of component i in the liquid, mol/L
	D_{ax}	Axial dispersion coefficient, m^2/s
	d_s	Diameter, m
	$k_{m,i}$	Mass transfer coefficient, m/s
	t	Time, s
	v	Flow rate, L/s
	x_x	Axial coordinate (length), m

In this study, axial dispersion was not included in the simulations. Another aspect that was taken into account was the movement of ions inside the resin particle pores. For ions movement in the pores, ResMod uses Nernst-Plank which is in Equation (13) (Laatikainen, 2014).

$$J_i = -D_{p,i}\left(\frac{\partial c_{p,i}}{\partial r} + \frac{z_i F c_{p,i}}{RT}\frac{\partial \varphi}{\partial r}\right) \quad (13)$$

Where,	$c_{p,i}$	Molar concentration of component i in pore, mol/L
	$D_{p,i}$	Pore diffusion coefficient of component i, m^2/s
	F	Faraday constant, As/mol
	J_i	Diffusion flux of component i, $mol/(m^2 s)$
	R	Gas constant, J/(mol·K)
	r	Radial coordinate, m
	T	Temperature, K
	φ	Electric potential, V

4. Separating LIB metals by ion exchange

There are several companies that are recycling batteries including lithium-ion batteries. Batteries can be recycled with several different methods for example with pyrometallurgy or hydrometallurgy and there are also combinations of different recycling methods (Swain, 2017). In pyrometallurgical processes, Cu, Ni, Co, and Fe can be recycled from LIB but Al, Li, and Mn are not regularly recovered from the waste (Gaines, 2018). Pyrometallurgical processes require lots of energy and high temperatures in its processes. Hydrometallurgy uses less energy and can be used to separate metals and compounds from complex solutions. (Dunn *et al.,* 2015; Gaines, 2018)

Currently, some of the recycling processes that are used are still in development and there is plenty of room for improvements. In many cases the waste stream contains valuable metals and materials. Some pyrometallurgical processes that are being used are shaft furnaces, calcination, and sintering. The hydrometallurgical processes used are leaching, solvent extraction, electrolysis, precipitation, and ion exchange. There are other processes and development of new methods is ongoing. (Velázquez-Martínez *et al.,* 2019; Sommerville *et al.,* 2021). Because environmental values have become more important, and the complexity of the waste has increased the interest towards recycling has grown.

4.1. Laboratory studies

In 2013 Badawy et al. studied Co separation from LIB waste. They studied how chelating resin separated Co from a leaching solution. First batteries were dismantled and treated first mechanically so extra Cu and Al could be removed. Then electrodes were leached by using 4 M HCl solution. Ion exchange was performed with several pH values between 3.5 to 6.5 and the used resin was chelating amidoxime resin. The equilibrium of the extraction of the metal ions is depending on pH and when pH is low the competition of the sites increases. In different pH values, the amount of sorped target metal can be changed. The best

results were achieved when pH was over 6 with 0.04 g/mL resin ratio. In this case, Co recovery was 100 %. When pH was 5.5 the recovery was 91 %. The process was continued with precipitation where spectrophotometrically detectable metals were precipitated. The end recovery of Co was 43 % at 6 pH case and at 5.5 pH case it was 66 %. There was noted that used polyamidoxime is not stable in acidic conditions. (Badawy *et al.*, 2014) However, only Co separation was studied so there is no information on how pure Co can be obtained from a multi-metal solution or how selective the separation process is. Also, resin regeneration was not studied. The acidic environment could be a problem in processes because the resin may not withstand the conditions.

Different resin adsorption was studied by Chiu and Chen (2017) in their study. They studied adsorption and its kinetics for LIB waste metals focusing on Ni and Co. Al was removed using NaOH before leaching which was performed with 3 N H_2SO_4. Tests were performed in pH values from 1 to 5 and studied resins were Amberlite IRC-748, Dowex M4195, Diaion CR-11, Purolite S 930, and Lewatit TP-272. M4195 and IRC748 were found to be the best resins for adsorbing Ni and Co. They also found out that M4195 resins adsorption is more ineffective at low concentrations and in the case of IRC748, the concentration has no effect on adsorption capacity at equilibrium. (Chiu and Chen, 2017)

Separation of metals from LIB waste by ion exchange using Dowex M4195 resin was studied by Strauss et al. (2021) in their study. Used test solution was made by leaching black mass with 1 M H_2SO_4 and ($FeSO_4$). Two columns were used to perform the separation and pH was adjusted to 1 during the test by using 2 M H_2SO_4. During wash cycles, 34.1 % of Ni was removed from the column and 36.2 % was removed by elution phase in 99.7 % purity. Some of the Ni was not removed from the resin during wash and elution cycles. In the case of Co, 26 % was removed from the column during the wash and 45 % during the elution. The elution solution Co purity was 98.9 %. Co and Ni were separated successfully and precipitated in 98.5 % and 99 % purities. Mn/Li product from raffinate was also obtained but its purity or yield was not reported. (Strauss *et al.*, 2021)

Separation of Mn, Zn, and Fe by ion exchange was studied by Lannoo et al. (2019). Studied battery type was alkaline battery. After leaching, Fe was precipitated by using NaOH. The solution had high Mn content which was 98.7 %. Ion exchange was performed using DOWEX M4195 resin to increase the purity of Mn for electrowinning. The separation between Mn and Zn succeeded and 99.975 % Mn purities were obtained. Higher purities could also be achieved by ending raffinate collection earlier. For Zn removal H_2SO_4 was used in elution step. 1 mol/L H_2SO_4 removed Zn effectively from the resin. (Lannoo *et al.*, 2019) Recycling of Zn could be profitable and studied recycling process was promising. Mn is most of least valuable metals when considering battery metals and its recycling may not be profitable. It is however in this case quite an effective way to achieve higher purities for the Mn.

Multi-metal LIB waste ion exchange was studied by Kaukinen (2019) in his master's thesis. In this study, the LIB waste solution was made by chemicals that were mixed to simulate solution from LIB waste leaching. The metals that were present in the used solution were Al, Co, Cu, Fe, Li, Mn, and Ni. Kaukinen studied different resins in metal separation, the purpose was to separate impurities Al, Cu, Fe, Ni, and Mn from the product stream that contained Co, Li, and Ni. Studied resins were Lewatit TP260, Purolite S-930, Finex CS12GC, and Finex CA16GC. The chelating resin TP260 performed the best and was able to separate Co, Li, and Ni from other metals. Al, Cu, Fe and Mn were sorped to resin and Co, Li, and Ni raffinate was obtained. Conditions were pH 1.8 and temperature 60 °C. TP260 resin performed quite well, and a purity of 99.5 % was achieved which is battery-grade purity. Regeneration of the resin was studied because of decreasing performance by elution with 1 M H_2SO_4, which was not enough because it could not remove Al and Fe from the resin. A cycle that contained elution with 2 M H_2SO_4 and 0.5 M $(COOH)_2$ was observed to remove most of the metals from the resin including Al and Fe. After this elution cycle, another sulfuric acid step was suggested to recover H^+ in the resin because there can be K ions bound to the resin. $K_2C_2O_4$ was used to produce $(COOH)_2$ and K ions can interact with the resin. This regeneration cycle was found to be suitable. (Kaukinen, 2019) The separation process was promising and if elution could be done in one step it could be the desired improvement.

The multi-metal separation studying was continued by Virolainen et al. paper (2021). Lewatit TP260 resin was used, and the experimented solution contained the same metals from the same chemicals as in Kaukinen's master thesis because it is based on it. The ion exchange process was optimized and in the regeneration step, the flow direction was changed during the elution step to achieve better regeneration. Two-step elution was still used. The suggested process overall gives over 99.6 % purity product and conditions were pH 1.8 and temperature 60 °C. (Virolainen *et al.*, 2021)

Li separation from Si, Al, and Fe was studied in Ningtyas et al. (2021). The used LIB waste came from used electric vehicles and a solution containing Fe, Al, Li, Si, Ni, Mn, Co, and Na. This differs from LIB waste obtained from mobile phones. Studied resins were DOWEX MSA, Amberlite IRA 410, and Amberjet 1200. DOWEX MSA was found to be a potential resin for Li and Si separation. (Ningtyas, *et al.*, 2021) However, this was from a solution that contained several metals, and it is unclear what are the purities of these two parts and how the resin affects other metals.

4.2. Simulation studies

Simulating ion exchange is a useful way to design and optimize processes because it can reduce the number of needed laboratory experiments. Laboratory experiments and measurements are necessary for the construction of accurate simulations of ion exchange systems. There are a lot of different mathematical models for ion exchange but those have their limitations, especially when the solution contains several different metals. To obtain accurate information for a certain system's kinetics and equilibrium, laboratory tests should be performed on multi-metal solutions, depending on what kind of separation is wanted.

Aalto has studied a way of modeling the ion exchange process for a multi-metal solution. A simulated system was made for a similar solution that has been studied earlier by Kaukinen (2019). Aalto (2021) modeled this process using ResMod

simulating tool capable to simulate ion exchange. The used equilibrium model in ResMod was NICA-IX, which is suited for multicomponent systems. Used NICA-IX and pore diffusion parameters were obtained by visually fitting them to laboratory tests by Kaukinen in his thesis (Kaukinen, 2019). This method has been good in two-component models but in this case, there is several components in the solution. The obtained modeling results were somewhat comparable to laboratory results, but peak values were not represented well. The modeled systems breakthroughs occurred usually later, and modeling of elution did not work. (Aalto, 2021) Diffusion parameters should be studied more and more laboratory tests are needed to obtain more accurate values for different simulation parameters. Also, a different model could be tried if improved values do not give better results.

5. Ion exchange laboratory experiments

In this thesis laboratory experiments were performed on solutions that were made synthetically to represent the solution obtained from LIB waste leaching. The LIB waste metals were studied one at a time. Kinetics of loading step were studied for each metal separately. When all metals can be simulated accurately these values could also be used in simulations of multi-metal system. This is needed for planning of the recycling process for LIB waste. All breakthrough experiments were performed with a column filled with Lewatit TP260 resin. Sulfates of the studied metals were dissolved into diluted 2 M H_2SO_4 media. The pH was adjusted by using NaOH pellets. Used chemicals are in Table (II).

Table II Chemical used in the tests.

Chemical	**Manufacturer**	**Purity**
$Al_2(SO_4)_3 \cdot 16H_2O$	KEBO Lab	N/A
$CoSO_4 \cdot 7H_2O$	VWR Chemicals	98 %
$CuSO_4$	VWR Chemicals	99.3 %
$Fe_2(SO_4)_3 \cdot x\ H_2O$	Alfa Aesar	>95 %
$Li_2SO_4 \cdot H_2O$	Acros Organics	>99 %
$MnSO_4 \cdot H_2O$	VWR Chemicals	99.8 %
Na_2SO_4	VWR Chemicals	99.5 %
$NiSO_4 \cdot 6H_2O$	VWR Chemicals	99 %
HCl	VWR Chemicals	Technical grade
H_2SO_4	VWR Chemicals	95 %
$K_2C_2O_4 \cdot H_2O$	J.T.Baker	>99 %
NaOH (pellets)	VWR Chemicals	98.8 %

The main goal was to study affinity constants and pore diffusion coefficients by using the breakthrough curves of the loading cycles of the ion exchange. Another goal was to gather more data about the ion exchange of LIB metals. The data was collected from loading and eluation of the packed bed column. The washing and the elution were also studied during these tests. When there is enough data, the affinity constants and pore diffusion coefficients can be determined by utilizing theoretical models. Modeled loadings were fitted visually against the measured data. To find out these values ResMod was used to simulate the loading. The test equipment is shown in Figure (5).

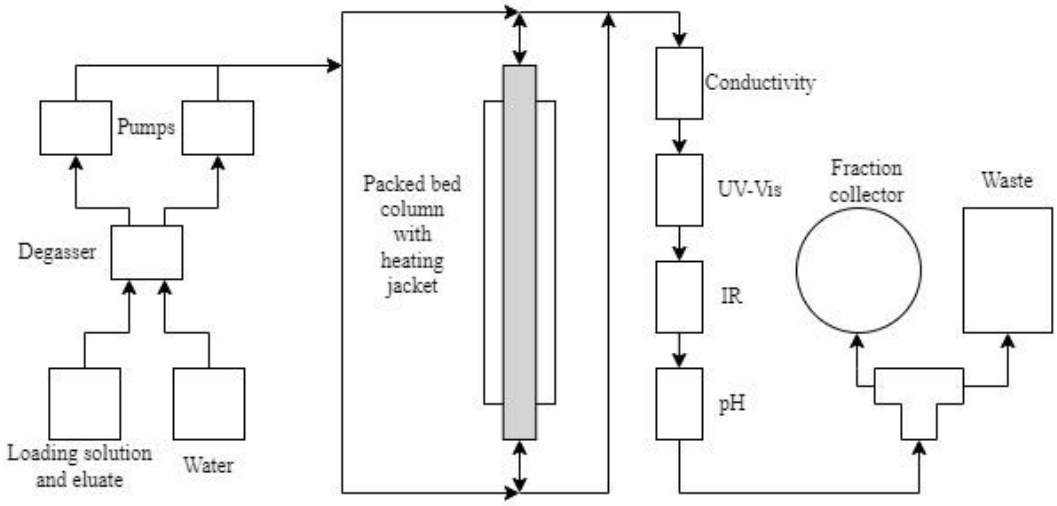

Figure 5 Test set-up used in breakthrough experiments.

The feed of the column was first pumped through degasser (Model DG-4400 by Degassex) after which were the pumps (Azura P4.1 by Knauer). There was one pump for loading solution and elution solution and one for water. There were backpressure valves after both pumps. The solutions continued to column with heating jacket (ECO15/120M3K-K by Kronlab). Heating of the column was done with heating recirculatory bath (C6 CS by Lauda). After column solution went through conductivity measurements (Conductivity meter 18 1500-00 by Pharmacia Biotech). Second measurement was UV-Vis detector (UV-900 by Amersham pharmacia biotech). Third was IR detector (RI 2000-F by Teopal). The last measurement was pH measurement (C3210 by Consort). After measurements, the flow was directed to fraction collector (Foxy R1 by Teledyne ISCO) or to waste container.

The collected samples were analyzed with ICP-MS (7900 by Agilent Technologies). Samples were diluted with matrix acid which consisted of purified water, 1 % HCl and 1 % HNO_3. The dilution was done in two steps where each dilution factor was 100. The final dilution was 10 000 times.

5.1. Ion exchange resin

The used ion exchange resin was Lewatit TP260. TP260 is a chelating resin whose functional group is aminomethylphosponic acid. The resin is sold when the functional group in Na^+-form and before, tests the resin is changed to H^+-form (*Product information Lewatit TP 260,* 2011). Aminomethylphosponic acid is shown in Figure (6). The pKa values for aminomethylphosponic functional groups are for the 1st 1.45 and for the 2nd 5.31 for the phosphonium groups and for amino group value is 11.0 (Nesterenko *et al.,* 1999).

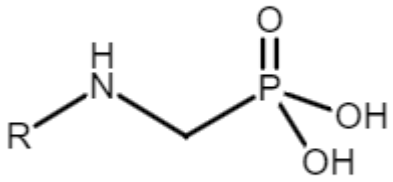

Figure 6 Aminomethylphosponic acid H^+-form on resin connected to resin styrene-divinylbenzene.

The selectivity of divalent cations for the Lewatit TP260 with aminomethylphosphonic acid as its functional group goes as follows U > Pb > Zn > Ni > Cd > Co > Mg > Sr > Ba >>> Na. From previous studies can be observed that trivalent cations bound strongly to the resin and their desorption requires large amount of suitable acid. (*Product information Lewatit TP 260*. 2011) More strongly bounding metal ions can push other weaker bounding ions out from the resin (Aalto, 2021). For eluation of trivalent cations, $(COOH)_2$ has been found to be a suitable acid (Kaukinen, 2019).

The resin needs to be prepared and turned to H^+-form before using it in ion exchange. The resin was rinsed with 1 M HCl and 1 M NaOH solution by turns removing Na from the resin and replacing it with H. The rinsing was started with

HCl and after the liquid from the column in acidic the resin was rinsed with purified water and after that NaOH solution was poured into the resin preparation column. Adding NaOH was continued until the liquid from the preparation column was alkaline. After every acid and basic phase, the resin was rinsed using deionized water. There were three HCl and two NaOH rinsing steps. The last dilution before water rinsing was performed with HCl which left the resin to H^+-form. When the resin is in Na-form it gives Na ions when water is run through it making its pH basic. This is wanted to avoid and is the main reason why the resin is changed to H-form before ion exchange experiments.

Bed porosity of the column resin bed was determined by injecting a pulse of blue dextran. 0.5 mL of blue dextran was injected in 1 BV/h flow rate in 60 min cycle times while deionized water was injected into the column. The amount of blue dextran from the outlet of the column was measured by using UV/Vis and IR analysis and absorbance data were read from a computer. 6 cycles were injected to the column in order to minimize the error. A mass center was calculated from the peaks and an average value was taken from the results. Bed porosity was calculated by using Equations (14), (15), (16), and (17).

$$\varepsilon_{bed} = \frac{V_{Bed,void}}{V_{Bed}} \tag{14}$$

Where V_{Bed} Volume of the resin bed, dm^3

$V_{Bed,\ void}$ Volume of the void of the resin bed, dm^3

ε_{bed} Bed porosity, -

$$V_{Bed,void} = \Delta t \cdot v \tag{15}$$

Where Δt Time interval, s

$$\Delta t = \frac{t_{inj}}{2} - t_{pmc} - t_{tube\ void} \tag{16}$$

Where t_{inj} Injection time of the solution, s

t_{pmc} Time value of the peak mass center, s

$t_{tube\ void}$ Time delay caused the volume of tubes and measuring devices, s

$$t_{pmc} = \frac{t_{0.5n+1}\left(0.5 - \frac{\frac{1}{2}\sum_{n=1}^{N0.5n-1}(t_{n+1}-t_n)\cdot(y_n+y_{n+1})}{\frac{1}{2}\sum_{n=1}^{N}(t_{n+1}-t_n)\cdot(y_n+y_{n+1})}\right) + t_{0.5n-1}\left(\frac{\frac{1}{2}\sum_{n=1}^{N0.5n+1}(t_{n+1}-t_n)\cdot(y_n+y_{n+1})}{\frac{1}{2}\sum_{n=1}^{N}(t_{n+1}-t_n)\cdot(y_n+y_{n+1})} - 0.5\right)}{\left(\frac{\frac{1}{2}\sum_{n=1}^{N0.5n+1}(t_{n+1}-t_n)\cdot(y_n+y_{n+1})}{\frac{1}{2}\sum_{n=1}^{N}(t_{n+1}-t_n)\cdot(y_n+y_{n+1})} - 0.5\right) + \left(0.5 - \frac{\frac{1}{2}\sum_{n=1}^{N0.5n-1}(t_{n+1}-t_n)\cdot(y_n+y_{n+1})}{\frac{1}{2}\sum_{n=1}^{N}(t_{n+1}-t_n)\cdot(y_n+y_{n+1})}\right)} \tag{17}$$

Where t_n Time of point n, s

t_{n+1} Time of point n+1, s

$t_{0.5n-1}$ Time of the measured y-value at the last point before the accumulated surface area of absorbance is ≤ 0.5 of the total surface area, s

$t_{0.5n+1}$ Time of the measured y-value value at the first point after the accumulated surface area of absorbance is ≥ 0.5 of the total surface area, s

y_n Absorbance of point x, -

y_{n+1} Absorbance of point x+1, -

N The end of data set

	$N_{0.5n-1}$	The last point before the accumulated surface area of absorbance is ≤ 0.5 of the total surface area
	$N_{0.5n+1}$	The first point after the accumulated surface area of absorbance is ≥ 0.5 of the total surface area

Total porosity can be calculated by using equation (18).

$$\varepsilon_{tot} = \varepsilon_{resin}(1 - \varepsilon_{bed}) + \varepsilon_{bed} \quad (18)$$

Where	ε_{tot}	Total porosity, -
	ε_{resin}	Resin porosity, -

Two different packed columns were used, and bed porosities were for 1st packed column 0.4348 and for 2nd packed columns 0.3977. Bed porosity values were used in simulations. For total bed porosities values were for 1st packed column 0.7219 and for 2nd packed columns 0.7037. Total bed porosity values were used to calculate mass balances. Porosities are needed for mass balances in the simulation.

5.2. Single metal tests

LIB waste metal solutions were studied, which were prepared by dissolving metal sulfate salts into a 1 M H_2SO_4 solution. The pH adjustments were done using NaOH pellets while the solution was heated to 60 °C. Al, Co, Cu, Fe, Li, Mn, and Ni were studied at pH 0, 1, and 1.8. Loading, washing, and elution were performed in the column which was filled with TP260 resin. Washing was done by deionized water and elution for Co, Cu, Ni, Li, and Mn with a 2 M H_2SO_4 solution. For elution of Al and Fe, 0.4 M $(COOH)_2$ was used after which 2 M H_2SO_4 was used for regeneration. Collected samples were analyzed with ICP-MS. Studied LIB metal and Na concentrations were measured from each sample. For H^+ concentration, pH meter results and Equation (19) were used.

$$a_{H^+} = 10^{-pH} \quad (19)$$

Where a_{H+} Activity of proton, -

Measurements of pH were used mainly to follow the change in the proton activity. Online measurements of pH were performed at ~25 °C and the adjustment of the pH of the feeding solution was done at 60 °C. The proton activity is different in these temperatures, so the calculated activity alters what have initially measured.

All tests and test phases were performed at a temperature of 60 °C. Flowrate in loading and elution were 2 BV/h and in the washing, the flowrate was 6 BV/h. General test parameters are shown in Table (III) and all tests and varied parameters are shown in Table (IV) and Table (V).

Table III Test variables in single metal tests.

Variable	**Values of the variable**
Flow rate loading and elution, BV/h	2
Flow rate washing, BV/h	6
Initial loading sulfuric acid concentration, M	1
Elution sulfuric acid concentration, M	2
Elution oxalic acid concentration for Fe and Al, M	0.4
Temperature, °C	60

Table IV Tests and their parameters.

Test	**Metal**	**Adjusted pH at 60 °C**	**Concentration of metal, g/L**	**Concentration Na, g/L**
1	Co	0.04	15.56	0.00
2	Co	1	15.59	34.32

3	Co	1.8	16.78	59.74
4	Cu	0.01	2.07	0.00
5	Cu	1	2.19	34.38
6	Cu	1.8	2.08	40.83
7	Ni	0.02	2.19	0.00
8	Ni	1	2.18	31.07
9	Ni	1.8	2.07	40.08
10	Li	0.02	2.58	0.00
11	Li	1	2.73	31.18
12	Li	1.8	2.55	42.99
13	Mn	0	2.48	0.00
14	Mn	1	2.34	28.33
15	Mn	1.8	2.24	49.11
16	Al	0.01	1.90	0.00
17	Al	1	1.79	27.82
18	Al	1.8	1.87	41.52
19	Fe	-0.06	0.66	0.00
20	Fe	1	0.68	31.21
21	Fe	1.8	0.63	40.05
22	Ni	1	1.61	26.38
23	Na	1	0.00	27.27
24	Na	1.8	0.00	39.26
25	Ni	1.8	2.30	40.80
26	Li	1.8	2.52	38.98
27	Cu	1.8	1.90	39.87
28	Mn	1.8	2.16	37.49
29	Co	1.8	16.11	40.87

Table V Tests and their parameters.

Test	Column bed height, mm	Bed porosity	Adjusted flow rate, mL/min	Void volume of tubes, mL	Flow direction
1	145	0.4348	0.85	3.2	T-to-B
2	145	0.4348	0.85	3.2	T-to-B
3	140	0.4348	0.83	3.2	T-to-B
4	138	0.4348	0.82	3.2	T-to-B
5	138	0.4348	0.82	3.2	T-to-B
6	137	0.4348	0.81	3.2	T-to-B
7	137	0.4348	0.81	3.2	T-to-B
8	137	0.4348	0.81	3.2	T-to-B
9	137	0.4348	0.81	3.2	T-to-B
10	138	0.4348	0.81	3.2	T-to-B
11	138	0.4348	0.81	3.2	T-to-B
12	138	0.4348	0.81	3.2	T-to-B
13	137	0.4348	0.81	3.25	T-to-B
14	136	0.4348	0.8	3.25	T-to-B
15	136	0.4348	0.8	3.25	T-to-B
16	136	0.4348	0.8	3.25	T-to-B
17	134	0.4348	0.79	3.25	T-to-B
18	133	0.4348	0.78	3.25	T-to-B
19	132	0.4348	0.78	4.2	B-to-T
20	133	0.4348	0.78	4.2	B-to-T
21	133	0.4348	0.78	4.2	B-to-T
22	134	0.3977	0.79	4.2	B-to-T
23	134	0.3977	0.79	4.2	B-to-T
24	132	0.3977	0.78	4.2	B-to-T
25	134	0.3977	0.79	4.2	B-to-T
26	145	0.3977	0.85	4.2	B-to-T
27	144	0.3977	0.85	4.2	B-to-T
28	143	0.3977	0.84	4.2	B-to-T

29	142	0.3977	0.84	4.2	B-to-T

The resin bed shrank between the tests and the gap between the bed and a frit of the column was fixed with an adjustment screw. The flow rates were adjusted so that 2, and 6 BV/h were achieved in each test. Flow direction was originally from top to bottom (T-to-B) but was changed from bottom to top (B-to-T) for last tests (19–29). Tests (22–29) were done at pH 1.8 for Co, Cu, Fe, Li, Mn, Na, and Ni when flow direction was B-to-T. In the case of the Fe, the flow direction was (B-to-T also at pH 0 and 1. The flow direction of Al tests (16–18) were B-to-T. The void volume between the column and fraction collector increased between tests when pH measurements and systems tubing were changed.

5.3.1. Single metal tests results

The tests 18, 21 and 24–29 loading, washing, and elution were done at pH 1.8 with flow direction from bottom to top excluding Al where the flow direction was from top to bottom. Every metal was tested separately but presented in the same plot in Figure (7). Y-axis is presented as c/c_0 and measured feeding concentrations (c_0) are presented in Table (VI). The Na curve is from its own test where its loading, washing, and elution were studied separately.

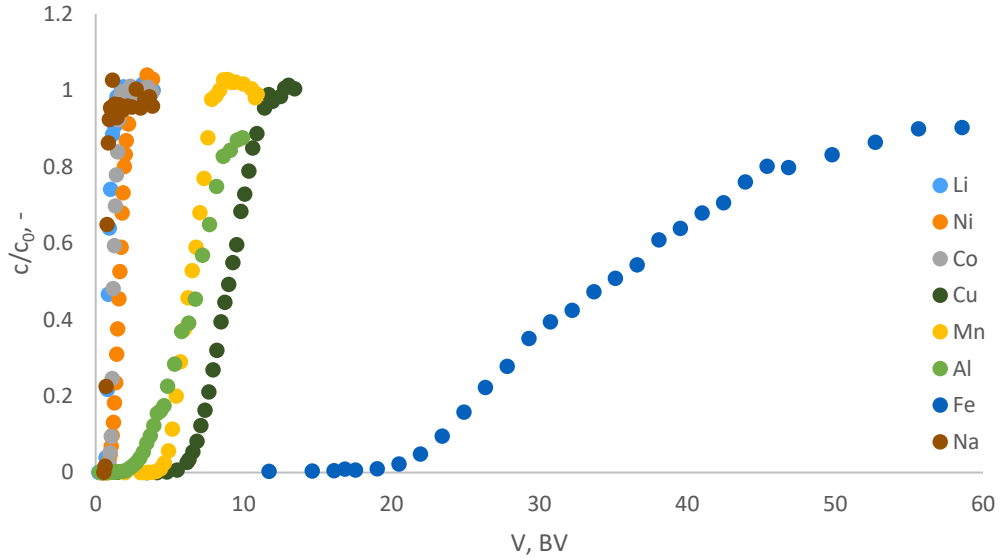

Figure 7 Loading of the resin for different metals at 60 °C. Flow rate was 2 BV/h. Flow direction was B-to-T expect for Al where flow direction was T-to-B. Each test was done separately.

Table VI Measured metal concentrations of feeding solutions at pH 1.8 from ICP-MS.

Metal	Al	Co	Cu	Fe	Li	Mn	Na	Ni
Concentration, g/L	1.9	16.1	1.9	0.6	2.5	2.2	39.3	2.3

The target metal ions Co, Li, and Ni breakthrough first with Na because they have lower sorption affinity than other metals. Fast breakthrough of Co, Li and Ni is desired because they are wanted to separate from other metals. Another group of metal ions, Al, Cu, and Mn breakthrough later between 3–7 bed volumes. These are the metals whose concentration in the product will limit the operation of the ion exchange column system. Fe is the last metal ion that breaks through the column.

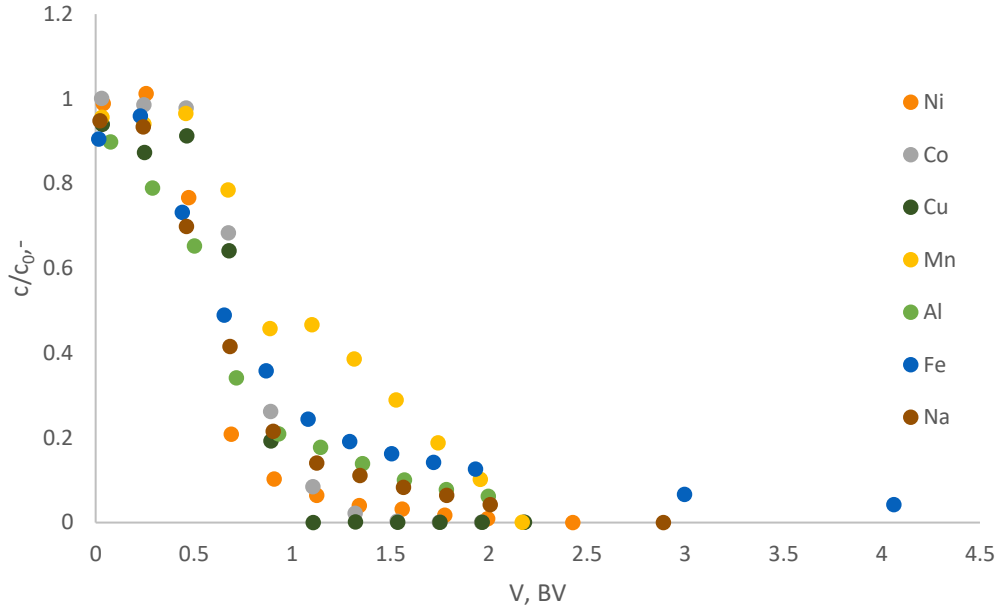

Figure 8 Washing of the resin for different metals at 60 °C. Flow rate 6 BV/h and flow direction was T-to-B. Each test was done separately.

Column washing is presented in Figure (8). There is not much difference between metals which was expected. Elution is presented in Figure (9). The elution of Co, Cu, Li, Mn, Ni, and Na were eluted with 2 M H_2SO_4. Al and Fe were eluted with 0.4 M $(COOH)_2$.

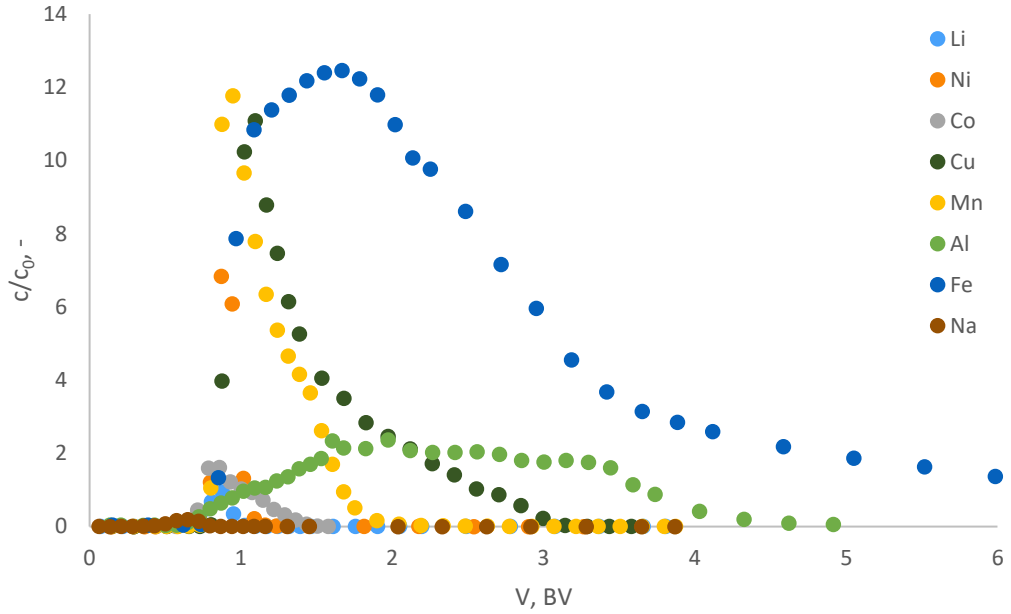

Figure 9 Elution of the resin for different metals at 60 °C. Flow rate was 2 BV/h. Flow direction was B-to-T expect for Al where flow direction was T-to-B. Each test was done separately.

The areas of the elution curves present the amount adsorbed by the resin in the column. Fe has the largest area, and its elution takes a long time. In total it takes about 30 BV. The full plot is in the Appendix I. These elution curves are in the same kind of groups as in loading. Al, Cu, and Mn have larger areas than Co, Li, Ni, and Na. These were measured separately so low-affinity metals will have smaller adsorption levels in a multi-metal system. Mass balances for loading and elution for tests presented above, were calculated by using Equations (20) and (21). Values of loaded and eluted amounts of metals per dry mass of the resin are presented in Table (VII).

$$q_{e,loa} = c_0\, v_{loa} \frac{z_c}{V_{BV}(1-\varepsilon_{tot,bed})\rho_{b,vet}(1-m_{vap})} \cdot \frac{1}{2}\sum_{n=1}^{N}(t_{n+1}-t_n)\cdot\left[\left(1-\frac{c_n}{c_0}\right)+\left(1-\frac{c_{n+1}}{c_0}\right)\right] - V_{void}c_o \frac{z_c}{V_{BV}(1-\varepsilon_{tot,bed})\rho_{b,vet}(1-m_{vap})} \quad (20)$$

Where,

c_n	Concentration at point n, mol/L
c_{n+1}	Concentration at point n+1, mol/L
m_{vap}	Mass of evaporated water per g of wet resin, g
$q_{e,loa}$	Loaded amount of metal per mass of the dry resin, meq/g
t_n	Time at point n, s
t_{n+1}	Time at point n+1, s
v_{loa}	Flow rate at loading, L/s
z_c	Charge of cation, -
$\rho_{b,vet}$	Density of wet resin, g/L

$$q_{e,elu} = c_0\, v_{elu} \frac{z_c}{V_{BV}(1-\varepsilon_{tot,bed})\rho_{b,vet}(1-m_{vap})} \cdot \frac{1}{2}\sum_{n=1}^{N}(t_{n+1}-t_n)\cdot\left[\left(\frac{c_n}{c_0}\right)+\left(\frac{c_{n+1}}{c_0}\right)\right] \quad (21)$$

Where,

$q_{e,elu}$	Eluted amount of metal per mass of the dry resin, meq/g
v_{elu}	Flow velocity of elution, L/s

Table VII Loaded and eluted amounts of metal per mass of the resin. Ion exchange tests (18, 21 and 24–29) were performed at pH 1.8, when flow direction was from bottom to top expect in Al tests where flow direction was top to bottom.

Metal	**Concentration (feed), g/L**	**q(loading), meq/g**	**q(elution), meq/g**
Li	2.5	0.4956	0.43635
Na	39.3	0.67803	0.50691
Co	16.1	1.8141	2.0847
Cu	1.9	3.0338	2.7969
Mn	2.2	2.7444	2.5454
Ni	2.3	0.51402	0.61265
Al	1.9	8.0818	7.3302
Fe	0.6	8.2837	8.2985

As expected, Al and Fe have the largest amount of metals sorped to the resin. Co, Cu, and Mn had similar q values in Table (VII). However, Co breakthrough occurs earlier in column experiments which is similar to Li and Ni with significantly lower values. This difference is most like due to the much higher Co concentration in the feeding solution. Similarities can be seen when comparing Table (VII) values to plots in Figures (7) and (9). The Cu and Mn have stronger affinity with the resin than Co but much lower than Al and Fe. Na has a larger value than expected since its interaction with the resin has been considered insignificant. These q values are probably because Na had a very high concentration in the loading solution. Na was the fastest metal to breakthrough and had the smallest area in the elution curves but had the largest concentration in the tests. Because of the large difference between concentrations these values are not directly comparable with each other. The lowest values were with Li and Ni which were also the fastest metals to breakthrough. This is a good thing because the binding of these metals is not desired.

5.3.2. Effect of pH

Ion exchange is a reversible reaction and the pH have a great effect on the binding of other metals. When the pH is low there is more active H^+ that competes the binding sites of the resin with other ions. For example, in the case of Mn and Cu where the interaction between metal ion and resin is quite strong, the pH has a large effect on the breakthrough curve, indicating a large capacity for the metal in the higher pH. The breakthrough curves are in Figures (10) and (11).

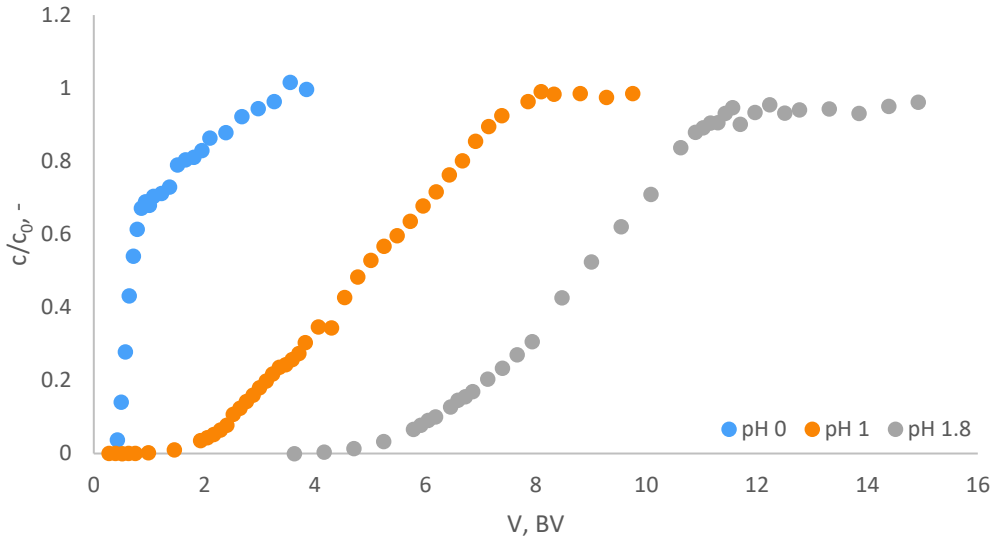

Figure 10 Breakthrough curves of Cu at different pH at 60°C when flow rate was 2 BV/h and flow direction was from bottom to top. The feed concentrations for Cu were for blue: 2.07 g/L, for orange: 2.19 g/L and for grey: 2.08 g/L.

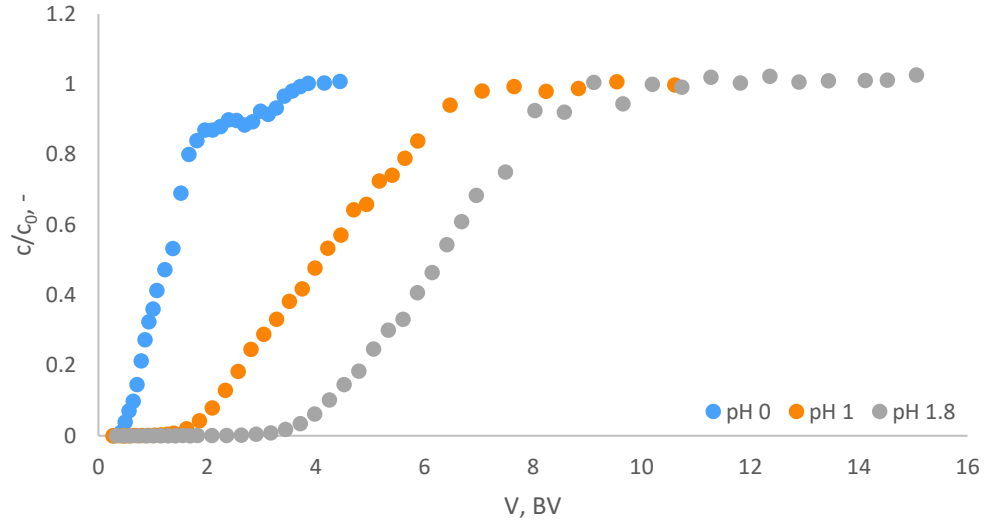

Figure 11 Breakthrough curves of Mn at different pH at 60°C when flow rate was 2 BV/h and flow direction was from bottom to top. The feed concentrations for Mn were for blue: 2.48 g/L, for orange: 2.34 g/L and for grey: 2.24 g/L.

Both Cu and Mn were as divalent metal ions in the solution. The observation is that the ion exchange is more effective when the pH is higher, and the activity of protons is smaller. Increasing the pH could be a way to increase the ion exchange of these metals with the resin. However, when considering a multi-metal solution, where Fe is present, Fe would start to precipitate when the pH is increased over 1.8 (Kaukinen, 2019).

For Fe, the increase of pH did not affect the ion exchange very much. Fe breakthrough curves are presented in Figure (12). Fe has a very strong interaction with the resin. It is stronger than H^+ and elution with 2 M H_2SO_4 is not possible. This is why the pH does not affect the ion exchange so much. An exception is at pH 1 where the interaction is smaller. The reason behind this is not clear and can be caused by high Na concentration in the feeding solution. Because NaOH is used to adjust the pH the Na could cause this difference. Another thing that could cause this difference is incomplete resin regeneration. The same resin was used for all Al and Fe tests.

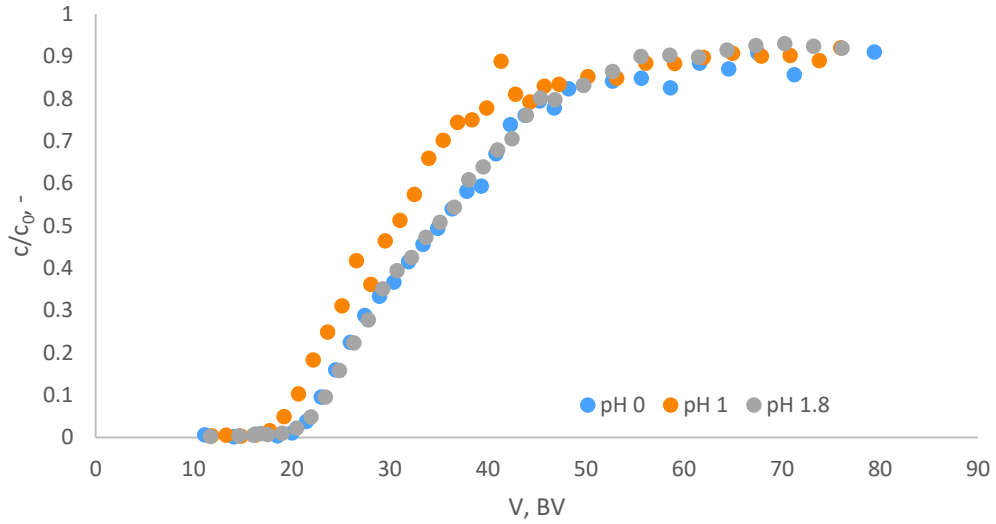

Figure 12 Breakthrough curves of Fe at different pH at 60°C when flow rate was 2 BV/h and flow direction was from bottom to top. The feed concentrations for Fe were for blue: 0.66 g/L, for orange: 0.68 g/L and for grey: 0.63 g/L.

Similar behavior was observed also in Al tests and all Al breakthrough curves are in Figure (13). Here the interaction is smaller than with Fe and the interaction changes more between different pH values. Al had the smallest capacity at pH 1. This was not studied further in this study.

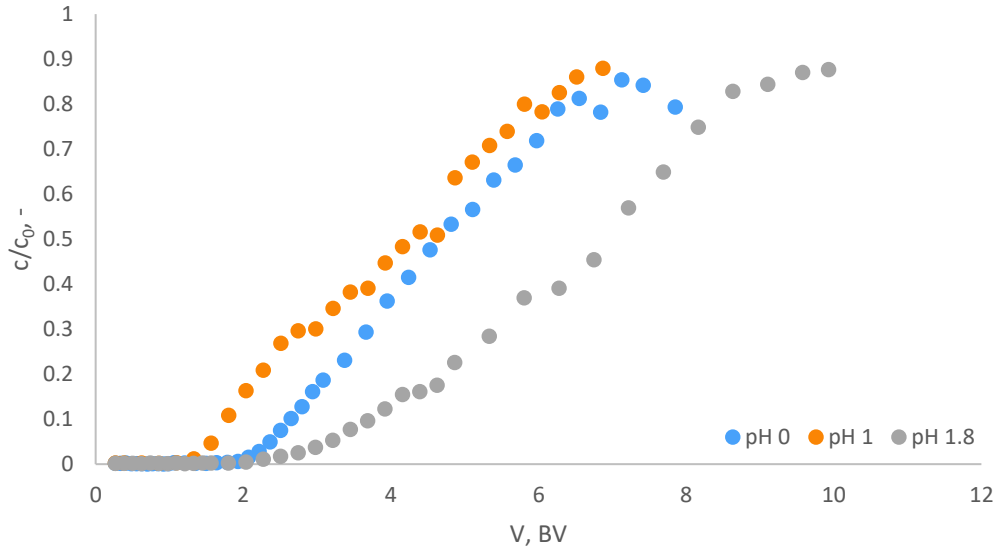

Figure 13 Breakthrough curves of Al at different pH at 60°C when flow rate was 2 BV/h and flow direction was from top to bottom. The feed concentrations for Al were for blue: 1.9 g/L, for orange: 1.79 g/L and for grey: 1.87 g/L.

5.3.3. Flow direction

The flow direction can have effect on the ion exchange experiments. Fluid dynamics affect how the concentration profiles behave in the column. Because channeling and viscous fingering can occur inside the column the concentration profile will be wider when feeding the column from the top. There is water inside the column in its pre-state. When acidic, more dense liquid, enters the column it can cause for example, the viscous fingering phenomena. (Homsy, 1987) Figure (14) shows Ni tests where the flow direction has been changed from top to bottom to bottom to top. Test were done at pH 1 and 1.8 with both flow directions.

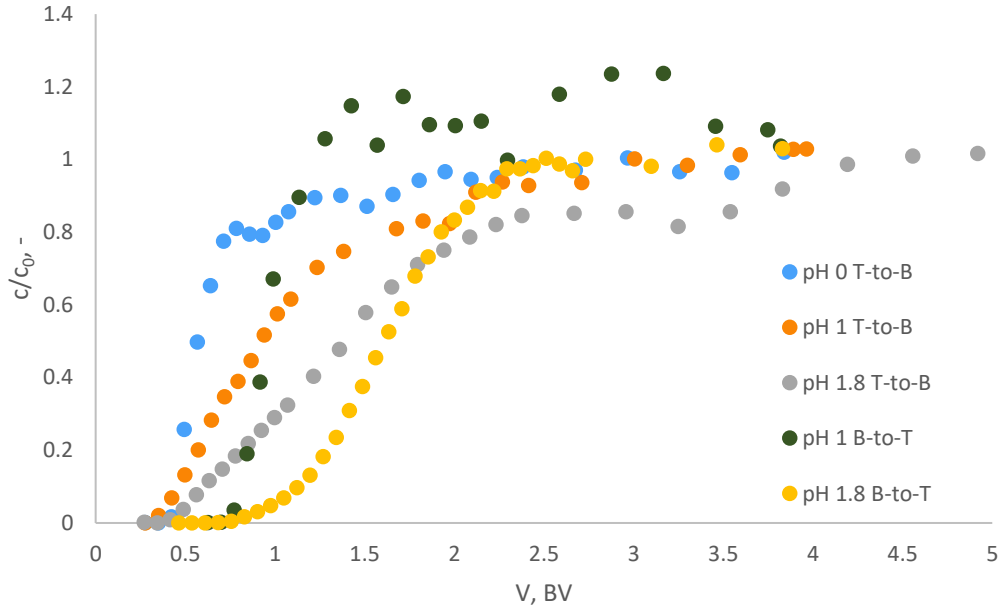

Figure 14 Ni breakthrough at pH 0, 1 and 1.8 in two different flow directions at 60 °C when flow rate was 2 BV/h. Ni feed concentrations were, for blue: 2.19 g/L, for orange: 2.18 g/L, for grey: 2.07 g/L, for green: 1.61 g/L and for yellow: 2.30 g/L.

When feeding of the column is done from the bottom, the breakthrough starts later, and the slope of the curve is steeper. This is significant when trying to estimate kinetic values by visually fitting simulated and measured breakthrough curves. The increase of the Ni concentration slowed down significantly at the end when the column was fed from the top. The mass transfer inside to column can cause this. This led to the fact that the complete breakthrough of loading took more time in the case where the feeding was done from the top, this can be seen in the pH 1.8 T-to-B curve. There is a possibility that in case of the 1.8 T-to-B tests the resin bed was not fully saturated. The difference of saturated resin bed between these two pH 1.8 tests, was about 2 bed volumes of feed solution. When the curves are steeper the resin bed utilization is higher, and the process would be more efficient.

To avoid the viscous fingering the feeding direction should be changed when the feed is changed. When metal ions had a strong interaction with the resin the effect of viscous fingering to the breakthrough curve disappears almost completely because the metal concentration profile did not go as fast through the column and

metal ions interacted more with the resin. The Cu breakthrough curves at pH 1.8 when the feeding was done from different directions is presented in Figure (15).

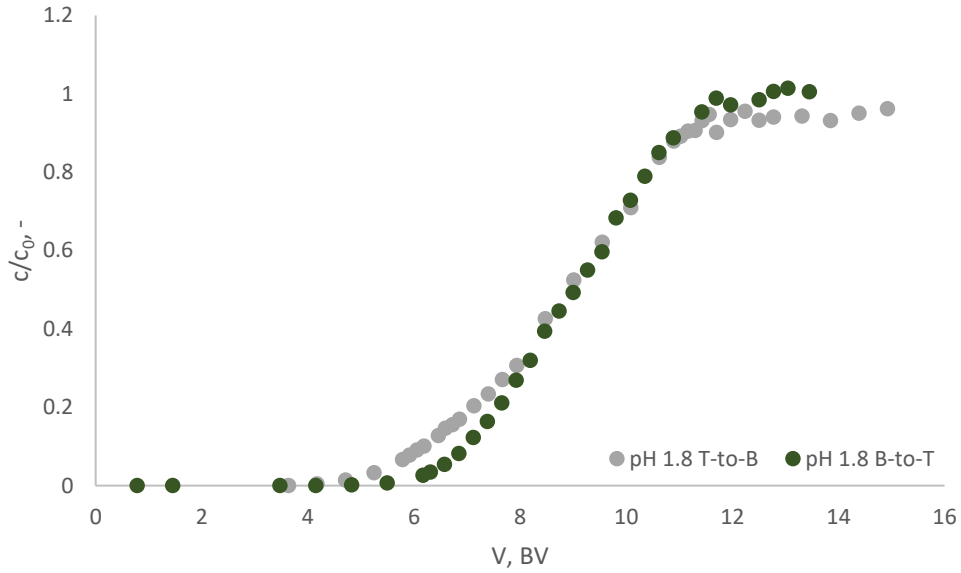

Figure 15 Cu breakthrough in pH 1.8 in two different feeding direction at 60 °C when flow rate was 2 BV/h. Feed concentrations for Cu were for grey: 2.08 g/L and for green: 1.90 g/L.

There is still a small difference between the Cu breakthrough curves, but this is not significant and will not affect the mathematical parameters or the column operation as significantly as with metals which have lesser interaction with the resin. The difference can be also caused by the inaccuracy in dilutions for ICP-MS on analysis or from the analysis itself.

5.3.4. Precipitations in tests

Elution of the Al and Fe was performed by using $(COOH)_2$. $(COOH)_2$ have been tested to be suitable for removing Al and Fe from the resin (Kaukinen, 2019). However, using $(COOH)_2$ has its own problems and, in the experiments, precipitations were observed. After the Al tests, precipitation was formed inside the

column and the precipitate did not dissolve into 2 M H_2SO_4. The precipitate inside the column is presented in Figure (16).

Figure 16 Precipitation inside ion exchange column after elution of Al.

This precipitate could be metal complexes. This precipitate was not studied further. In the case of Fe, precipitates formed into collected test tubes a couple of days after the column run. The samples were already measured with ICP-MS before any visible precipitation had formed. The precipitation formed in the sample tubes that contained the highest amount of Fe. In Figure (17) is the Fe precipitation in the test tubes.

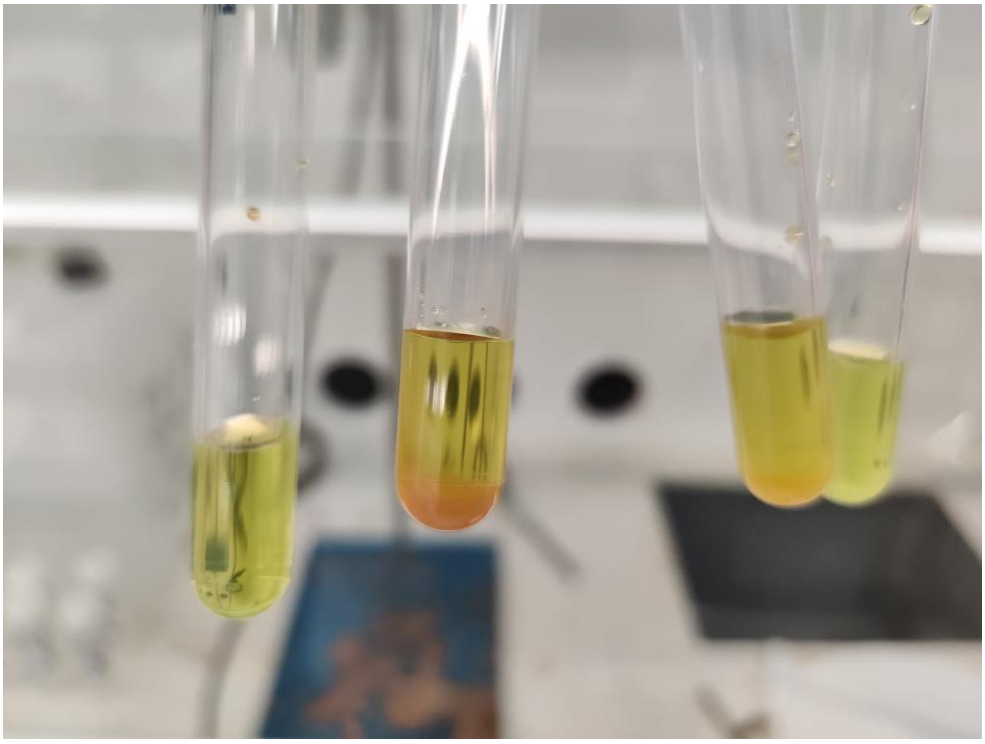

Figure 17 Precipitation in collected samples from Fe test from test 21.

The precipitation was not studied because it was not in the scope of this study. But according to the literature, it could be $Fe(OH)_3$ depending on the color of the precipitate. Also, when eluting with $(COOH)_2$ the pH of the system increases around 6 what makes the precipitation of Fe possible. (Niu *et al.*, 2021) The amount of precipitate increased when the sample was allowed to stand longer.

After the tests the resin particles were studied by taking SEM pictures of fresh resin and resin after Al and Fe tests. SEM pictures are in Figure (18).

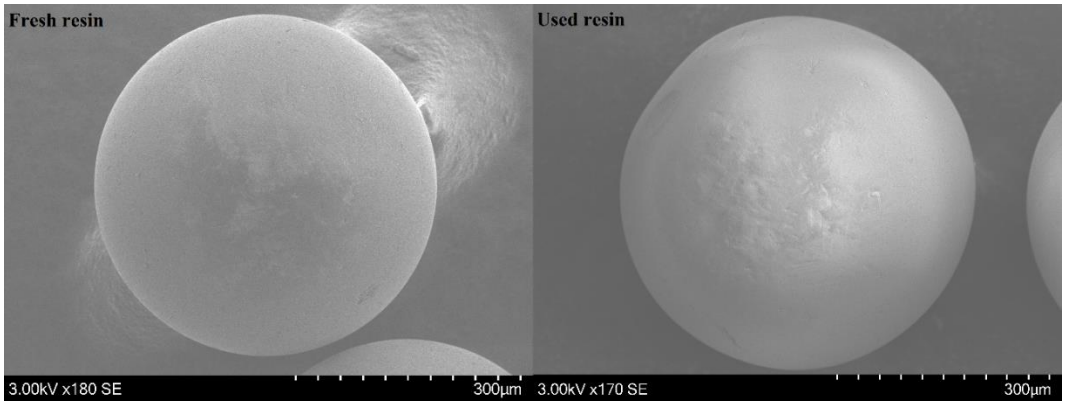

Figure 18 SEM pictures of Lewatit TP 260 resin, on the left is fresh resin and on the right is used resin.

The precipitation seemed to be only in the liquid part but not on top of the resin. In this study, the effect of these precipitations was assumed to be negligible. Especially for the loading which was the main focus of this study. However, Al can cause problems with the operation of the columns in the industrial case if $(COOH)_2$ is used. The precipitate which was observed in the Al test can pile up into tubes/pipes, resin bed, and resin pores clogging them during the cycles. Also, it will take up space in the column and affect the flow inside the column. Other eluents should be studied to replace $(COOH)_2$. Considering the Fe precipitation, the problem is not as crucial because it forms much slower outside the column and when using ion exchange for separating metals from multi-metal solution, Fe will not build up so much onto the resin.

6. Modelling of ion exchange of the LIB metals

Affinity constant parameters of NICA-IX equilibrium model and pore diffusion coefficients were fitted visually against measured data from breakthrough experiments. Loading of the ion exchange column was studied especially. NICA-IX was selected because it is capable to simulate multi-metal solutions and non-ideal competitive ion exchange. (Laatikainen, 2014) It has also been used previously in studies giving promising results. Tests used for fitting were performed at pH 1.8 at 60 °C when the feeding was done from bottom to top to reduce

disturbance of the breakthrough curve caused by fluid dynamics. Exception with Al where the flow direction was from top to bottom. The test was not redone for simulations because the flow direction did not have a large effect on the breakthrough curve when metal had a strong interaction with the resin. This was discussed in chapter 5.3.3. Fitted parameters were affinity coefficient and pore diffusion coefficient.

6.1. Simulation tool parameters

To make the studied parameters for metals comparable among themselves, other parameters H, SO_4, and Na parameters were fixed to be the same in every simulation. Used parameters and their values in the ResMod are shown in Table (VIII).

Table VIII Parameters used in ResMod when simulating loading steps.

Parameter	**Unit**	**Value**
Resin max capacity	mol/kg	2.3
Resin charge (Al and Fe)	-	-2
Resin charge (Co, Cu, Li, Mn, Ni)	-	-1
Number of mixing stages	pcs	50
Particle diameter	mm	0.55
Bed porosity (Al and Fe)	-	0.4348
Bed porosity (Co, Cu, Li, Mn, Ni)	-	0.3977
Time step	s	1
H affinity constant, log(K)	-	0
H pore diffusion coefficient	m^2/s	$1 \cdot 10^{-9}$
Na affinity constant, log(K)	-	-1.8
Na pore diffusion coefficient	m^2/s	$1 \cdot 10^{-12}$
SO4 affinity constant, log(K)	-	-20
SO4 pore diffusion coefficient	m^2/s	$4 \cdot 10^{-14}$

The ion-specific non-ideality constant parameters in NICA-IX are kept as 1 for every component. The affinity constant of H is kept as reference value which the values of other components are compared. This is made because it makes the case simpler and the finding of suitable values for affinity constant and pore diffusion coefficient doable without using a solver. The resin properties at ResMod are presented in Figure (19). Because of assumed electroneutrality in the system, every site of the resin is always bound to a metal ion or H ion.

Figure 19 Resin properties set in ResMod.

These values were used for all other metals excluding Al and Fe. For Al and Fe, the charge of the functional group was decreased to -2. This is because fitting this breakthrough curve, the breakpoint, or shape of the curve, was not able to fit with functional group charge -1. Because of different charges, all the results cannot be used at the same time with other metals without changing the affinity constants and pore diffusion coefficients. The difference is probably because of the nature of Al^{3+} and Fe^{3+} and their stronger affinity towards the ion exchange resin. Al and Fe can probably interact with amino group of the resins functional group. If this is the case, it could explain why value -1 was not enough. The strong affinity could also explain

why 2 M H_2SO_4 cannot remove these metals from the resin. However, this was not explored any further in this study and is one important thing to study in the future.

6.2. Simulation results

After column experiments, all metals were simulated utilizing breakthrough data from the tests. The chosen tests were at pH 1.8 when flow direction was from bottom to top. In this way, the breakthrough curves were smoothest without many disturbances. In each simulation one battery metal ion, Na ion, H ion, and SO_4 ion were simulated. The results of the simulated breakthrough of single battery metal tests are displayed in Figures (20), (21), (22), (23), (24), (25), and (26).

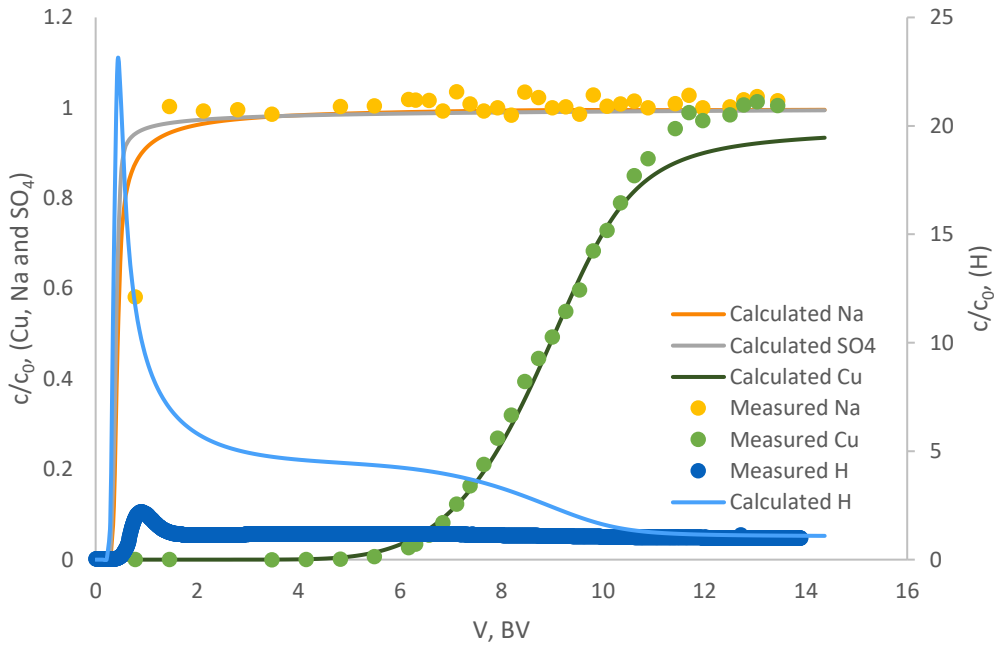

Figure 20 Simulated and measured breakthrough curves of Cu test at 60 °C. The feed concentration of Cu was 1.89 g/L and flow rate was 2 BV/h.

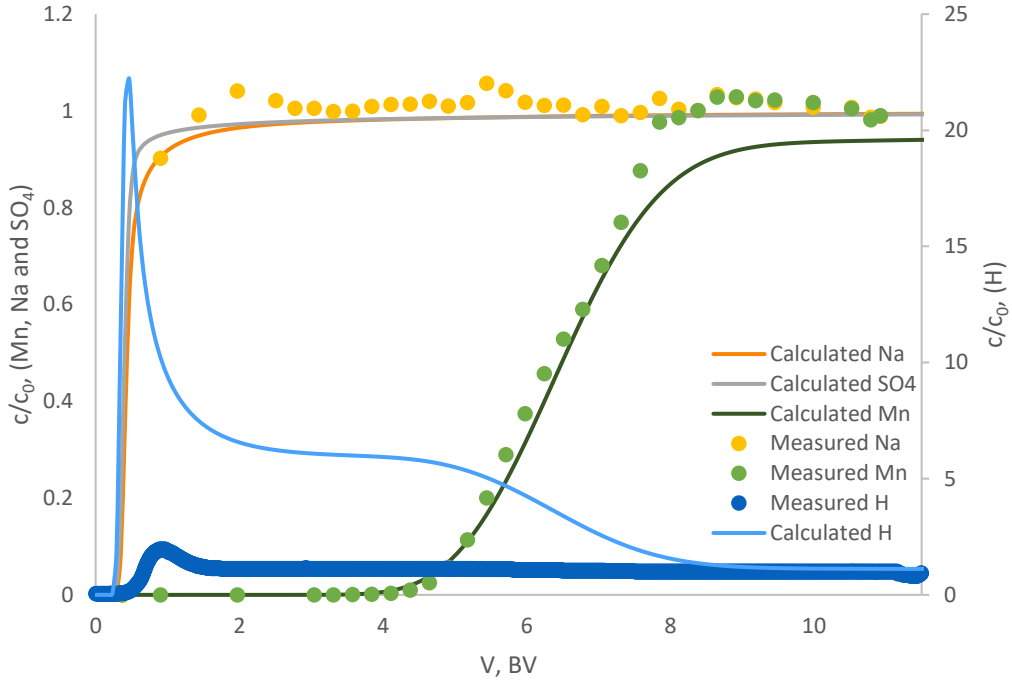

Figure 21 Simulated and measured breakthrough curves of Mn test at 60 °C. The feed concentration of Mn was 2.16 g/L and flow rate was 2 BV/h.

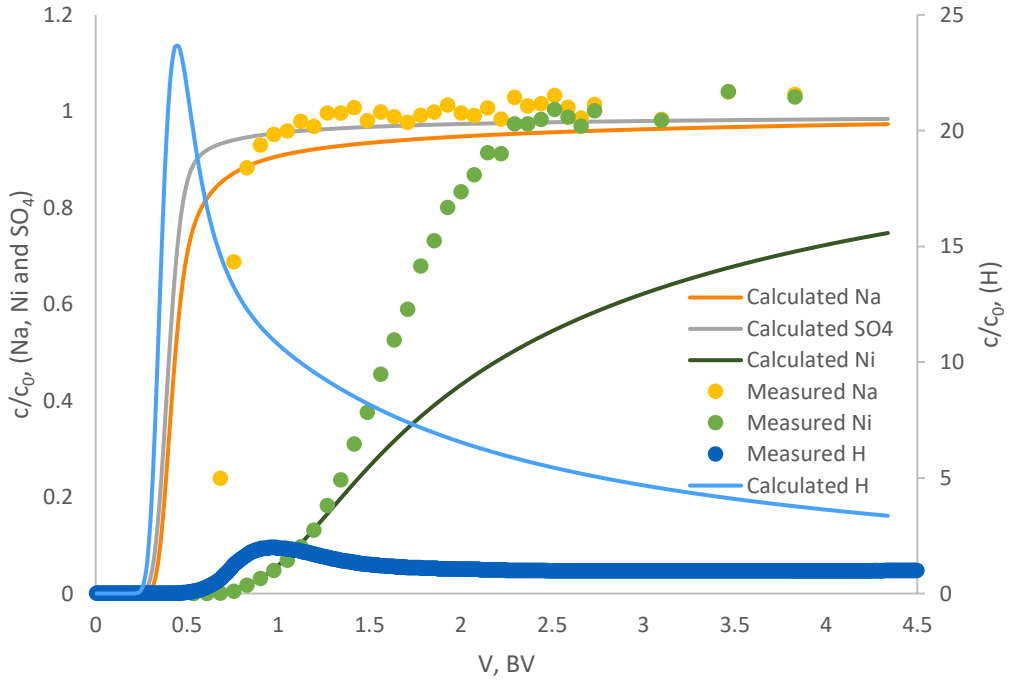

Figure 22 Simulated and measured breakthrough curves of Ni test at 60 °C. The feed concentration of Ni was 2.30 g/L and flow rate was 2 BV/h.

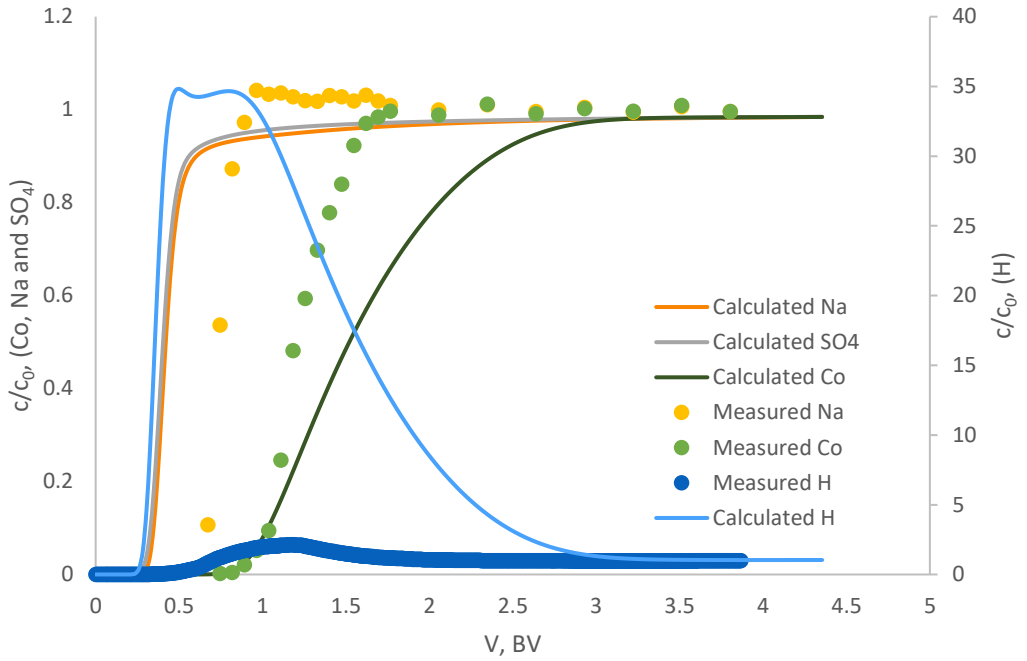

Figure 23 Simulated and measured breakthrough curves of Co test at 60 °C. The feed concentration of Co was 16.11 g/L and flow rate was 2 BV/h.

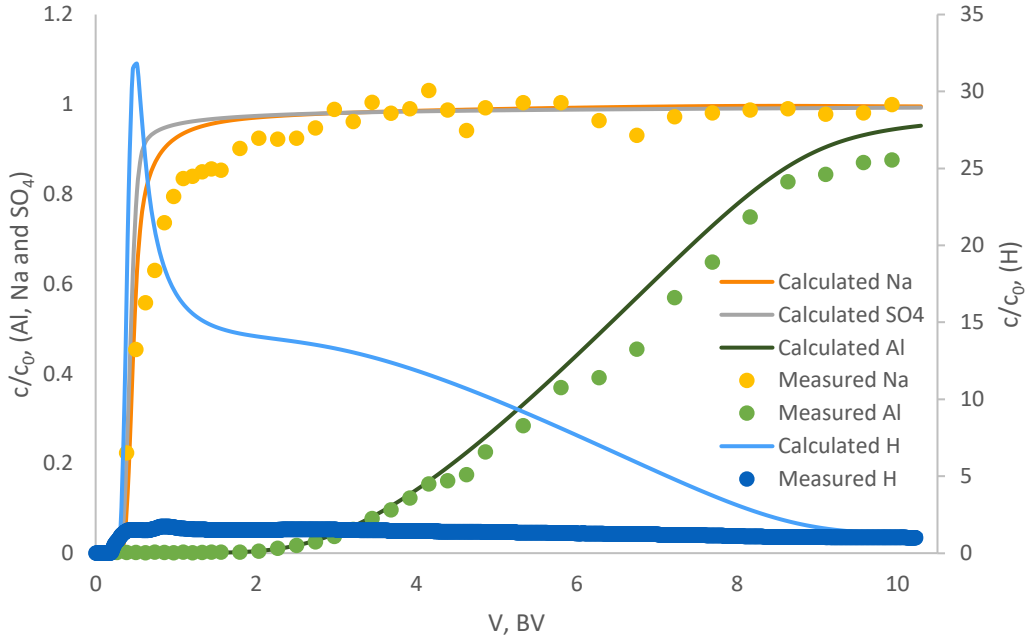

Figure 24 Simulated and measured breakthrough curves of Al test at 60 °C. The feed concentration of Al was 1.87 g/L and flow rate was 2 BV/h.

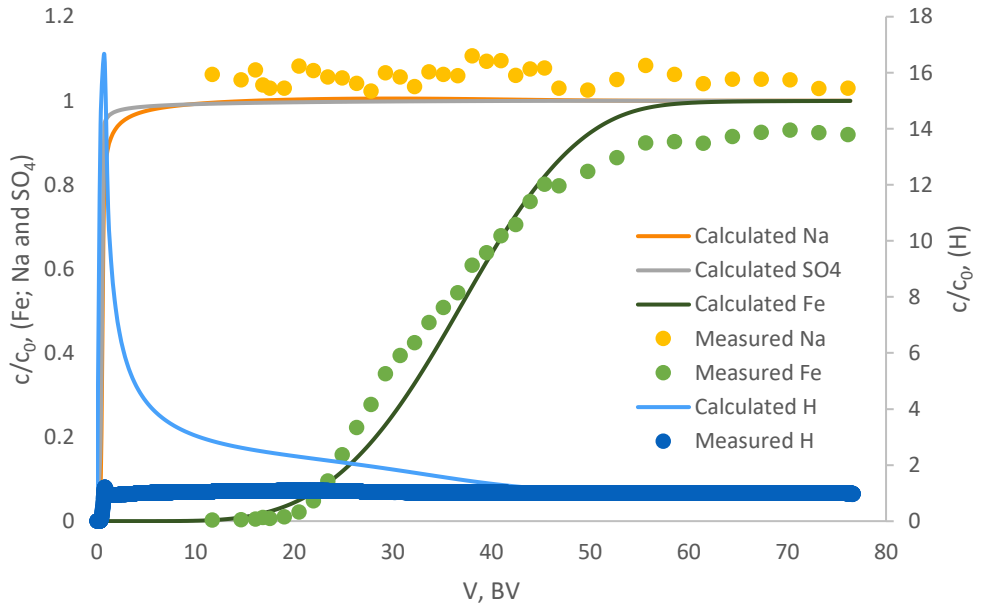

Figure 25 Simulated and measured breakthrough curves of Fe test at 60 °C. The feed concentration of Fe was 0.63 g/L and flow rate was 2 BV/h.

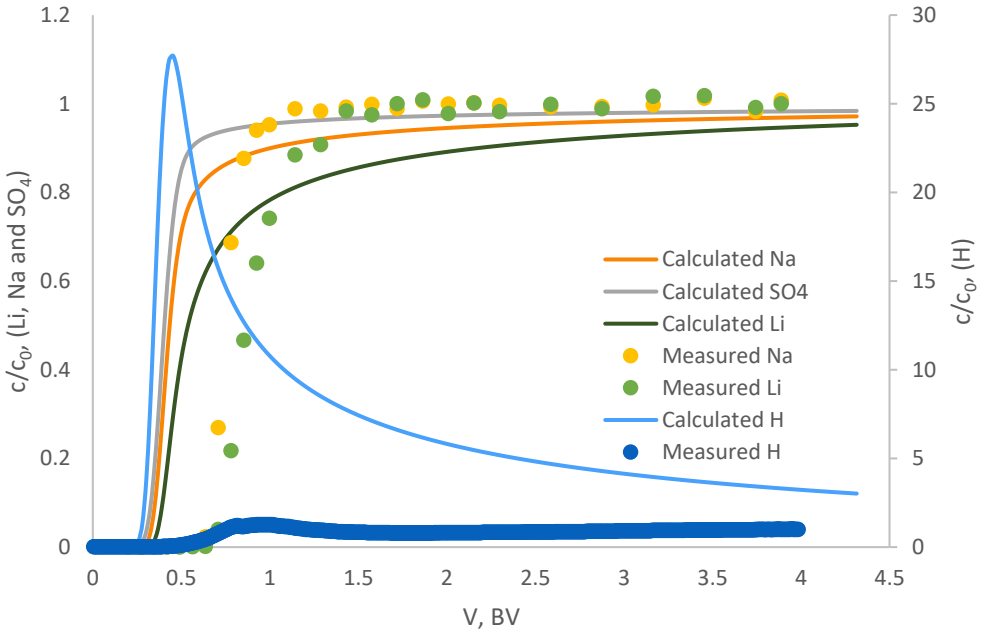

Figure 26 Simulated and measured breakthrough curves of Li test at 60 °C. The feed concentration of Li was 2.52 g/L and flow rate was 2 BV/h.

Great fits were achieved with Cu, Mn, Fe, and Al. The fit between the simulated curve and measured values is quite good. Breakthrough is at the same point and the slope is mostly the same but, in the end, the simulated curve does not reach c/c_0 value 1 at same time than the measured values. When simulating longer the simulated values reached the value 1. Na measured and simulated values were quite the same and because of the long run, the breakthrough point of Na is not visible in most plots because it breaks through so early. This is because analyzed fractions of the loading were taken later because LIB metals took more time to break through the column. For H ion concentration the simulated peak is approximately at the same point as the measured peak. However, the scale of the H ion is completely different and far from each other. Except in the Cu and Ni tests where the H concentrations were close.

The fits of Co, Li and Ni were lacking. The breakthrough points of Co and Ni and beginning of the curve are good. However, then the deviation between simulated curve and measured curve starts to grow when moving along the X-axis. At the end of the tests the simulated, and measured values were quite apart from each other. Li was very fast and came through from the columns just barely later than Na. Accurate modeling of Li was not able be done and simulated breakthrough point occurred much earlier than in experimental case. This can be caused by a lack of simulated fluid dynamics in the system. Also, when the interaction between the resin and metal-ion is low, the binding of the Na ions will increase. The simulated and measured Na breakthroughs in this Li case were also different from each other. The simulated breakthrough occurs much earlier than the measured curve. Na is most likely underrepresented in this case and in reality interreacts much more with the resin. Na could be studied more and fit own affinity constant for it. When Na has accurate affinity constant the modeling of low-affinity LIB metals could be done more accurately. The simulated Li was fitted to represent somewhat the same kind of breakthrough curve as in measured Na and Li values.

For Fe and Al, the capacity of the resin was different. The capacity was increased because fitting the simulated loadings curves to measured ones were not possible with lower capacity. The capacity of resin is constant, but in this case of Al and Fe have a strong affinity and they can probably bind to both phosphonium groups and

even with the amino group. With the higher capacity, the simulation was able to make a good representation of the experimental data. However, in both cases simulated and measured H^+ concentrations were far away from each other. For Na, the curves fit but there is no measured data at the beginning. The first analyzed data points start around 10 BV when the Na is already leveled. However, Na comes through so fast that it is hard to read from a long tests like Al and Fe. All fitted model parameters for each metal are given in Table (IX).

Table IX Pore diffusion coefficients and affinity coefficients from fitted simulated breakthrough curves.

Metal	**Ion charge**	**Pore diffusion coefficient, D_p, m^2/s**	**Affinity constants, log(K), -**
Li	1	$8.5 \cdot 10^{-12}$	-1.4
Co	2	$6.0 \cdot 10_{-10}$	0.07
Cu	2	$7.0 \cdot 10^{-11}$	0.43
Mn	2	$9.5 \cdot 10^{-10}$	0.24
Ni	2	$1.0 \cdot 10^{-10}$	-0.4
Al	3	$6.5 \cdot 10^{-12}$	0.63
Fe	3	$8.5 \cdot 10^{-12}$	1.15

Like in Figure (7), the affinity constant values of the metals increase in order of breakthrough points similarly as in the plot. Fe and Al have the largest affinity constant. Then comes Cu and Mn with a bit lower value. And the lowest, which also breakthrough first Li, Ni, and Co. The pore diffusion coefficient values, affect how the ions travel in the system and do not directly affect the NICA-IX model itself. However, it affects the whole system and in that way the breakthrough curve of the loading profile. With right pore diffusion coefficient value, a better fit and more accurate affinity constants can be fitted. Pore diffusion coefficient also had a quite large effect when simulating the system and adjusting them made the fit better in most cases. In the case where the fits were not so good, Ni, Co and Li, the pore diffusion coefficient does not represent the reality so well. In these cases, the affinity constant plays a bigger role.

The affinity constant and pore diffusion coefficients were determined using the experimental data of the loading step. These values were tried also in the simulation of the elution phase. In those cases, the values from loading simulations did not fit the elution curve at all. Because a large difference was observed between experimental data and simulated elution curves it can be concluded that simulating the elution requires its own affinity constants. It would need separate simulations to determine those values for elution. Studying elution was not continued further in this thesis. Simulation of the Cu elution is shown in Figure (27).

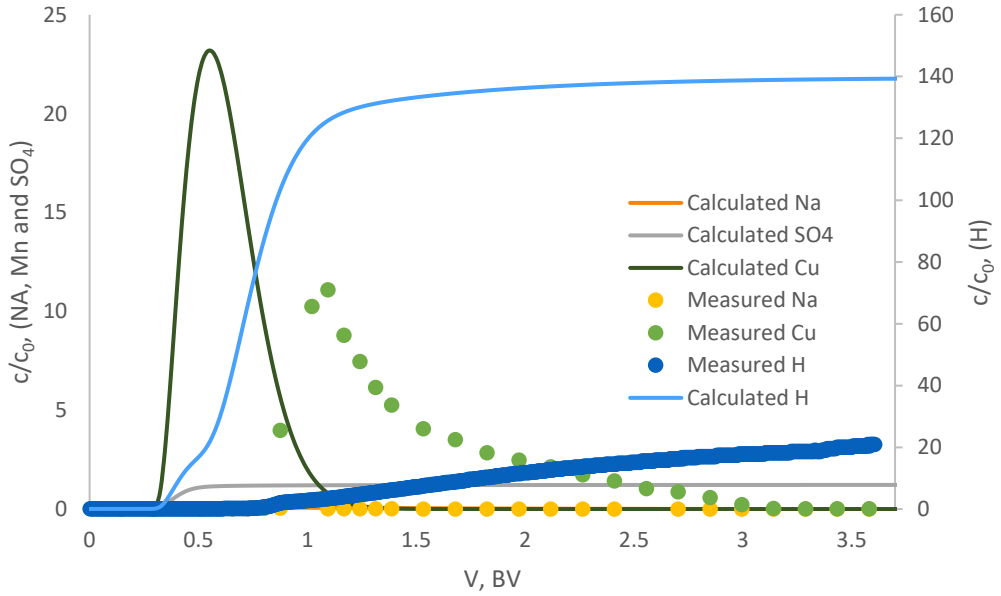

Figure 27 Simulated and measured elution curves of Cu at 60 °C. Flow direction was B-to-T and flow rate was 2 BV/h. Cu feeding concentration was 1.89 g/L.

The fit of simulated and measured elution curves was not good when used affinity constants and pore diffusion coefficients were the same as in the loading simulation. The simulated elution curve came out of the column much earlier than the experimental data. For elutions 2 M H_2SO_4 was used which will favor protons on the competition of resin sites and sorped metal ions detach from the resin.

Washing of the metals was also tried to be simulated and the washing of the Cu is shown in Figure (28). Used affinity constants and pore diffusion coefficients were the same as in the loading simulations of the Cu.

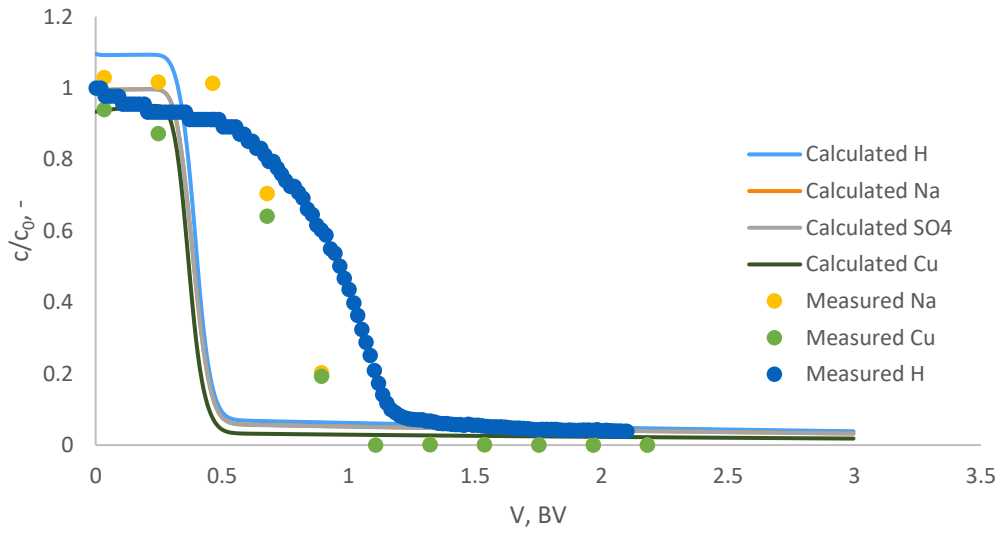

Figure 28 Simulated and measured washing curves of Cu at 60 °C. Flow direction was T-to-B and flow rate was 6 BV/h. Cu feeding concentration was 1.89 g/L.

As in the elution, the modeled curve behaves faster than the experimental data. In this case, there is only water pumped into the column. In the simulation, the concentration of the components dropped close to 0 already in a bed volume of 0.5. With experiments, this took over 1 bed volume. When water is injected into the column there is no major ion exchange phenomenon. In this case, the difference can be caused by fluid dynamics in the system. Another notable thing is the time needed to perform the simulated washing steps which were often much longer than simulations of loading and elution. For example, while the loading simulation took 50 minutes, the washing simulation could take 9 hours. Also, a very small timestep was needed in order to avoid errors during the modeling. Difficulties can be numerical when the ResMod is calculating very small values. However, this was not investigated further in this thesis.

There is a need to make the simulation with the same resin properties. To make it possible to make representative multi-metal simulation, affinity constant values of single metal experiments in needed to study under the same conditions. It was tried in this work, but it was not achieved to perform such simulations. More experiments with different flow rates and concentrations are needed to determine more accurate affinity constant values for the metals. Table (IX) values work in this studied case, but the case might be different when using these on another test where these same metals are studied or modeled. The NICA-IX model is workable for this kind of system. However, modeling of Al, Fe, and elution needs still work. Al and Fe needed different resin properties and that is why their results cannot directly use with other metals. Adding modeling of fluid dynamics for accurate low affinity metal simulations could be beneficial. Next step in the simulations is to use these values to simulate a multi-metal system and making it accurate. This is needed because planning simulated moving bed (SMB) and industrial-scale processes is simpler when the whole system can be simulated.

7. Conclusion

Recycling batteries is crucial to maintain the sufficiency of metallic raw materials is wanted to maintain. Especially recycling of Li, Co, and Ni is important. The current consumption of metals is high and virgin deposits cannot meet the demand in the future. Many of the metals and their ions are hazardous. So, recycling spent batteries will decrease the risk of them causing harm to the environment. Also, the ethic of the production of some metals can be questionable. This is especially the case when considering metals that are used in batteries. The usage of batteries in different applications have been drastically increased during the past years. At the same time recycling of batteries is still at quite a small scale. Increasing the recycling of batteries will also improve their sustainability.

Ion exchange processes are a good way to separate different compounds like metals from each other. Batteries include many different metals and not all of them are

valuable enough to be recycled back to pure metal or different compounds. That is why separating valuable metals from lesser metals is necessary when considering the profitability of the recycling process.

Breakthrough experiments for one LIB waste metal at a time were performed with Lewatit TP260 resin with aminomethylphosphonic acid functional group. Lewatit TP260 can separate Co, Li, and Ni from Al, Cu, Fe, and Mn. The concentrations of the metals in the solutions were chosen to represent the concentrations of the leachate obtained from LIB waste. Varied experimental conditions were pH and flow direction. Collected samples from loading, washing, and elution were analyzed with ICP-MS. These results were used in modeling the ion exchange with the NICA-IX model. Affinity constants and pore diffusion coefficients were determined by fitting measured and simulated breakthrough curves visually.

In small-scale ion exchange systems flow direction can play a big role when the breakthrough is fast. In those cases, the fluid dynamics will affect the concentration profile drastically and viscous fingering can occur. The affinity of the resin towards the metal ions increased when the pH was increased. The estimated affinity constant and pore diffusion coefficients were able to simulate the breakthrough curves accurately and gave promising results. With accurate values more complex simulations of ion exchange of battery metals like simulated moving bed configuration could be done. But before that modeling of the elution step and modeling of the multi-metal ion exchange, are needed.

References

Aalto, M. (2021) *Modelling of Ion exchange process in purification of lithium-ion battery leachate.*

Abdel-Monem, M., Hegazy, O., Omar, N., Trad, K., Van den Bossche, P. and Van Mierlo, J. (2017) *Lithium-ion batteries: Comprehensive technical analysis of second-life batteries for smart grid applications.* pp. P.1.

A Vision for a Sustainable Battery Value Chain in 2030: Unlocking the Full Potential to Power Sustainable Development and Climate Change Mitigation. (2019) World Economin Forum. Available at: https://www.weforum.org/reports/a-vision-for-a-sustainable-battery-value-chain-in-2030/ (Accessed: 31.8.2022).

Badawy, S.M., Nayl, A.A., El Khashab, R.A. and El-Khateeb, M.A. (2014) 'Cobalt separation from waste mobile phone batteries using selective precipitation and chelating resin', *Journal of Material Cycles and Waste Management*, 16(4), pp. 739-746. doi: https://doi.org/10.1007/s10163-013-0213-y.

Baum, Z.J., Bird, R.E., Yu, X. and Ma, J. (2022) 'Lithium-Ion Battery Recycling─Overview of Techniques and Trends', *ACS Energy Letters*, 7(2), pp. 712-719. doi: https://doi.org/10.1021/acsenergylett.1c02602.

Brückner, L., Frank, J. and Elwert, T. (2020) 'Industrial recycling of lithium-ion batteries—A critical review of metallurgical process routes', *Metals*, 10(8), pp. 1107.

Chiu, K. and Chen, W. (2017) 'Recovery and separation of valuable metals from cathode materials of spent lithium-ion batteries (LIBs) by ion exchange', *Science of Advanced Materials*, 9(12), pp. 2155-2160. doi: https://doi.org/10.1166/sam.2017.3214.

Choi, D., Shamim, N., Crawford, A., Huang, Q., Vartanian, C.K., Viswanathan, V.V., Paiss, M.D., Alam, M.J.E., Reed, D.M. and Sprenkle, V.L. (2021) 'Li-ion battery technology for grid application', *Journal of Power Sources*, 511, pp. 230419. doi: https://doi.org/10.1016/j.jpowsour.2021.230419.

Dunn, J.B., Gaines, L., Kelly, J.C., James, C. and Gallagher, K.G. (2015) 'The significance of Li-ion batteries in electric vehicle life-cycle energy and emissions and recycling's role in its reduction', *Energy & environmental science*, 8(1), pp. 158-168. doi: https://doi.org/10.1039/C4EE03029J.

DuPont Ion Exchange Resins Resin wear-out guidelines (2019) DuPont, https://www.dupont.com/content/dam/dupont/amer/us/en/water-solutions/public/documents/en/45-D01119-en.pdf.

European Commission (2020) 'Critical Raw Materials Resilience: Charting a Path towards Greater Security and Sustainability. COM 474 Final', .

European Lithium (2020) *Lithium.* Available at: https://europeanlithium.com/lithium/ (Accessed: 30.90.2022).

Fisher, K.G. (2011) *Cobalt processing developments.* The Southern African Institute of Mining and Metallurgy, pp. 237.

Free, M.L. (2022) *Hydrometallurgy: Fundamentals and Applications.* 2nd edn. Cham: Springer International Publishing.

Gaines, L. (2018) 'Lithium-ion battery recycling processes: Research towards a sustainable course', *Sustainable Materials and Technologies,* 17. doi: https://doi.org/10.1016/j.susmat.2018.e00068.

Georgi-Maschler, T., Friedrich, B., Weyhe, R., Heegn, H. and Rutz, M. (2012) 'Development of a recycling process for Li-ion batteries', *Journal of Power Sources,* 207, pp. 173-182.

Girish, C.R. (2017) 'Various isotherm models for multicomponent adsorption: a review', *Int.J.Civ.Eng.Technol,* 8(10), pp. 80-86.

Gupta, A. and Balomajumder, C. (2015) 'Simultaneous adsorption of Cr(VI) and phenol onto tea waste biomass from binary mixture: Multicomponent adsorption, thermodynamic and kinetic study', *Journal of Environmental Chemical Engineering,* 3(2), pp. 785-796. doi: https://doi.org/10.1016/j.jece.2015.03.003.

Helbig, C., Bradshaw, A.M., Wietschel, L., Thorenz, A. and Tuma, A. (2018) 'Supply risks associated with lithium-ion battery materials', *Journal of Cleaner Production,* 172, pp. 274-286. doi: https://doi.org/10.1016/j.jclepro.2017.10.122.

Homsy, G.M. (1987) 'Viscous fingering in porous media', *Annual Review of Fluid Mechanics,* 19(1), pp. 271-311. doi: https://doi.org/10.1146/annurev.fl.19.010187.001415.

Inglezakis, V.J. and Zorpas, A. (2012) 'Fundamentals of Ion Exchange Fixed-Bed Operations', in Dr., I. and Luqman, M. (eds.) *Ion Exchange Technology I: Theory and Materials* Dordrecht: Springer Netherlands, pp. 121-161.

International Nickel Study Group (2021) *Production, Usage and Price* . Available at: https://insg.org/index.php/about-nickel/production-usage/ (Accessed: 24.11.2021).

Jung, J.C., Sui, P. and Zhang, J. (2021) 'A review of recycling spent lithium-ion battery cathode materials using hydrometallurgical treatments', *Journal of Energy Storage,* 35, pp. 102217. doi: https://doi.org/10.1016/j.est.2020.102217.

Kaukinen, A. (2019) 'Ion exchange in hydrometallurgical recycling of Li-ion battery metals: production of Li-Ni-Co mixture.

Kinniburgh, D.G., van Riemsdijk, W.H., Koopal, L.K., Borkovec, M., Benedetti, M.F. and Avena, M.J. (1999) 'Ion binding to natural organic matter: competition, heterogeneity, stoichiometry and thermodynamic consistency', *Colloids and Surfaces A: Physicochemical and Engineering Aspects*, 151(1), pp. 147-166. doi: https://doi.org/10.1016/S0927-7757(98)00637-2.

Laatikainen, M. (2014) *ResMod Toolbox for Parameter Estimation and Process Simulation in Ion Exchange and Adsorption.*

Langmuir, I. (1918) 'The adsorption of gases on plane surfaces of glass, mica and platinum.', *Journal of the American Chemical Society*, 40(9), pp. 1361-1403.

Lannoo, S., Vilas-Boas, A., Sadeghi, S.M., Jesus, J. and Soares, Helena M. V. M. (2019) 'An environmentally friendly closed loop process to recycle raw materials from spent alkaline batteries', *Journal of Cleaner Production*, 236, pp. 117612. doi: https://doi.org/10.1016/j.jclepro.2019.117612.

Lebron, Y.A.R., Moreira, V.R. and Amaral, M.C.S. (2021) 'Metallic ions recovery from membrane separation processes concentrate: A special look onto ion exchange resins', *Chemical Engineering Journal*, 425, pp. 131812. doi: https://doi.org/10.1016/j.cej.2021.131812.

Li, J., Wang, G. and Xu, Z. (2016) 'Environmentally-friendly oxygen-free roasting/wet magnetic separation technology for in situ recycling cobalt, lithium carbonate and graphite from spent LiCoO2/graphite lithium batteries', *Journal of hazardous materials*, 302, pp. 97-104. doi: https://doi.org/10.1016/j.jhazmat.2015.09.050.

Liu, C., Lin, J., Cao, H., Zhang, Y. and Sun, Z. (2019) 'Recycling of spent lithium-ion batteries in view of lithium recovery: A critical review', *Journal of Cleaner Production*, 228, pp. 801-813. doi: https://doi.org/10.1016/j.jclepro.2019.04.304.

Lithium-Ion Battery Recycling Market. (2021) Available at: https://www.fortunebusinessinsights.com/industry-reports/lithium-ion-battery-recycling-market-100244 (Accessed: 21.8.2022).

Luca, C., Vlad, C.D. and Bunia, I. (2009) 'Trends in weak base anion exchangers resins', *Revue Roumaine de Chimie*, 54(2), pp. 107-117.

Miyabe, K. and Guiochon, G. (2003) 'Measurement of the parameters of the mass transfer kinetics in high performance liquid chromatography', *Journal of separation science; J.Sep.Science*, 26(3-4), pp. 155-173. doi: 10.1002/jssc.200390024.

Naushad, M. and Al-Othman, Z.A. (2013) *A book on ion exchange, adsorption and solvent extraction.* Hauppauge, N.Y: Nova Science Publishers, Inc.

Nesterenko, P.N., Shaw, M.J., Hill, S.J. and Jones, P. (1999) 'Aminophosphonate-Functionalized Silica: A Versatile Chromatographic Stationary Phase for High-Performance Chelation Ion Chromatography', *Microchemical Journal*, 62(1), pp. 58-69. doi: https://doi.org/10.1006/mchj.1999.1717.

Ningtyas, R.P., Wirawan, S.K. and Purnomo, C.W. (2021) *Lithium purification from spent li-ion batteries leachate using ion exchange resin.* AIP Publishing LLC, .

Niu, Z., Li, G., He, D., Fu, X., Sun, W. and Yue, T. (2021) 'Resource-recycling and energy-saving innovation for iron removal in hydrometallurgy: Crystal transformation of ferric hydroxide precipitates by hydrothermal treatment', *Journal of hazardous materials*, 416, pp. 125972. doi: https://doi.org/10.1016/j.jhazmat.2021.125972.

Porvali, A., Aaltonen, M., Ojanen, S., Velazquez-Martinez, O., Eronen, E., Liu, F., Wilson, B.P., Serna-Guerrero, R. and Lundström, M. (2019) 'Mechanical and hydrometallurgical processes in HCl media for the recycling of valuable metals from Li-ion battery waste', *Resources, Conservation and Recycling*, 142, pp. 257-266. doi: https://doi.org/10.1016/j.resconrec.2018.11.023.

Product information Lewatit TP 260 (2011) Lanxess, https://www.lenntech.com/Data-sheets/Lewatit-TP-260-L.pdf.

Pudas, J., Erkkila, A. and Viljamaa, J. (2015) *Battery recycling method.* Authoring organisation. US 8,979,006 B2. Available at: (Accessed: .

Ruthven, D.M. (1984) *Principles of adsorption and adsorption processes.* John Wiley & Sons.

Scrosati, B. (2011) 'History of lithium batteries', *Journal of Solid State Electrochemistry*, 15(7), pp. 1623-1630. doi: https://doi.org/10.1007/s10008-011-1386-8

Shamsuddin, M. (2021) *Physical Chemistry of Metallurgical Processes, Second Edition.* Cham: Springer International Publishing AG.

Sole, K.C., Mooiman, M. and Hardwick, E. (2016) *Present and future applications of ion exchange in hydrometallurgy: an overview.* At Cambridge UK, pp. 2016.

Sommerville, R., Zhu, P., Rajaeifar, M.A., Heidrich, O., Goodship, V. and Kendrick, E. (2021) 'A qualitative assessment of lithium ion battery recycling processes', *Resources, Conservation and Recycling*, 165, pp. 105219. doi: https://doi.org/10.1016/j.resconrec.2020.105219.

Strauss, M.L., Diaz, L.A., McNally, J., Klaehn, J. and Lister, T.E. (2021) 'Separation of cobalt, nickel, and manganese in leach solutions of waste lithium-ion batteries using Dowex M4195 ion exchange resin', *Hydrometallurgy*, , pp. 105757. doi: https://doi.org/10.1016/j.hydromet.2021.105757.

Swain, B. (2017) 'Recovery and recycling of lithium: A review', *Separation and Purification Technology*, 172, pp. 388-403. doi: https://doi.org/10.1016/j.seppur.2016.08.031.

Talens Peiró, L., Villalba Méndez, G. and Ayres, R.U. (2013) 'Lithium: Sources, Production, Uses, and Recovery Outlook', *JOM*, 65(8), pp. 986-996. doi: https://doi.org/10.1007/s11837-013-0666-4.

Tisserant, A. and Pauliuk, S. (2016) 'Matching global cobalt demand under different scenarios for co-production and mining attractiveness', *Journal of Economic Structures*, 5(1), pp. 4. doi: https://doi.org/10.1186/s40008-016-0035-x.

Trading Economics. (2022) Available at: https://tradingeconomics.com (Accessed: 27.7.2022).

U.S. Geological Survey (2022) *Mineral commodity summaries 2022.* U.S. Geological Survey. Available at:(Accessed: 24.8.2022).

U.S. Geological Survey (2021) *Nickel Statistics and Information.* Available at: https://www.usgs.gov/centers/national-minerals-information-center/nickel-statistics-and-information (Accessed: 27.1.2022).

U.S. Geological Survey (2011) *Mineral commodity summaries 2011.* U.S. Geological Survey. Available at:(Accessed: 24.8.2022).

Vanderbruggen, A., Gugala, E., Blannin, R., Bachmann, K., Serna-Guerrero, R. and Rudolph, M. (2021) 'Automated mineralogy as a novel approach for the compositional and textural characterization of spent lithium-ion batteries', *Minerals Engineering*, 169, pp. 106924. doi: https://doi.org/10.1016/j.mineng.2021.106924.

Velázquez-Martínez, O., Valio, J., Santasalo-Aarnio, A., Reuter, M. and Serna-Guerrero, R. (2019) 'A critical review of lithium-ion battery recycling processes from a circular economy perspective', *Batteries*, 5(4), pp. 68.

Virolainen, S., Wesselborg, T., Kaukinen, A. and Sainio, T. (2021) 'Removal of iron, aluminium, manganese and copper from leach solutions of lithium-ion battery waste using ion exchange', *Hydrometallurgy*, 202, pp. 105602. doi: https://doi.org/10.1016/j.hydromet.2021.105602.

Warner, J. (2015) *The handbook of lithium-ion battery pack design : chemistry, components, types and terminology.* Waltham, MA: Elsevier Inc.

Zheng, X., Zhu, Z., Lin, X., Zhang, Y., He, Y., Cao, H. and Sun, Z. (2018) 'A Mini-Review on Metal Recycling from Spent Lithium Ion Batteries', *Engineering*, 4(3), pp. 361-370. doi: https://doi.org/10.1016/j.eng.2018.05.018.

Appendices

Appendix I All laboratory test results from ICP-MS

Appendix II Simulated and measured washing and elution curves

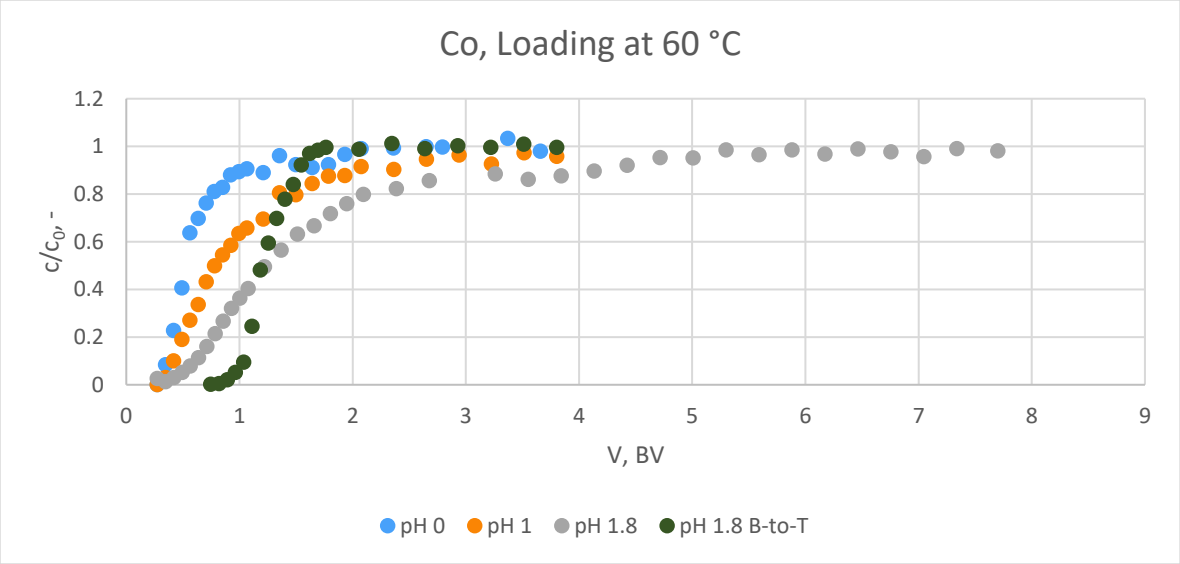
Co, Loading at 60 °C
c/c0, -
V, BV
pH 0
pH 1
pH 1.8
pH 1.8 B-to-T

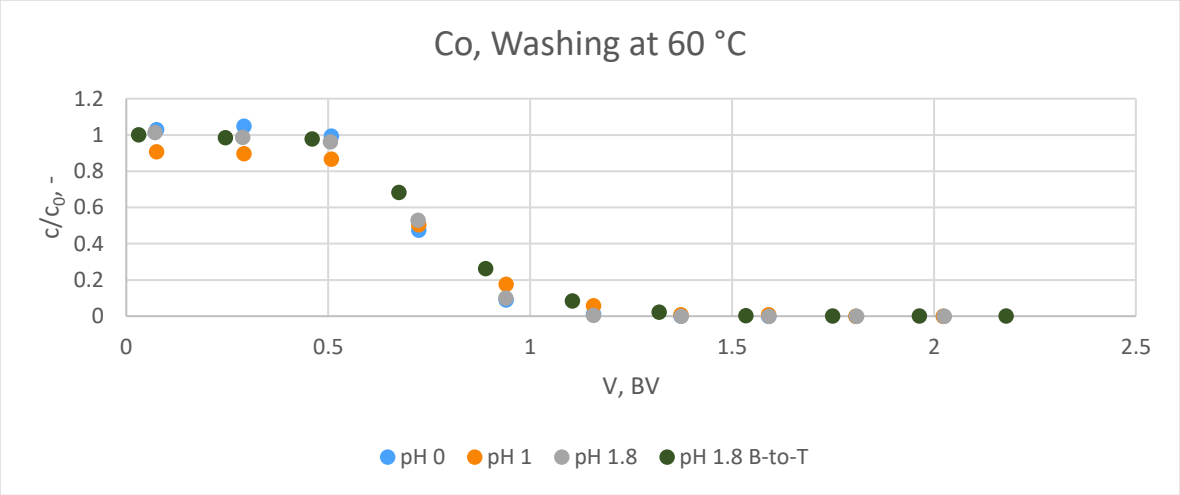
Co, Washing at 60 °C
c/c0, -
V, BV
pH 0
pH 1
pH 1.8
pH 1.8 B-to-T

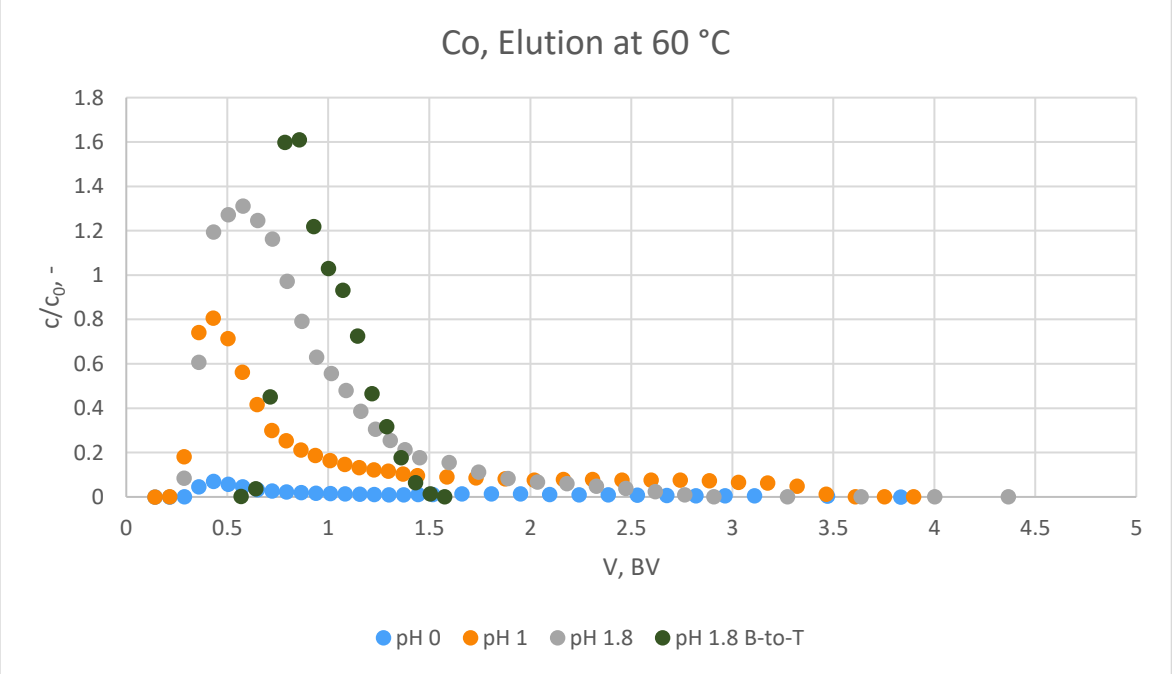
Co, Elution at 60 °C
c/c0, -
V, BV
pH 0
pH 1
pH 1.8
pH 1.8 B-to-T

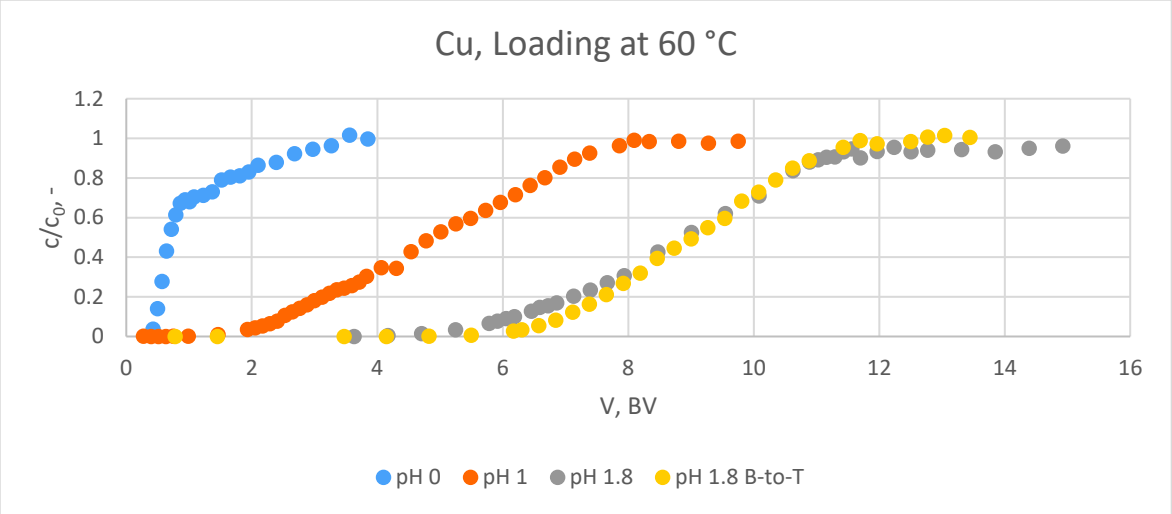
Cu, Loading at 60 °C
c/c0, -
V, BV
pH 0
pH 1
pH 1.8
pH 1.8 B-to-T

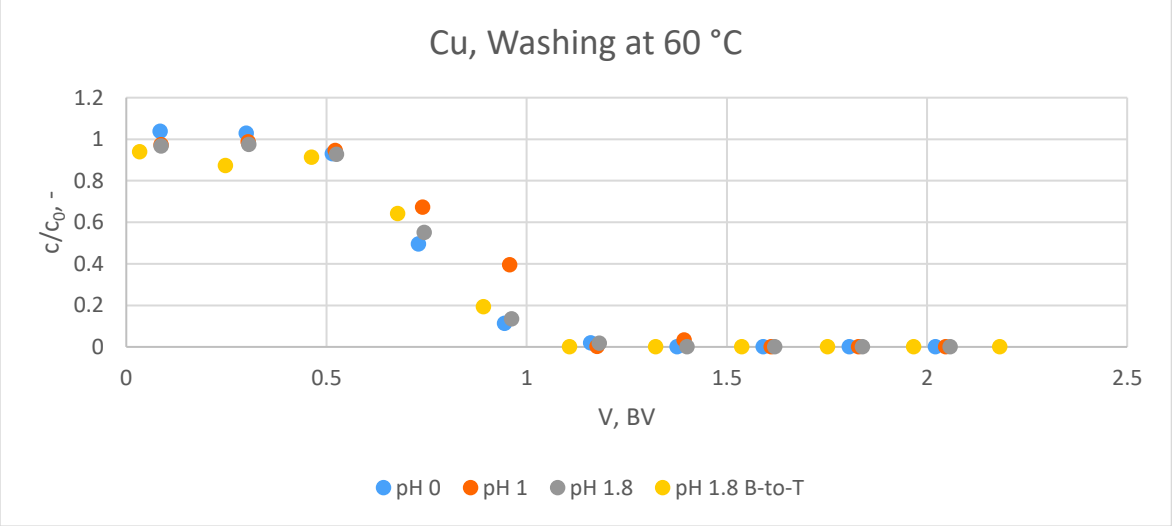
Cu, Washing at 60 °C
c/c0, -
V, BV
pH 0
pH 1
pH 1.8
pH 1.8 B-to-T

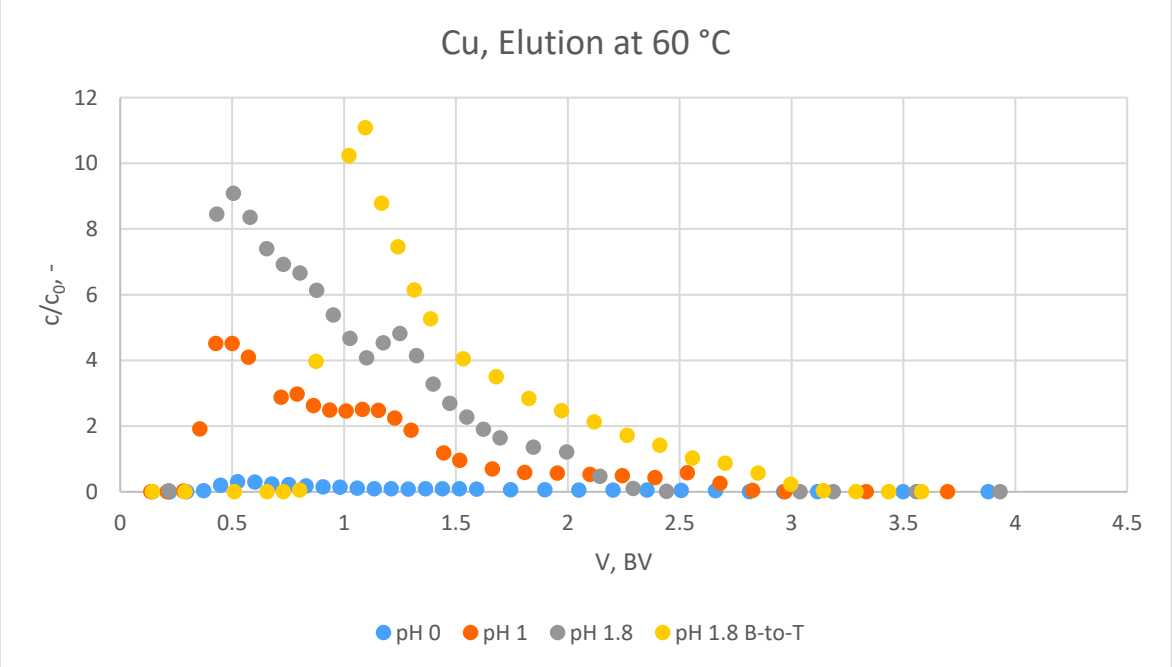
Cu, Elution at 60 °C
c/c0, -
V, BV
pH 0
pH 1
pH 1.8
pH 1.8 B-to-T

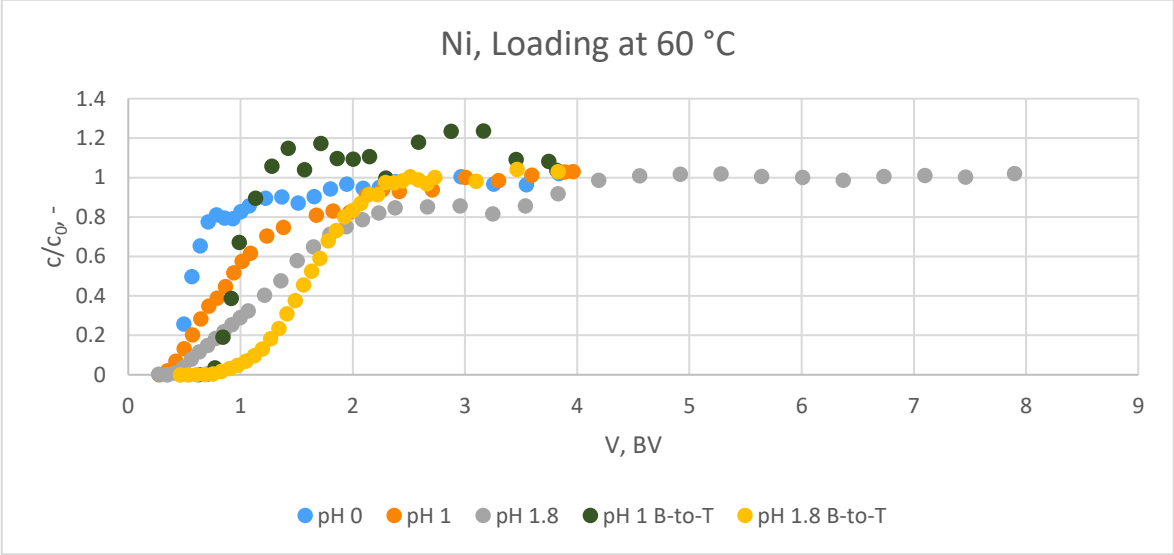
Ni, Loading at 60 °C
c/c0, -
V, BV
pH 0
pH 1
pH 1.8
pH 1 B-to-T
pH 1.8 B-to-T

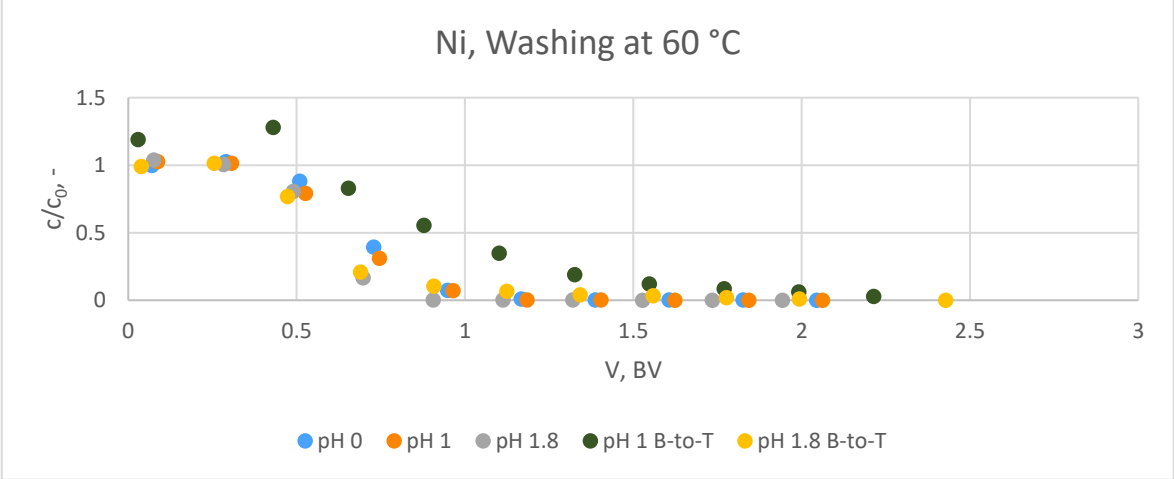
Ni, Washing at 60 °C
c/c0, -
V, BV
pH 0
pH 1
pH 1.8
pH 1 B-to-T
pH 1.8 B-to-T

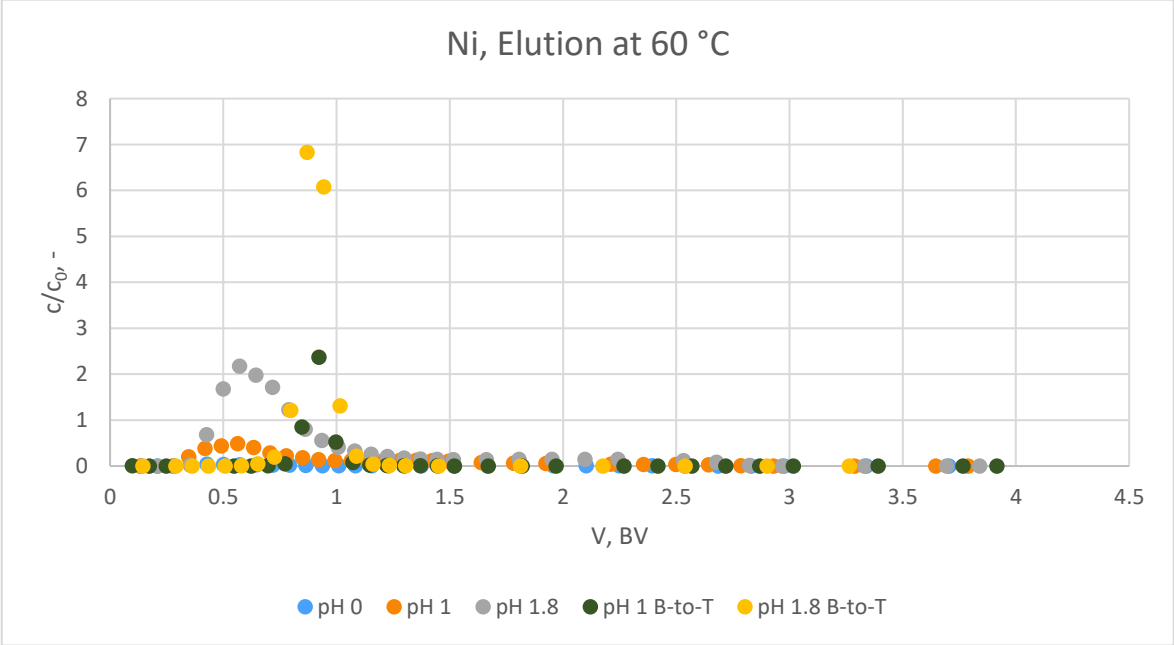
Ni, Elution at 60 °C
c/c0, -
V, BV
pH 0
pH 1
pH 1.8
pH 1 B-to-T
pH 1.8 B-to-T

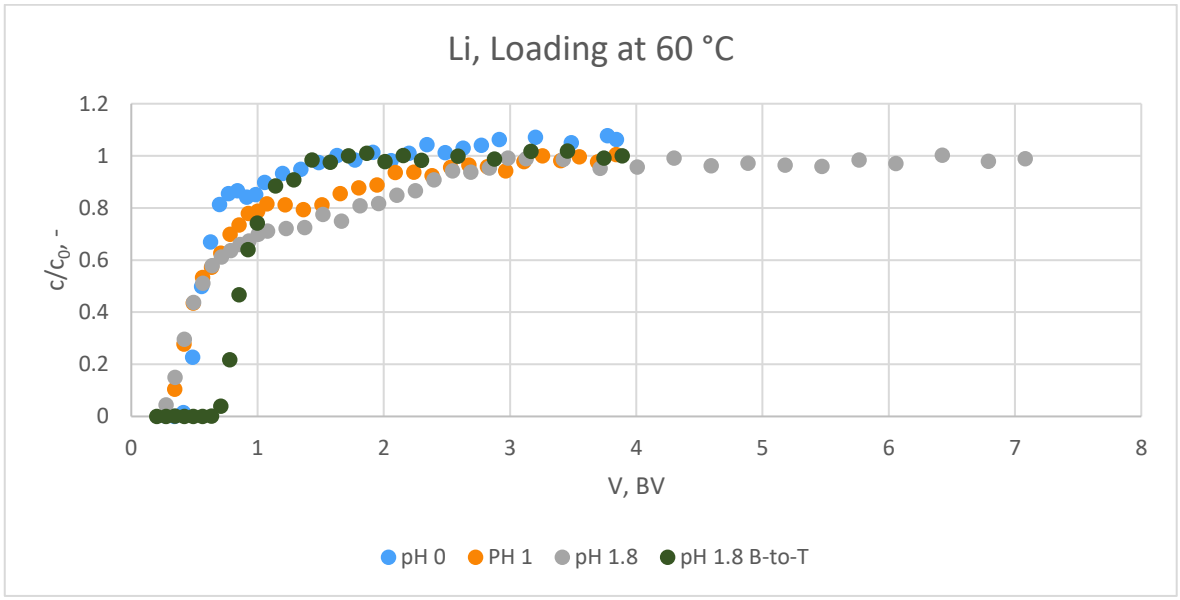
Li, Loading at 60 °C
c/c0, -
V, BV
pH 0
PH 1
pH 1.8
pH 1.8 B-to-T

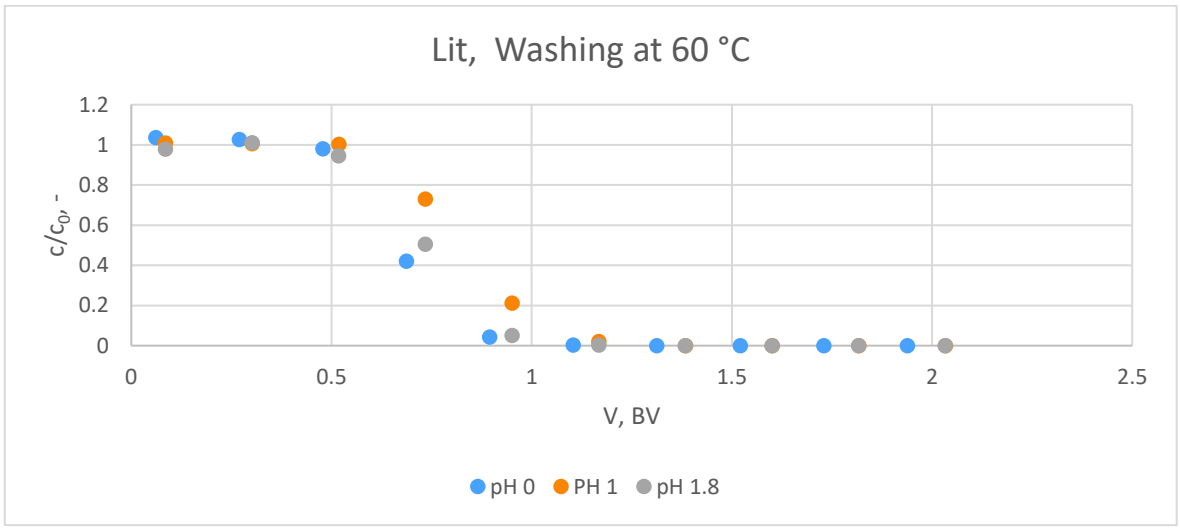
Lit, Washing at 60 °C
c/c0, -
V, BV
pH 0
PH 1
pH 1.8

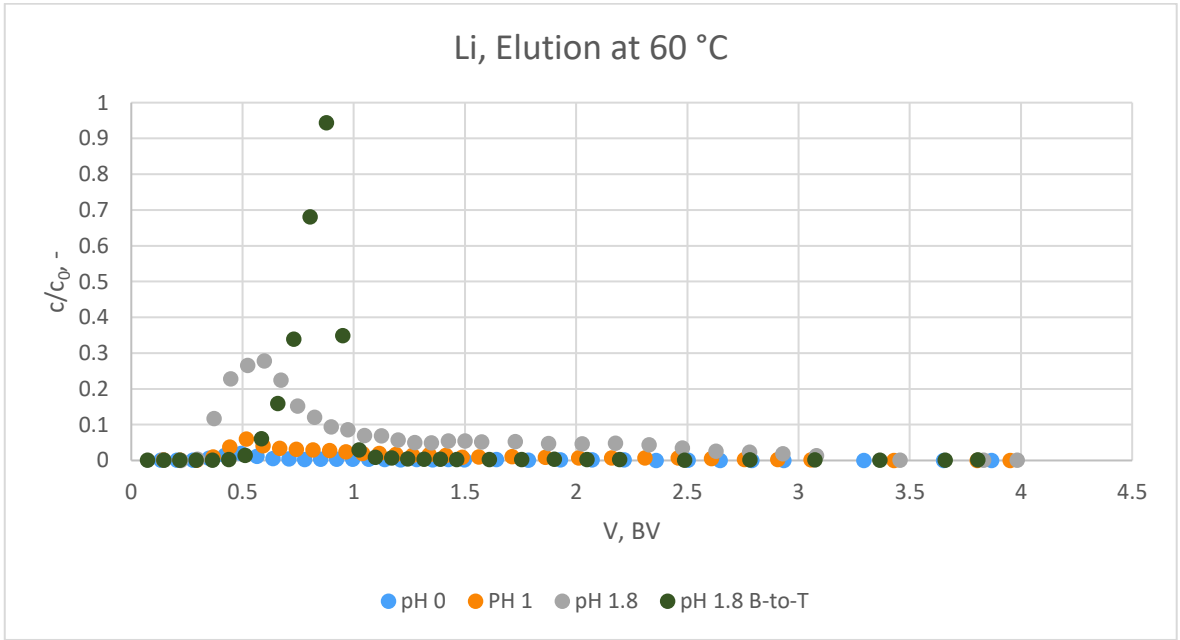
Li, Elution at 60 °C
c/c0, -
V, BV
pH 0
PH 1
pH 1.8
pH 1.8 B-to-T

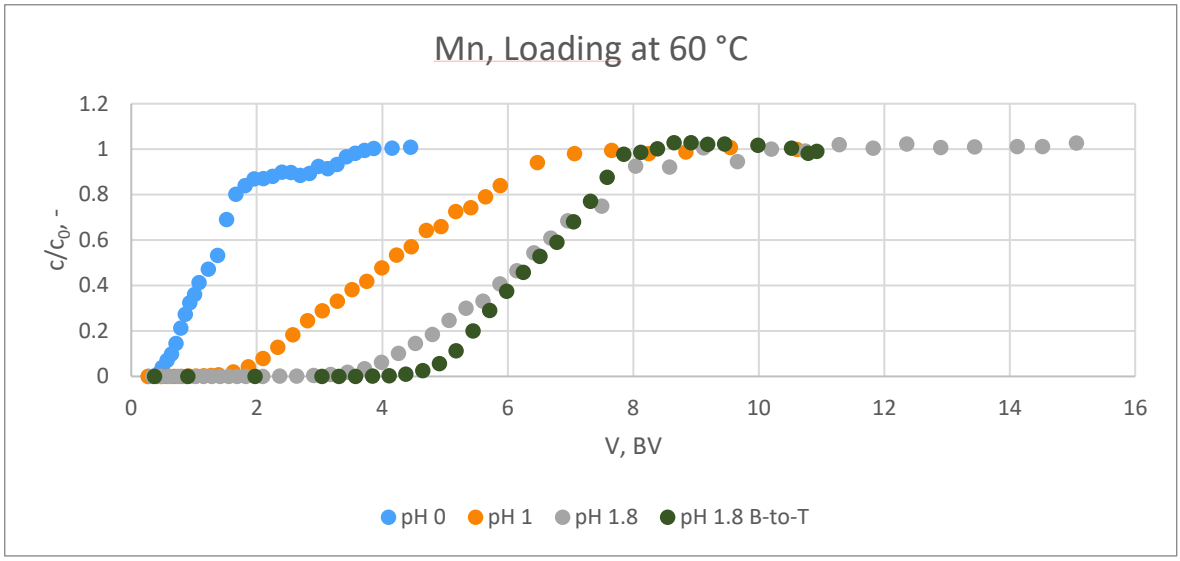
Mn, Loading at 60 °C
c/c0, -
V, BV
pH 0
pH 1
pH 1.8
pH 1.8 B-to-T

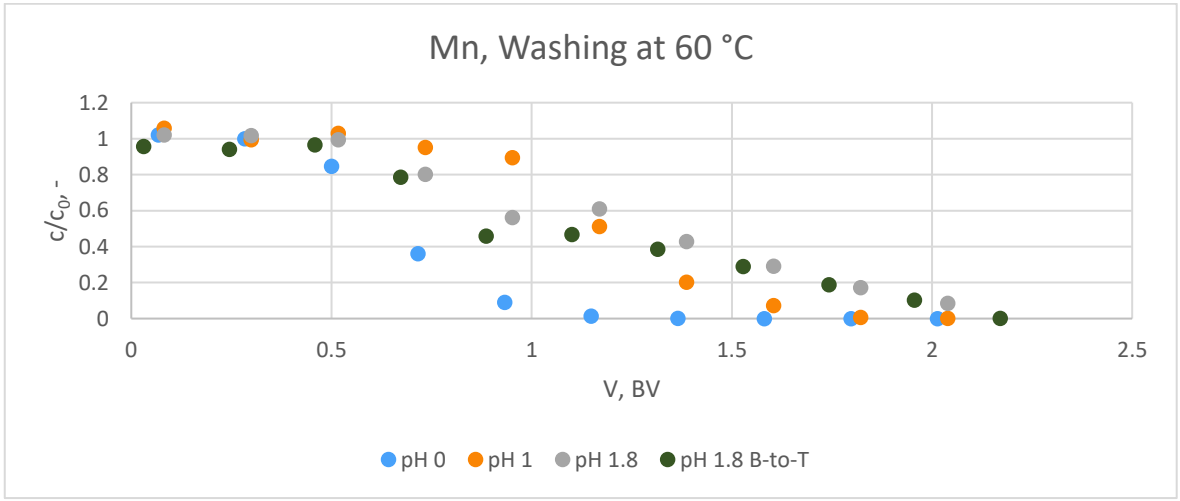
Mn, Washing at 60 °C
c/c0, -
V, BV
pH 0
pH 1
pH 1.8
pH 1.8 B-to-T

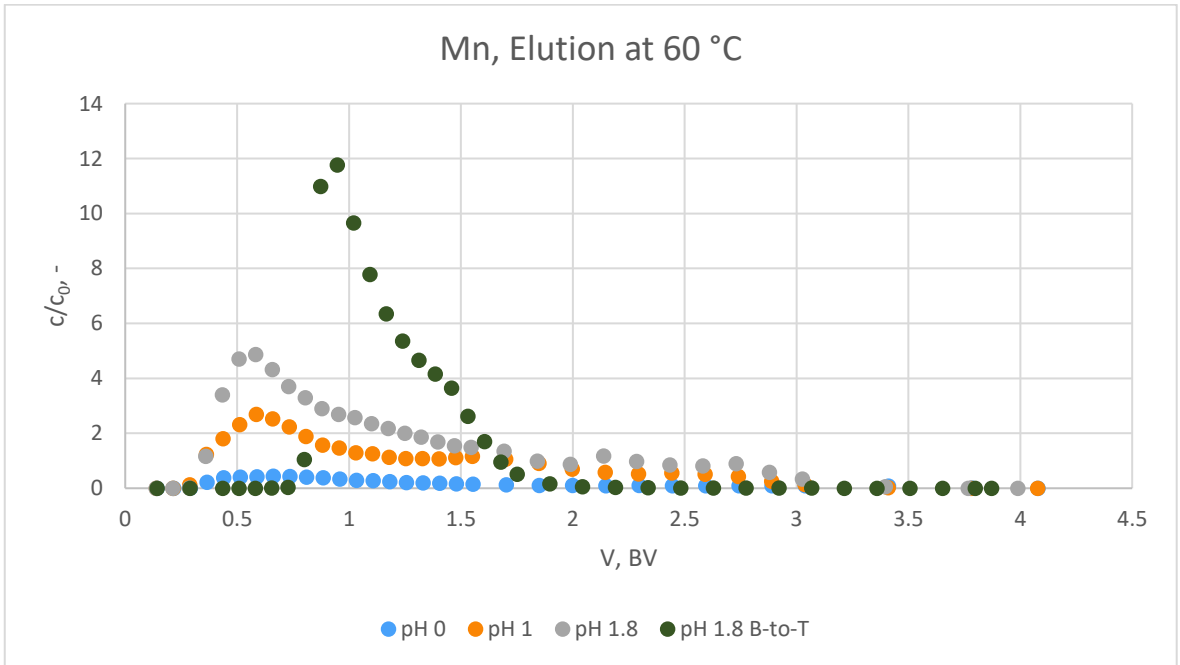
Mn, Elution at 60 °C
c/c0, -
V, BV
pH 0
pH 1
pH 1.8
pH 1.8 B-to-T

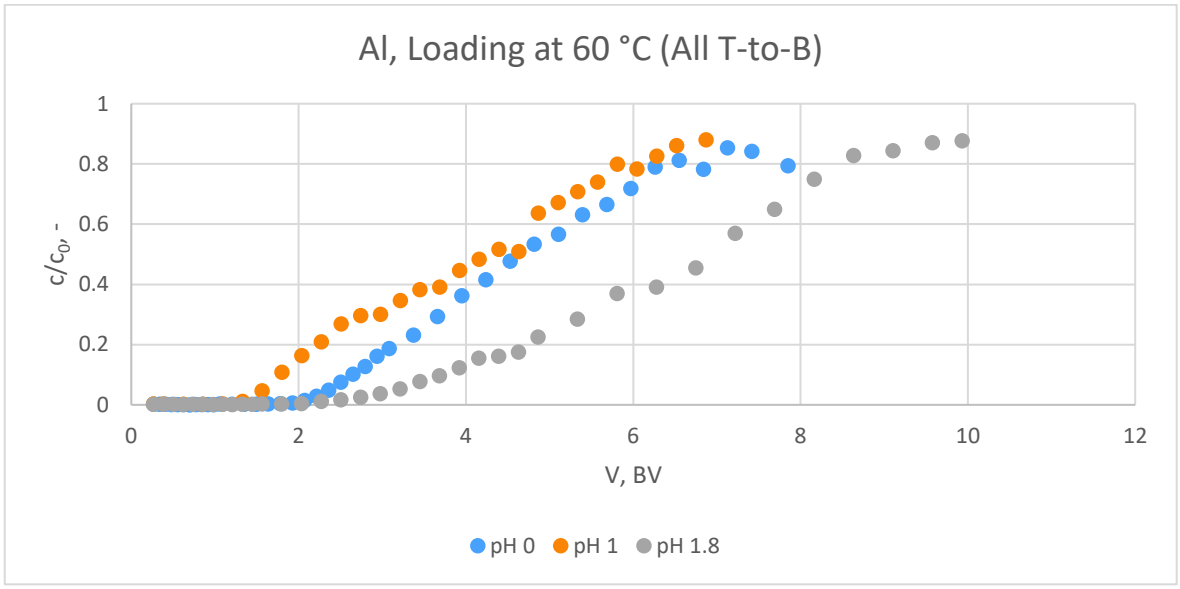
Al, Loading at 60 °C (All T-to-B)
c/c0, -
V, BV
pH 0
pH 1
pH 1.8

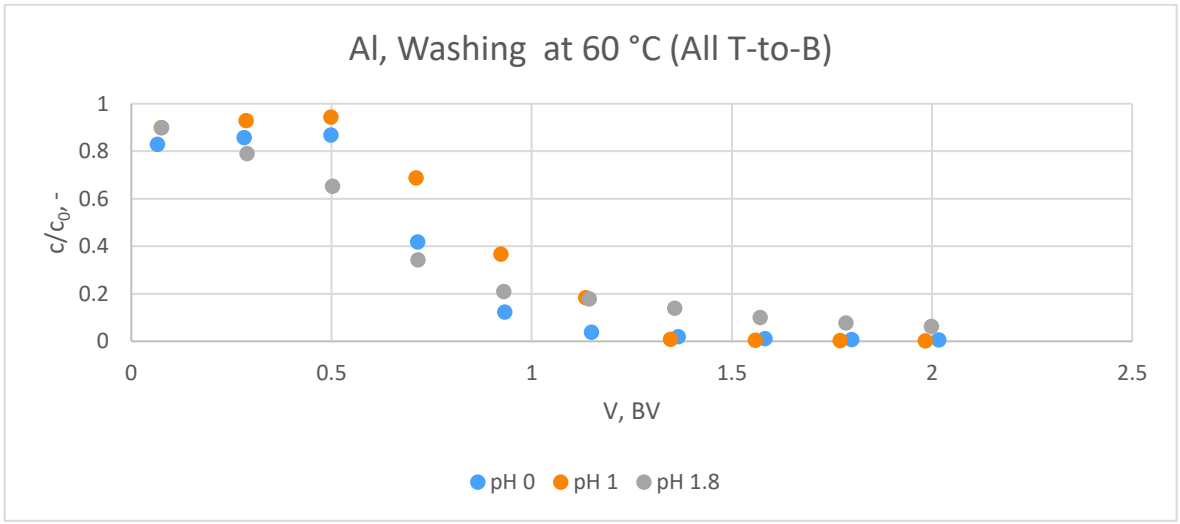
Al, Washing at 60 °C (All T-to-B)
c/c0, -
V, BV
pH 0
pH 1
pH 1.8

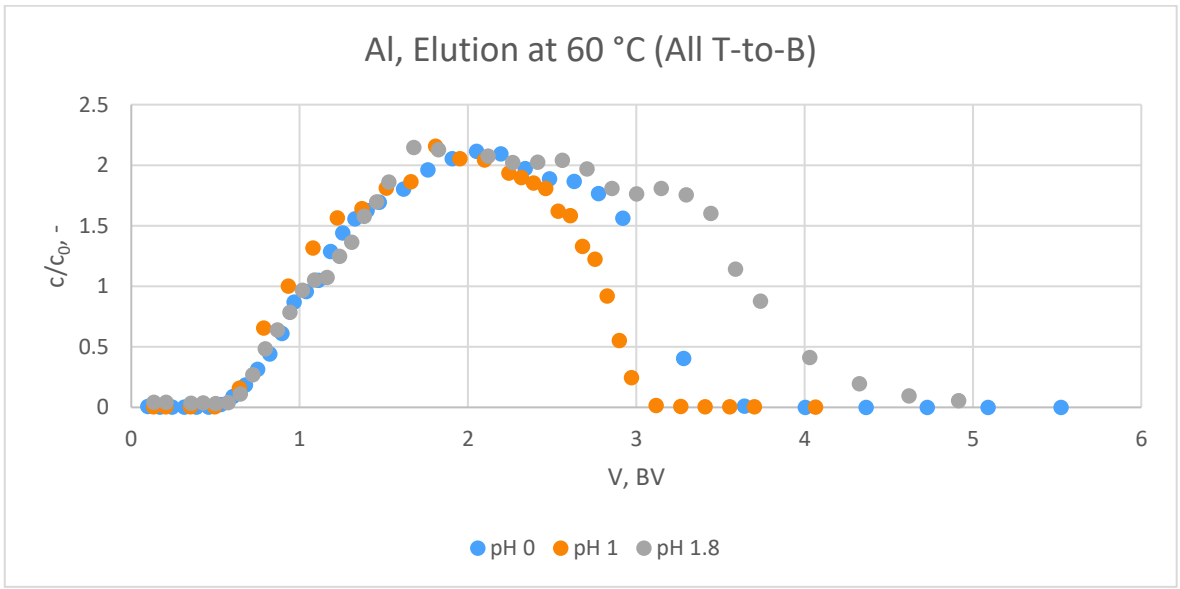
Al, Elution at 60 °C (All T-to-B)
c/c0, -
V, BV
pH 0
pH 1
pH 1.8

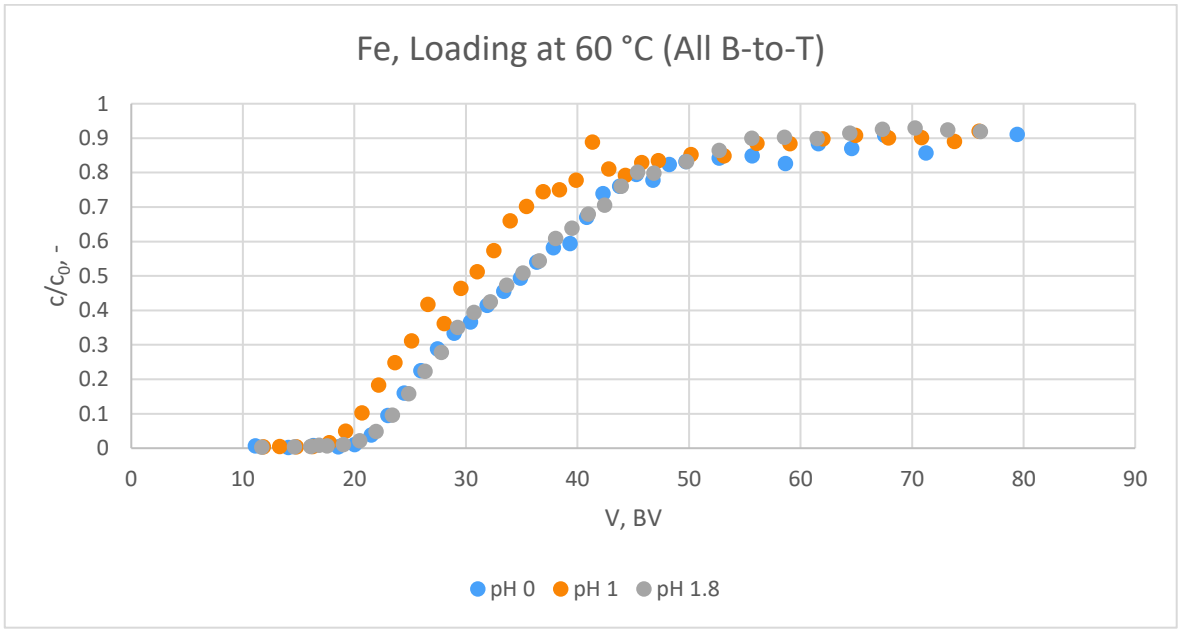
Fe, Loading at 60 °C (All B-to-T)
c/c0, -
V, BV
pH 0
pH 1
pH 1.8

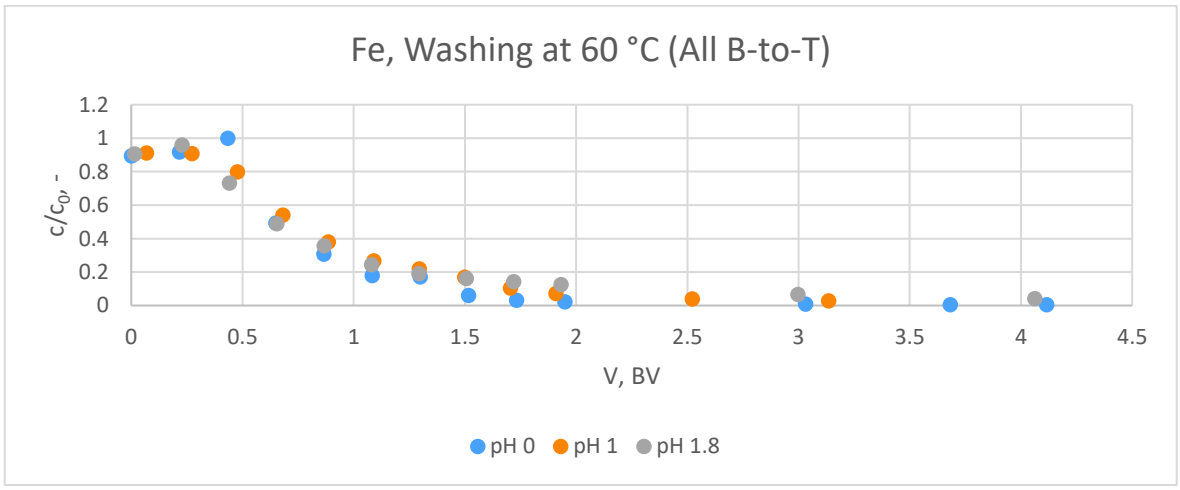
Fe, Washing at 60 °C (All B-to-T)
c/c0, -
V, BV
pH 0
pH 1
pH 1.8

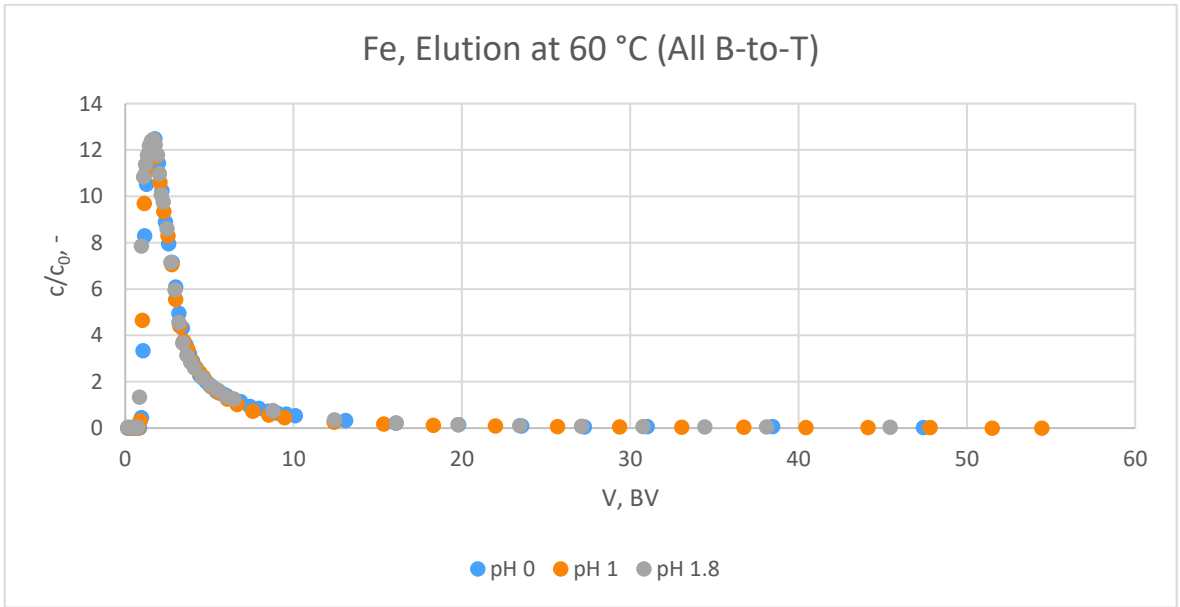
Fe, Elution at 60 °C (All B-to-T)
c/c0, -
V, BV
pH 0
pH 1
pH 1.8

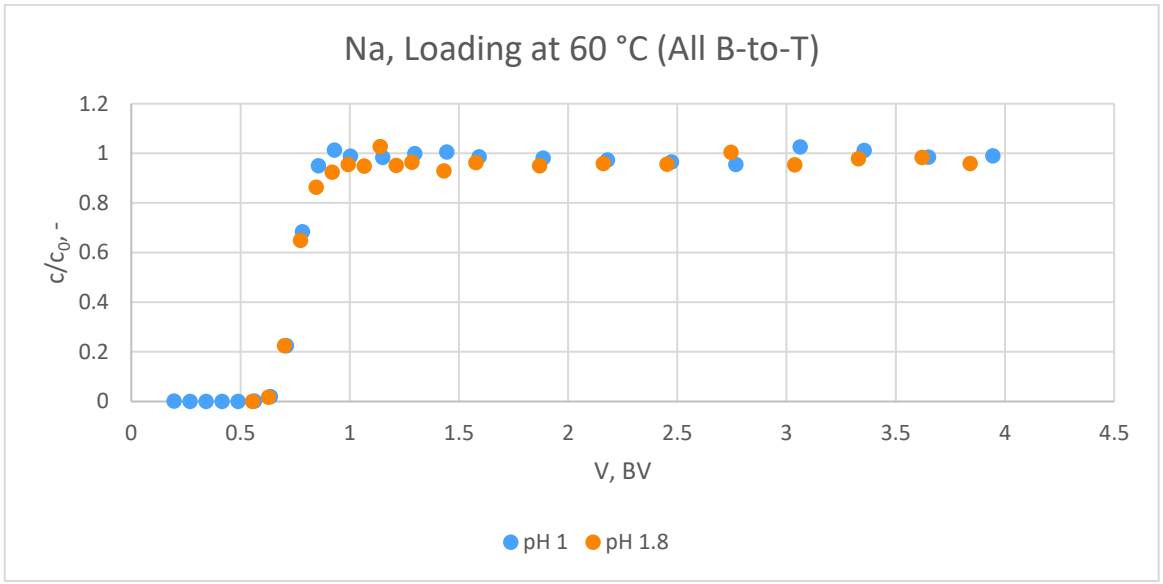
Na, Loading at 60 °C (All B-to-T)
c/c0, -
V, BV
pH 1
pH 1.8

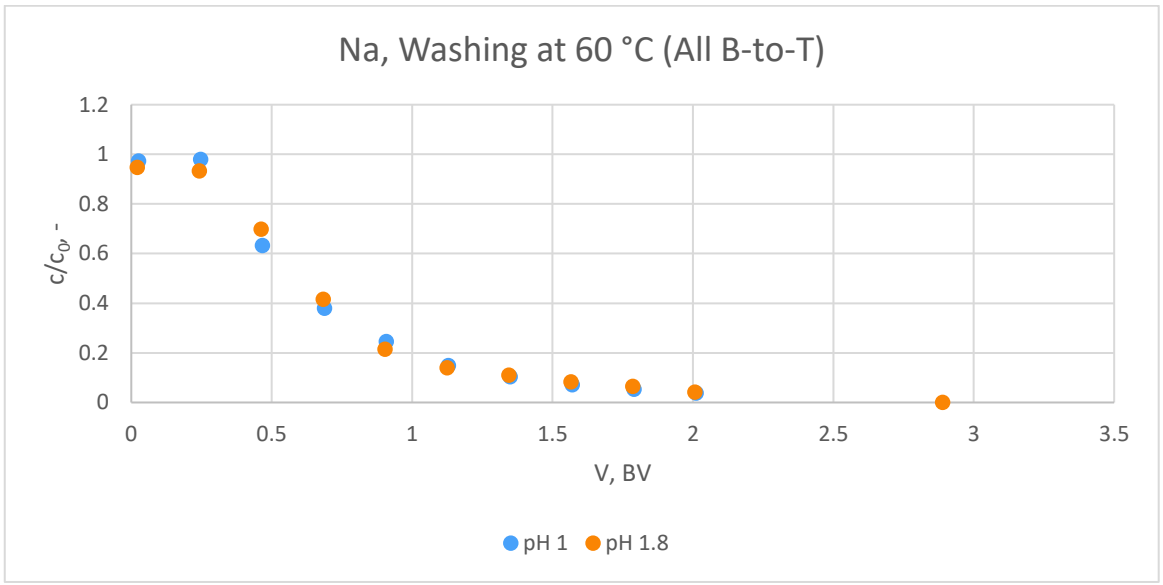
Na, Washing at 60 °C (All B-to-T)
c/c0, -
V, BV
pH 1
pH 1.8

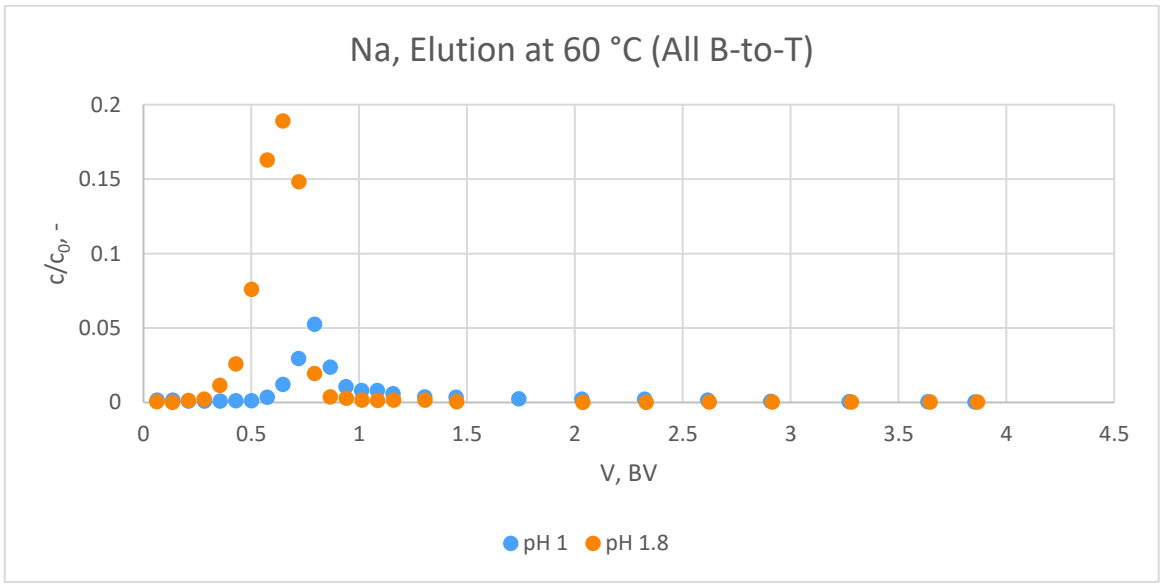
Na, Elution at 60 °C (All B-to-T)
c/c0, -
V, BV
pH 1
pH 1.8

Appendix II Simulated and measured washing and elution curves

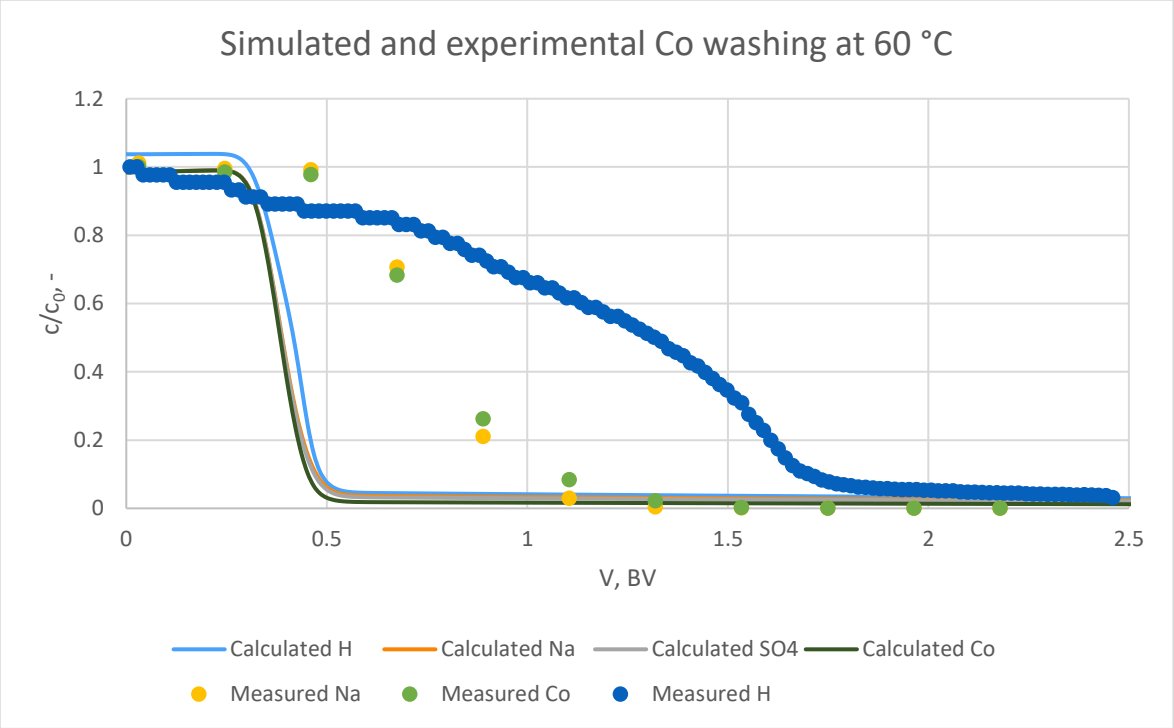

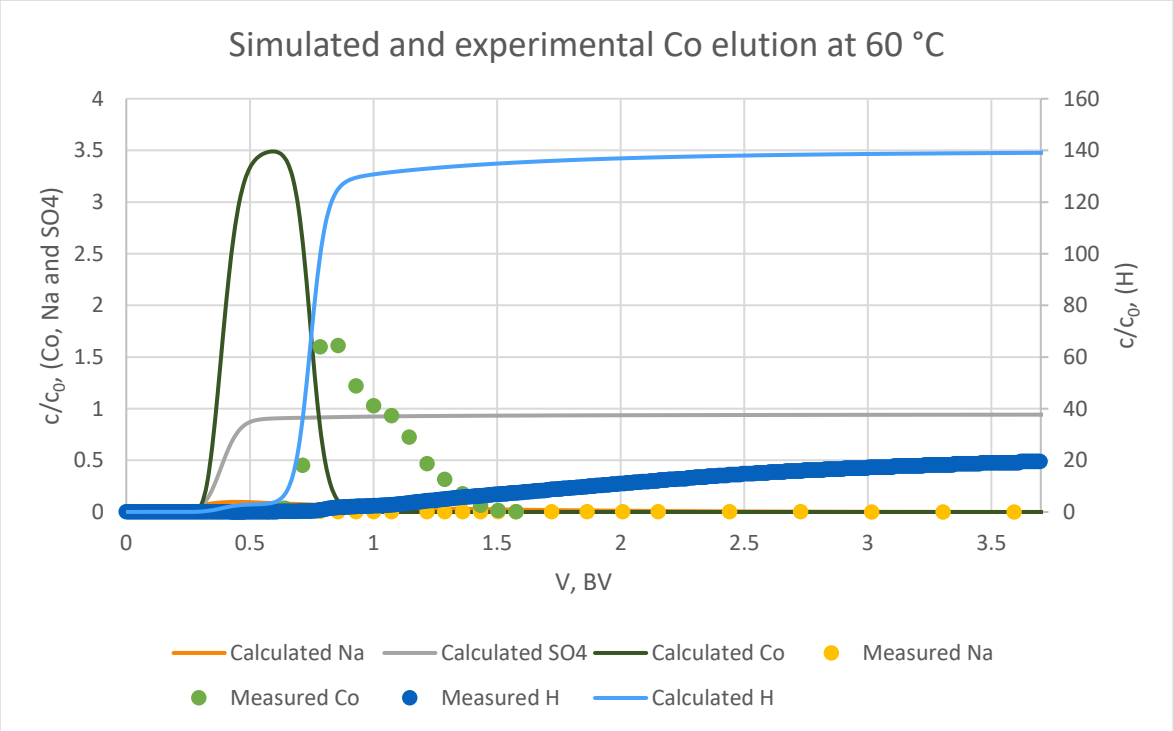

Appendix II Simulated and measured washing and elution curves

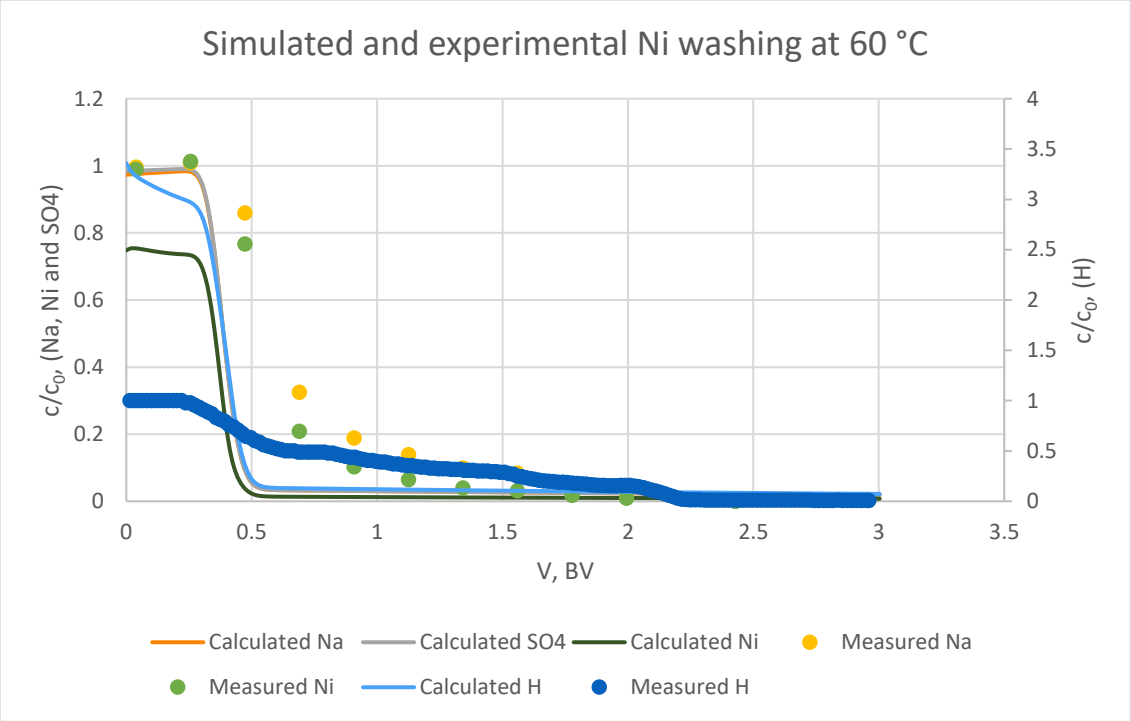

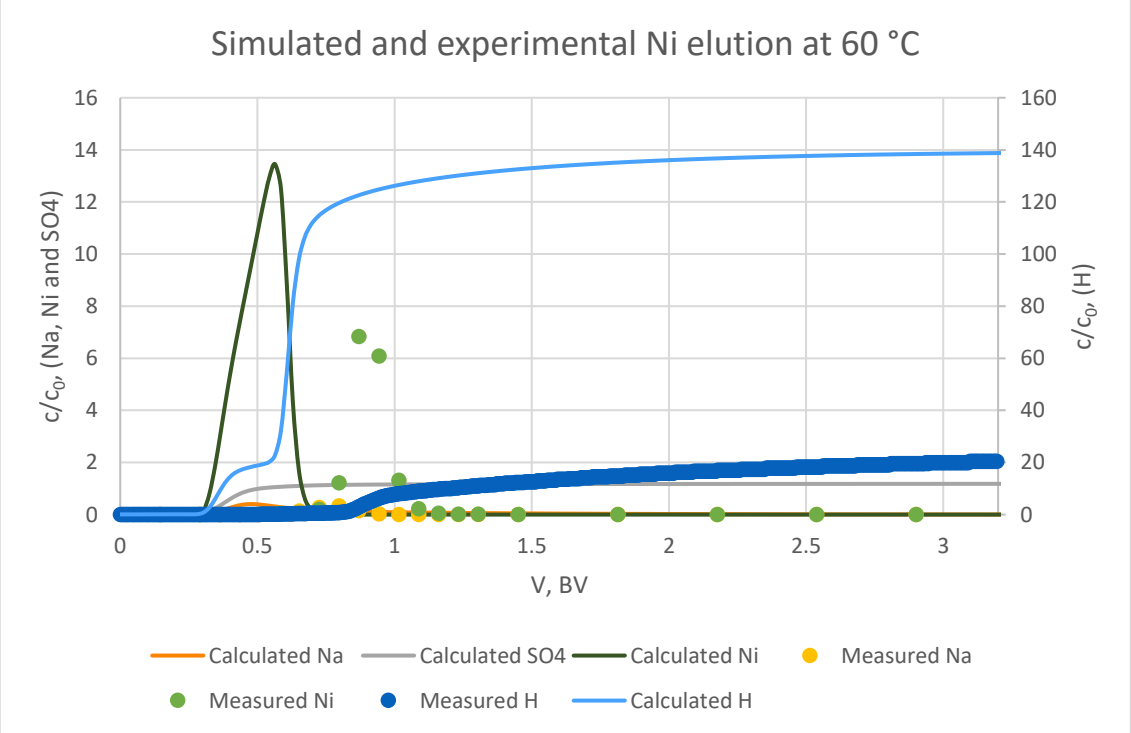

Appendix II Simulated and measured washing and elution curves

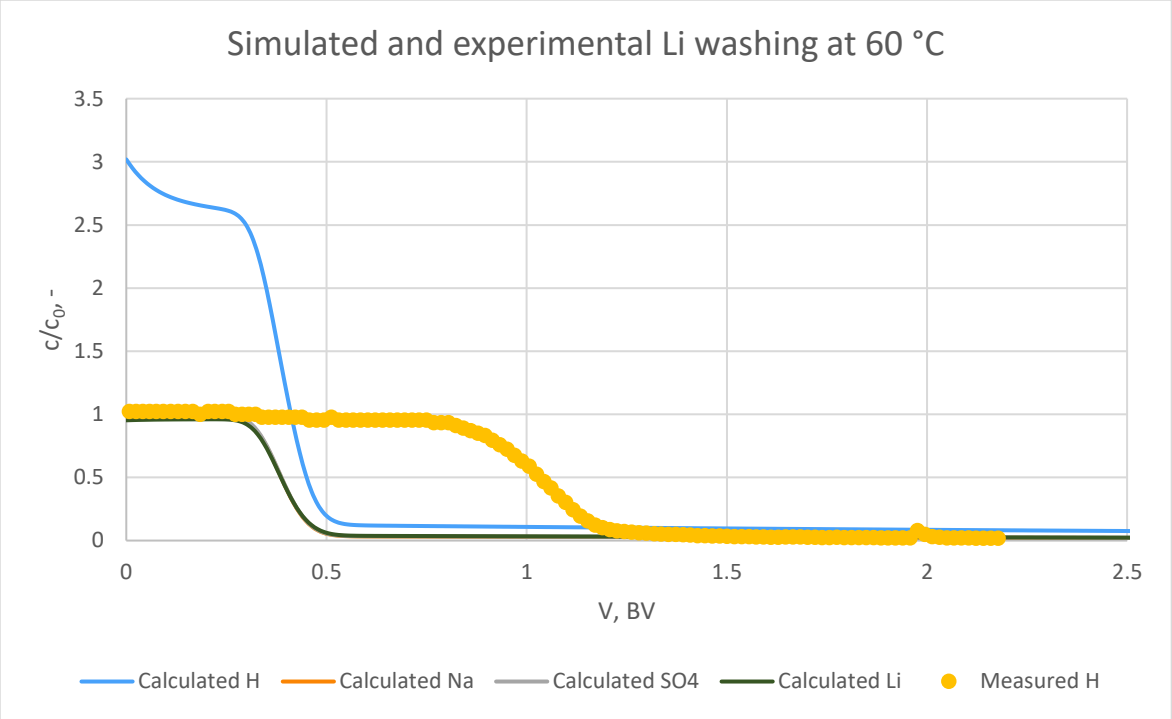

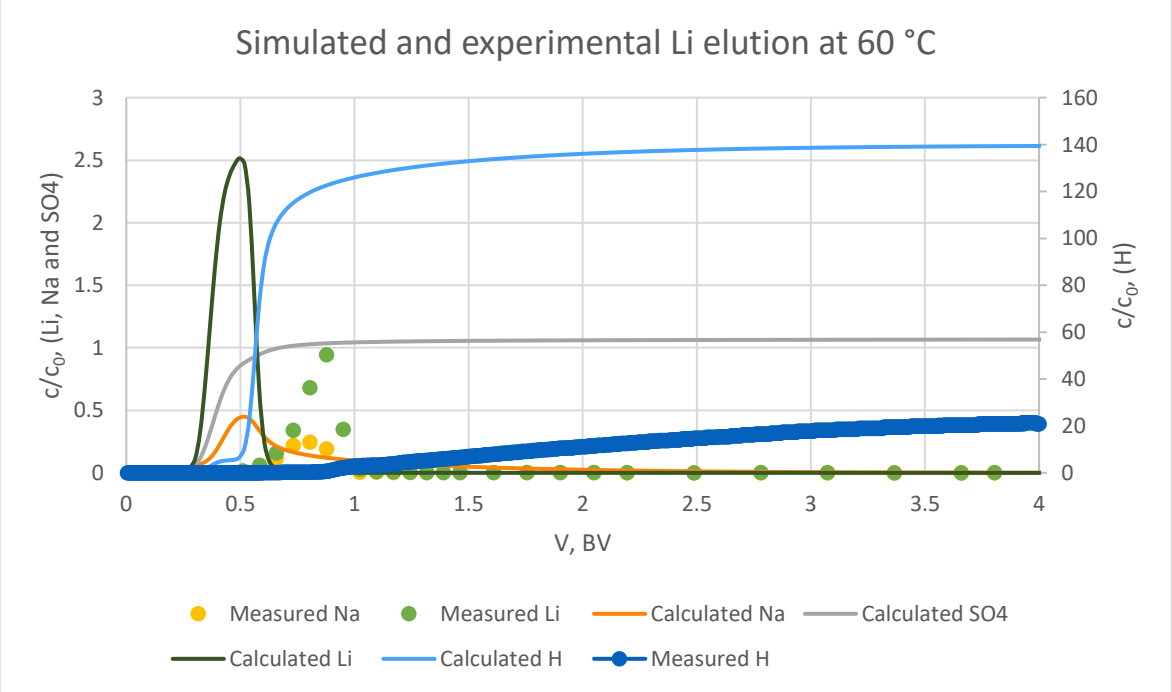

Appendix II Simulated and measured washing and elution curves

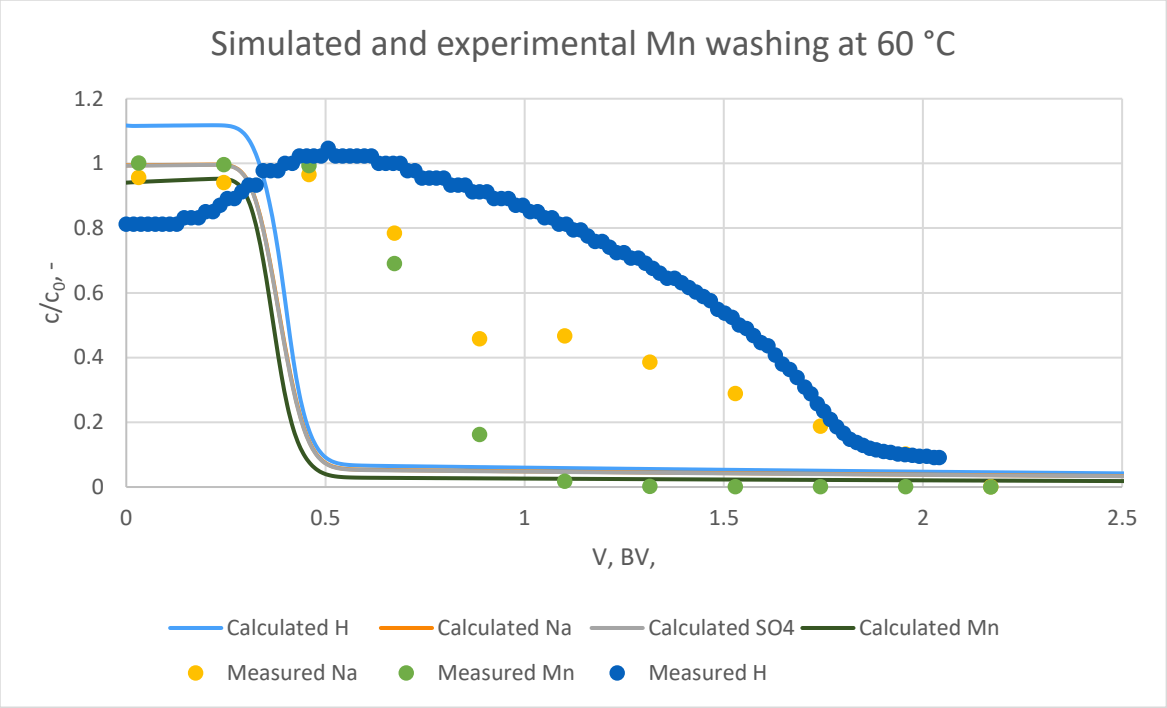

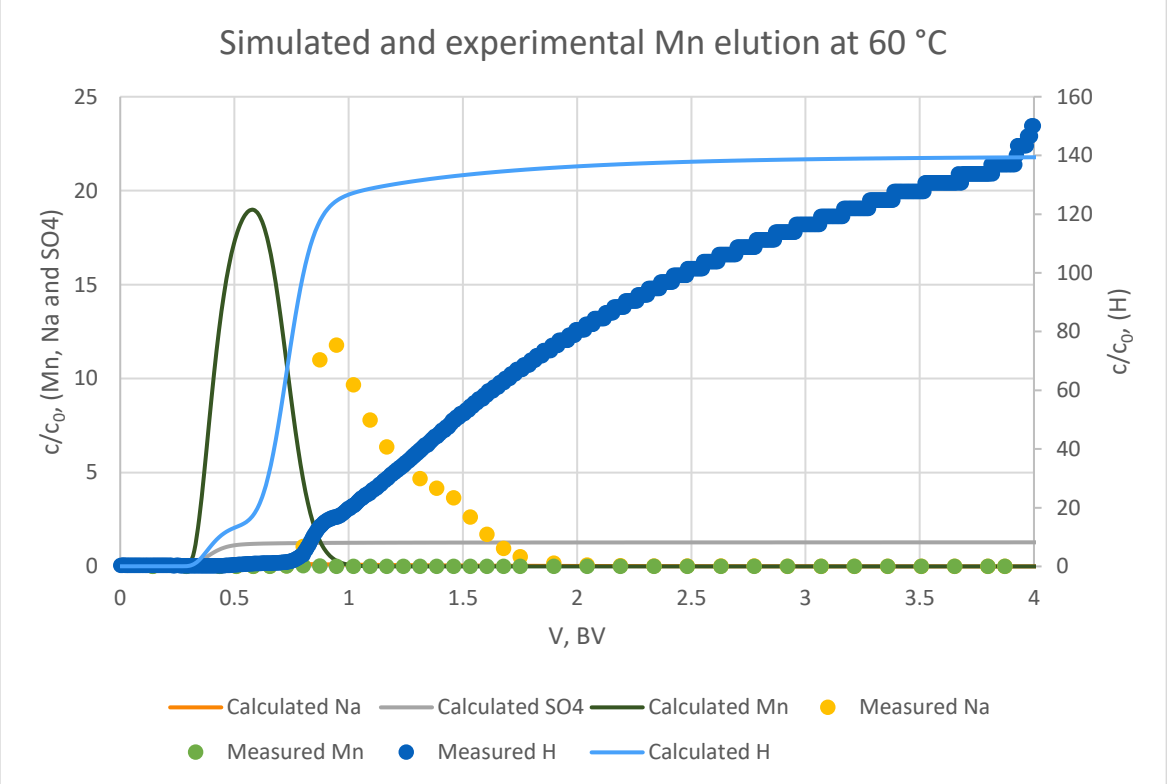

Appendix II Simulated and measured washing and elution curves

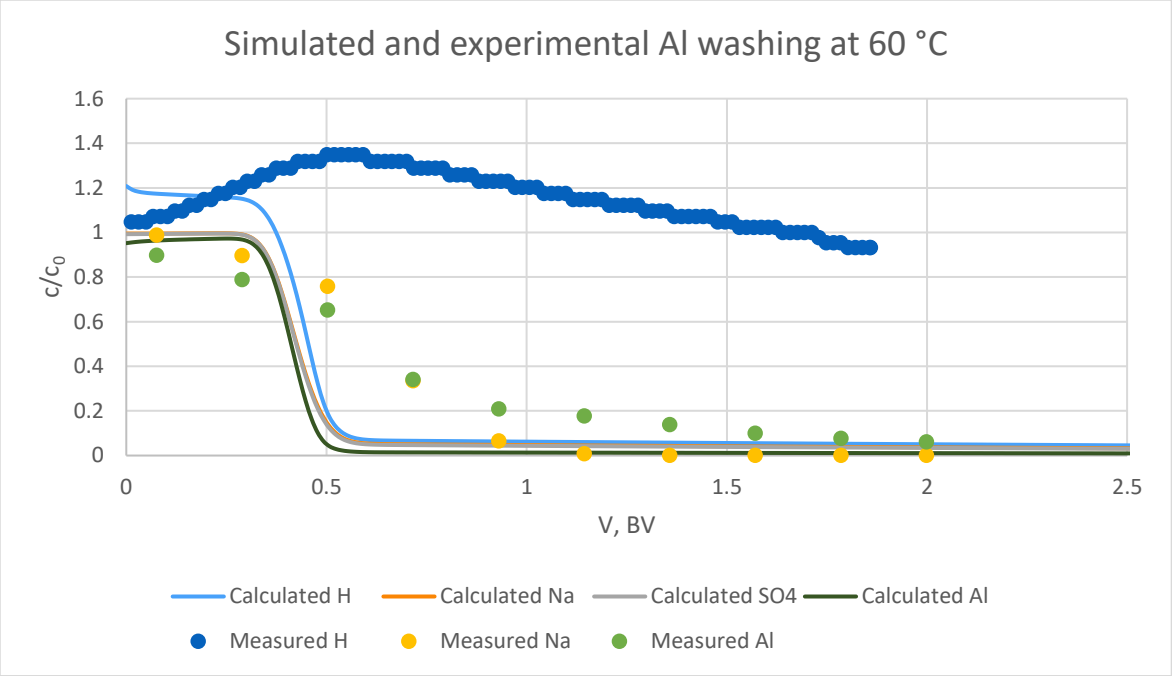

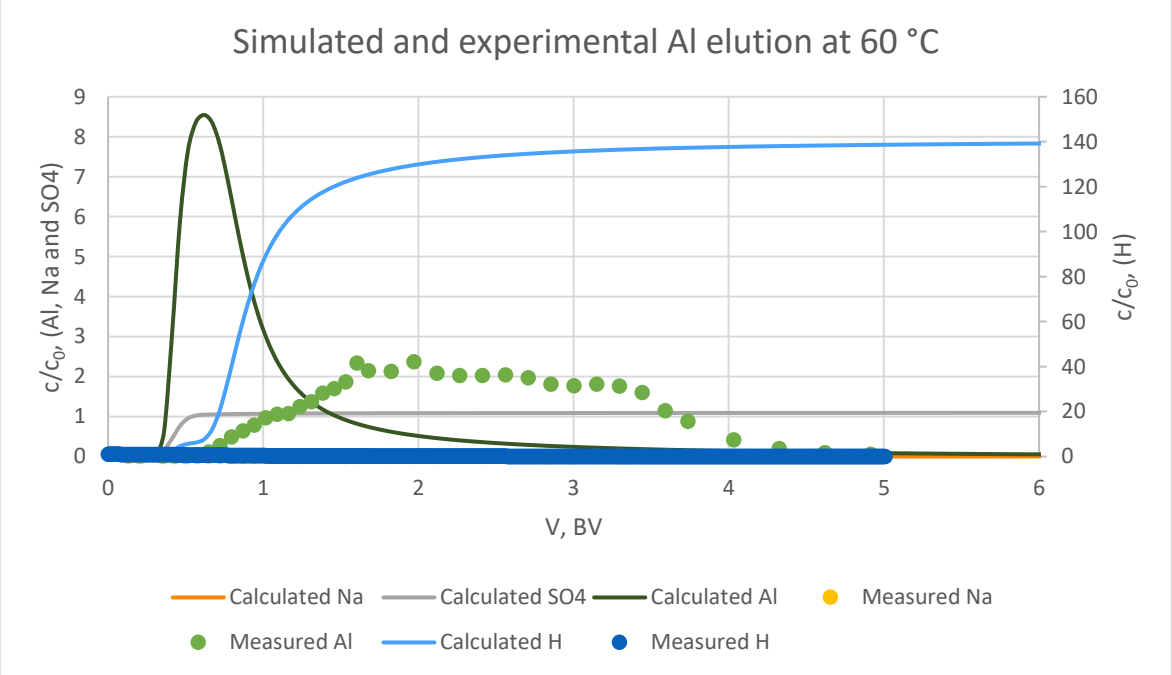

Appendix II Simulated and measured washing and elution curves